BENZIMIDAZOLE DERIVATIVES OF PERYLENE DIIMIDE FOR ORGANIC FIELD-EFFECT TRANSISTOR

Mr. Tianchai Chooppawa

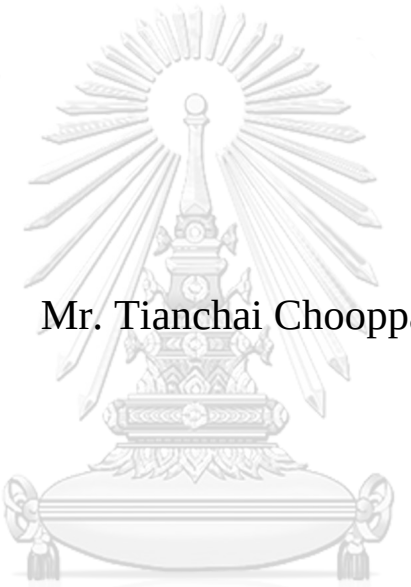

จุฬาลงกรณ์มหาวิทยาลัย
Chulalongkorn University

A Dissertation Submitted in Partial Fulfillment of the Requirements
for the Degree of Doctor of Philosophy in Chemistry
Department of Chemistry
Faculty of Science
Chulalongkorn University
Academic Year 2018
Copyright of Chulalongkorn University

อนุพันธ์เบนซิมิดาโซลของเพอรีลีนไดอิไมด์สำหรับทรานซิสเตอร์สนามไฟฟ้าอินทรีย์

นายเธียรชัย ชุปวา

จุฬาลงกรณ์มหาวิทยาลัย
CHULALONGKORN UNIVERSITY

วิทยานิพนธ์นี้เป็นส่วนหนึ่งของการศึกษาตามหลักสูตรปริญญาวิทยาศาสตรดุษฎีบัณฑิต
สาขาวิชาเคมี ภาควิชาเคมี
คณะวิทยาศาสตร์ จุฬาลงกรณ์มหาวิทยาลัย
ปีการศึกษา 2561
ลิขสิทธิ์ของจุฬาลงกรณ์มหาวิทยาลัย

Thesis Title	BENZIMIDAZOLE DERIVATIVES OF PERYLENE DIIMIDE FOR ORGANIC FIELD-EFFECT TRANSISTOR
By	Mr. Tianchai Chooppawa
Field of Study	Chemistry
Thesis Advisor	Associate Professor PAITOON RASHATASAKHON, Ph.D.
Thesis Co Advisor	Professor Vinich Promarak, Ph.D.

Accepted by the Faculty of Science, Chulalongkorn University in Partial Fulfillment of the Requirement for the Doctor of Philosophy

..... Dean of the Faculty of Science
(Professor POLKIT SANGVANICH, Ph.D.)

DISSERTATION COMMITTEE

..... Chairman
(Associate Professor VUDHICHAI PARASUK, Ph.D.)

..... Thesis Advisor
(Associate Professor PAITOON RASHATASAKHON, Ph.D.)

..... Thesis Co-Advisor
(Professor Vinich Promarak, Ph.D.)

..... Examiner
(Assistant Professor SAKULSUK UNARUNOTAI, Ph.D.)

..... Examiner
(Assistant Professor WORAWAN BHANTHUMNAVIN, Ph.D.)

..... External Examiner
(Assistant Professor Nakorn Niamnont, Ph.D.)

จุฬาลงกรณ์มหาวิทยาลัย
CHULALONGKORN UNIVERSITY

เธียรชัย ชุปวา : อนุพันธ์เบนซิมิดาโซลของเพอรีลีนไดอิไมด์สำหรับทรานซิสเตอร์สนามไฟฟ้าอินทรีย์. (BENZIMIDAZOLE DERIVATIVES OF PERYLENE DIIMIDE FOR ORGANIC FIELD-EFFECT TRANSISTOR) อ. ที่ปรึกษาหลัก : รศ. ดร.ไพฑูรย์ รัชตะสาคร, อ.ที่ปรึกษาร่วม : ศ. ดร.วินิช พรมอารักษ์

การละลายได้น้อยของอนุพันธ์เพอรีลีนที่มีเสถียรภาพทางความร้อนสูงเป็นปัจจัยสำคัญที่ขัดขวางการนำสารดังกล่าวไปใช้เป็นชิ้นงานทรานซิสเตอร์สนามไฟฟ้าอินทรีย์ ในงานวิจัยนี้ผู้วิจัยได้พยายามเพิ่มการละลายเพื่อนำไปใช้ในการศึกษาสมบัติทรานซิสเตอร์สนามไฟฟ้าอินทรีย์ของอนุพันธ์เบนซิมิดาโซลจากเพอริลีนไดอิไมด์ที่มีการปรับแต่งหมู่แอริลอกซีในโครงสร้างแกนของเพอริลีนไดอิไมด์ อย่างไรก็ตามพบว่าไอโซเมอร์ของสารที่สังเคราะห์ทั้งหมดยังคงละลายได้น้อยในตัวทำละลายอินทรีย์จึงทำให้ไม่สามารถแยกและทำให้บริสุทธิ์ได้ ดังนั้นแผนการสังเคราะห์และสารเป้าหมายจึงเปลี่ยนเป็นอนุพันธ์เบนโซไตรเอซาทรุกซีนซึ่งละลายได้ดีในตัวทำละลายอินทรีย์ อาทิ โทลูอีนและไดคลอโรมีเทน โดยพบว่าอนุพันธ์เบนโซไตรเอซาทรุกซีนนี้ไม่เหมาะที่จะนำมาใช้เป็นทรานซิสเตอร์สนามไฟฟ้าอินทรีย์ อย่างไรก็ตามผู้วิจัยพบว่าอนุพันธ์เบนโซไตรเอซาทรุกซีนที่สมมาตรและมีหมู่เฮกซิลเป็นส่วนประกอบแสดงสมบัติการนำส่งโฮลดีกว่าสารทีพีดีซึ่งหาซื้อได้เมื่อขึ้นรูปเป็นไดโอดอินทรีย์เปล่งแสง

จุฬาลงกรณ์มหาวิทยาลัย
CHULALONGKORN UNIVERSITY

สาขาวิชา เคมี

ปีการศึกษา 2561

ลายมือชื่อ
นิสิต .....
ลายมือชื่อ อ.ที่ปรึกษา
หลัก .....
ลายมือชื่อ อ.ที่ปรึกษา
ร่วม .....

5672818923 : MAJOR CHEMISTRY
KEYWORD: organic field-effect transistor, organic light emitting diode, hole-transporting property

Tianchai Chooppawa : BENZIMIDAZOLE DERIVATIVES OF PERYLENE DIIMIDE FOR ORGANIC FIELD-EFFECT TRANSISTOR. Advisor: Assoc. Prof. PAITOON RASHATASAKHON, Ph.D. Co-advisor: Prof. Vinich Promarak, Ph.D.

The poor solubility of perylene derivatives has been a key factor that prohibits the application of these thermally stable compounds in organic field-effect transistors (OFET) devices. In this research, the effort to enhance the solubility and exploring FET property of benzimidazole derivatives of perylene diimide were investigated. The perylene diimide core structure was functionalized by aryloxy moieties. Unfortunately, the isomeric products were still poorly soluble in common organic solvents, which made them impossible to separate and purify. Thus, the synthetic plan and goal were completely revised to the benzotriazatruxene derivatives, which were highly soluble in organic solvents such as dichloromethane and toluene. It was found that these newly designed compound were not suitable for OFET application, However, the C3-symmetric benzotriazatruxene containing hexyl group exhibited better hole transporting properties than the commercial *N,N′*-Bis(3-methylphenyl)-*N,N′*-diphenylbenzidine (TPD).

จุฬาลงกรณ์มหาวิทยาลัย
CHULALONGKORN UNIVERSITY

Field of Study:	Chemistry	Student's Signature .....
Academic Year:	2018	Advisor's Signature .....
		Co-advisor's Signature .....

ACKNOWLEDGEMENTS

First of all, I would like to thank Associate Professor Paitoon Rashataskhon, Ph.D. my advisor, Professor Vinich Promarak, Ph.D., my co-advisor, and the members Material Advancement via Proficient Synthesis (MAPS) for supporting my thesis regarding fluorescent compounds and their property measurements. Not only giving me an opportunity to study and achieve this research, Associate Professor Paitoon also provides me Teacher Assistant scholarship (TA) and Research Assistant scholarship (RA), from Chulalongkorn university.

I appreciate IMS-IIPA (Institute for Molecular Science International Internship Program in Asia) scholarship for foreign students to fulfill my research experience regarding field-effect measurement. Especially, Professor Dr. Hiroshi M. Yamamoto and his members provided nice opportunity and hospitality supported by MEXT Nanotechnology Platform Program (Molecule and Material Synthesis), and Equipment Development Center (Institute for Molecular Science; IMS).

Furthermore, this thesis would not have been accomplished without many precious and valuable advice and comments from all my thesis committee, Associate Professor Vudhichai Parasuk, Ph.D., Assistant Professor Worawan Bhanthumnavin, Ph.D., Assistant Professor Sakulsuk Unarunotai, Ph.D. and Assistant Professor Nakorn Niamnont, Ph.D.

Ultimately, I am most grateful to my mother, my aunt, Ms. Sophin, and all family members for their personal supports at all times.

Tianchai Chooppawa

จุฬาลงกรณ์มหาวิทยาลัย
Chulalongkorn University

TABLE OF CONTENTS

Page

..... iii
ABSTRACT (THAI) iii
.....iv
ABSTRACT (ENGLISH).....iv
ACKNOWLEDGEMENTS.....v
TABLE OF CONTENTS.....vi
List of tables.....ix
List of figures.....x
CHAPTER 1 INTRODUCTION.....1
1.1. Organic field-effect-transistor (OFET).....1
1.2. Band insulator.....3
1.3. Perylene 4
1.4. Benzimidazole of perylene diimide derivatives 6
1.5. Organic Light Emitting Diodes (OLEDs).....10
1.6. Truxene and triazatruxene derivatives.....12
1.7. Coating techniques.....13
1.8. Objectives 16
CHAPTER 2 EXPERIMENTAL.....18
2.1. Materials and instruments.....18
2.2. Synthesis.....19
Bromination of perylene-3,4,9,10-tetracarboxylic dianhydride.....19
1,7-dibromo-*N,N'*-diphenyl-3,4,9,10-perylenetetracarboxylic diimide (DB-PTCDI-PH).....20
1,6,7-tribromo-*N,N'*-diphenyl-3,4,9,10-perylenetetracarboxylic diimide (TB-PTCDI-PH).....20

จุฬาลงกรณ์มหาวิทยาลัย
Chulalongkorn University

1,7-di(4-methoxyphenoxy)-*N,N'*-diphenyl-3,4,9,10-perylenetetracarboxylic diimide (DM-PTCDI-PH) 21

1,7-di(4-methoxyphenoxy)-3,4,9,10-perylenetetracarboxylic dianhydride (DM-PTCDA) 22

B-octyl-9-BBN (9-octyl-9-borabicyclo[3.3.1]nonane) 22

4,5-dioctyl-1,2-phenylenediamine 22

Dibromo perylene benzimidazole containing octyl groups 23

Dibromo perylene benzimidazole containing methyl groups (reaction was in acetic acid) 24

Dibromo perylene benzimidazole containing methyl groups (reaction was in propionic) (DB-BP-C1) 24

1,7-di(4-*t*-butyl-phenoxy)-perylene benzimidazole containing methyl groups (DTP-BP-C1) 25

Dimethyl-4,4'-(perylene benzimidazole-1,7-diylbis(oxy))dibenzoate containing methyl groups (DAP-BP-C1) 26

1,7-diphenoxy-perylene benzimidazole containing methyl groups (DP-BP-C1) 26

6,13-dihydro-5*H*-benzo[*i*]benzo[6,7]indolo[2,3-*a*]benzo[6,7]indolo[2,3-*c*]carbazole (A-BTT) and 12,19-dihydro-5*H*-benzo[*i*]benzo[6,7]indolo[3,2-*a*]benzo[6,7]indolo[3,2-*c*]carbazole (S-BTT) 27

5,6,13-trihexyl-6,13-dihydro-5H-benzo[i]benzo[6,7]indolo[2,3-a]benzo[6,7]indolo[2,3-c]carbazole (A-BTT-C6) 29

5,12,19-trihexyl-12,19-dihydro-5*H*-benzo[*i*]benzo[6,7]indolo[3,2-*a*]benzo[6,7]indolo[3,2-*c*]carbazole (S-BTT-C6) 30

N-ethyl benzo[g]indole 31

N, *N*, *N*-triethyl-benzotriazatruxene (S-BTT-C2) via *N*-ethyl benzo[g]indole 31

N-hexyl benzo[g]indole 32

N, *N*, *N*-trihexyl-benzotriazatruxene (S-BTT-C6) via *N*-hexyl benzo[g]indole 32

2.3. OFET evaluation 33

2.3.1. OFET fabrication 33

2.3.2. OFET performance investigation 34

จุฬาลงกรณ์มหาวิทยาลัย
Chulalongkorn University

2.4. OLED evaluation 35
2.4.1. OLED fabrication 35
2.4.2. OLED performance investigation 36
CHAPTER 3 RESULTS AND DISCUSSION 37
3.1. Synthesis and characterization of benzimidazole perylene derivatives via hydrolysis 38
3.2. Synthesis and characterization of benzimidazole perylene derivatives via brominated perylene benzimidazole 40
3.3. Synthesis and characterization of benzotriazatruxene derivatives 44
3.4. Thermal characterization of benzotriazatruxene derivatives 46
3.5. Photophysical properties of benzotriazatruxene derivatives 47
3.6. FET properties of benzotriazatruxene derivatives 50
3.7. Hole transporting properties of benzotriazatruxene derivatives in OLEDs 59
CHAPTER 4 CONCLUSIONS 62
REFERENCES 64
APPENDIX 70
VITA 93

จุฬาลงกรณ์มหาวิทยาลัย
Chulalongkorn University

List of tables

Page

Table 3.1 Photophysical and electrochemical properties of A-BTT, S-BTT, A-BTT-C6 and S-BTT-C6 50

Table 3.2 Annealing temperature for 1 hour and SAM effect on DFM image of benzotriazatruxene films via the solution-deposition process (thickness is below the image) 51

Table 3.3 Summary of mobility values for evaporated A-BTT and S-BTT on bare substrates 59

Table 3.4 Electroluminescent properties of device 1-5 61

จุฬาลงกรณ์มหาวิทยาลัย
Chulalongkorn University

List of figures

Page

Figure 1.1 Schematic of p- and n- transistor....2

Figure 1.2 (a) Idealized energy diagram of OFET at $V_G = V_D = 0$. (b) At $V_G > 0$ and $V_D = 0$ (c) At $V_G < 0$ and $V_D = 0$ (d) at $V_G > 0$ and $V_D > 0$ (e) at $V_G < 0$ and $V_D < 0$ 3

Figure 1.3 Metal, semiconductor and insulator according to band theory.....4

Figure 1.4 Structure of perylene-3,4,9,10-tetracarboxylic dianhydride (PTCDA).....5

Figure 1.5 Electron mobility of various PTCDI with thermal treatment.....5

Figure 1.6 I_d-V_d of 30 nm PTCDI-C13 film (a) before and (b) after annealing at 140 ^oC.....6

Figure 1.7 Synthesis route for pyridyl-fused perylene bisimides 6

Figure 1.8 Structure of benzimidazole derivatives in a patent.....7

Figure 1.10 Structure and normalzied absorption and emission spectrum of bis(trifluoromethyl)-substituted-3,4,9,10-perylene tetracarboxylic bis(benzimidazole) regioisomers.....8

Figure 1.9 Structure and normalzied absorption and emission spectrum of 1,6,7,12-tetrakis(aryloxy)-3,4,9,10-perylenetetracarboxdiimide derivatives.....8

Figure 1.11 Synthesis of asymmetric soluble perylene imide benzimidazole.....9

Figure 1.12 I_d-V_g and $I_{d1/2}$-V_g characteristics of perylenebis-benzimidazole on benzocyclobutane.....9

Figure 1.13 (a) CRT, (b) LCD, (c) plasma, and (d) OLED displays in computer monitor.....10

Figure 1.14 Comparison of brightness and contrast between OLED and LCD display 10

Figure 1.15 Light-emitting mechanism in an OLED device (HIL = hole-injection layer; HTL = hole-transporting layer; EML = emissive layer; ETL = electron-transporting layer; EIL = electron-injection layer) 11

Figure 1.16 Chemical structures of NPD and TPD.....11

Figure 1.17 Two derivatives of carbazole with truxene as a core structure 12

Figure 1.18 Chemical structures of truxene derivatives with carbazole and pyrene moieties.....13

จุฬาลงกรณ์มหาวิทยาลัย
Chulalongkorn University

Figure 1.19 Chemical structures of triazatruxene derivatives with substituent at 3, 8, 13 positions 13

Figure 1.20 I_d-V_g of spin-coated N,N'-bis-(1-pentyl)hexyl-3,4,9,10-perylene diimide film 15

Figure 1.21 Chemical structures of pyrenyl triazatruxene containing benzyl moiety 15

Figure 1.22 Target perylenebis-benzimidazole derivatives 16

Figure 1.23 Target molecules containing benzotriazatruxene 17

Figure 2.24 Device scheme for OFET investigation 35

Figure 2.25 Illustration of our fabricated devices 36

Figure 3.26 Bromination and imidization of perylene 38

Figure 3.27 Synthesis strategy of benzimidazole perylene via hydrolysis 39

Figure 3.28 Synthesis of perylene benzimidazole derivatives via brominated perylene benzimidazole 40

Figure 3.29 FTIR results (wavenumber (cm-1) and transmittance) of reaction in (top) acetic acid (bottom) propionic acid (red line: product; blue line: PTCDA) 42

Figure 3.30 Solubility of synthesized perylene-benzimidazole regioisomers in methylenechloride (left) toluene (right) 43

Figure 3.31 Synthesis of A-BTT and S-BTT 44

Figure 3.32 Synthesis of N,N,N-trialkyl benzotriazatruxene via N-alkyl-1H-benzo[g]indole 45

Figure 3.33 Synthesis of A-BTT-C6 and S-BTT-C6 46

Figure 3.34 DSC thermograms of A-BTT, S-BTT, A-BTT-C6 and S-BTT-C6 47

Figure 3.35 Absorption and emission spectra of A-BTT and A-BTT-C6 in THF 48

Figure 3.36 Absorption and emission spectra of S-BTT and S-BTT-C6 in THF 48

Figure 3.37 Example of failed result (I_d-V_g characteristic) such as from spin-coated S-BTT-C6 51

Figure 3.38 DFM images of (a) A-BTT and (b) S-BTT without annealing of evaporated film 57

Figure 3.39 Electrical characterization (top) A-BTT, (bottom) S-BTT of evaporated sample without annealing. 58

Figure 3.40 Illustration of our fabricated devices 60

Figure 3.41 Current density and luminance vs. voltage (J-V-L) characteristic of 61

จุฬาลงกรณ์มหาวิทยาลัย
Chulalongkorn University

Figure A. 42 GC-MS spectrum of 4,5-dioctyl-1,2-phenylene diamine 70

Figure A. 43 ^{1}H-NMR spectrum of 1,7-dibromo-N,N-diphenyl-perylene-3,4,9,10-tetracarboxylic diimide (DB-PTCDI-PH).....70

Figure A. 44 ^{1}H-NMR spectrum of 1,6,7-tribromo-N,N-diphenyl-perylene-3,4,9,10-tetracarboxylic diimide (TB-PTCDI-PH) 71

Figure A. 45 ^{1}H-NMR spectrum of 1,7-di(4-methoxy-phenoxy)-N,N-diphenyl-perylene-3,4,9,10-tetracarboxylic diimide (DM-PTCDI-PH) 71

Figure A. 46 MALDI-TOF mass spectrum of DB-BP-C1 72

Figure A. 47 LC-MS mass spectrum of DTP-BP-C1 72

Figure A. 48 LC-MS mass spectrum of DAP-BP-C1.....73

Figure A. 49 LC-MS mass spectrum of DP-BP-C1.....73

Figure A. 50 ^{1}H-NMR spectrum of 6,13-dihydro-5H-benzo[i]benzo[6,7]indolo[2,3-a]benzo[6,7]indolo[2,3-c]carbazole (A-BTT) 74

Figure A. 51 ^{13}C-NMR spectrum of 6,13-dihydro-5H-benzo[i]benzo[6,7]indolo[2,3-a]benzo[6,7]indolo[2,3-c]carbazole (A-BTT) 74

Figure A. 52 MALDI-TOF mass spectrum of 6,13-dihydro-5H-benzo[i]benzo[6,7]indolo[2,3-a]benzo[6,7]indolo[2,3-c]carbazole (A-BTT).....75

Figure A. 53 ^{1}H-NMR spectrum of 12,19-dihydro-5H-benzo[i]benzo[6,7]indolo[3,2-a]benzo[6,7]indolo[3,2-c]carbazole (S-BTT) 75

Figure A. 54 ^{13}C-NMR spectrum of 12,19-dihydro-5H-benzo[i]benzo[6,7]indolo[3,2-a]benzo[6,7]indolo[3,2-c]carbazole (S-BTT) 76

Figure A. 55 MALDI-TOF mass spectrum of 12,19-dihydro-5H-benzo[i]benzo[6,7]indolo[3,2-a]benzo[6,7]indolo[3,2-c]carbazole (S-BTT).....76

Figure A. 56 ^{1}H-NMR spectrum of 5,6,13-trihexyl-6,13-dihydro-5H-benzo[i]benzo[6,7]indolo[2,3-a]benzo[6,7]indolo[2,3-c]carbazole (A-BTT-C6).....77

Figure A. 57 ^{13}C-NMR spectrum of 5,6,13-trihexyl-6,13-dihydro-5H-benzo[i]benzo[6,7]indolo[2,3-a]benzo[6,7]indolo[2,3-c]carbazole (A-BTT-C6).....77

Figure A. 58 MALDI-TOF mass spectrum of 5,6,13-trihexyl-6,13-dihydro-5H-benzo[i]benzo[6,7]indolo[2,3-a]benzo[6,7]indolo[2,3-c]carbazole (A-BTT-C6).....78

Figure A. 59 ^{1}H-NMR spectrum of 5,12,19-trihexyl-12,19-dihydro-5H-benzo[i]benzo[6,7]indolo[3,2-a]benzo[6,7]indolo[3,2-c]carbazole (S-BTT-C6).....78

Figure A. 60 ^{13}C-NMR spectrum of 5,12,19-trihexyl-12,19-dihydro-5H-benzo[i]benzo[6,7]indolo[3,2-a]benzo[6,7]indolo[3,2-c]carbazole (S-BTT-C6).....79

Figure A. 61 MALDI-TOF mass spectrum of 5,12,19-trihexyl-12,19-dihydro-5H-benzo[i]benzo[6,7]indolo[3,2-a]benzo[6,7]indolo[3,2-c]carbazole (S-BTT-C6).....79
Figure A. 62 DI-GC-MS spectrum of N-ethyl-benzo[g]indole 80
Figure A. 63 DI-GC-MS spectrum of N, N, N-triethyl-benzotriazatruxene (S-BTT-C2).....80
Figure A. 64 DI-GC-MS spectrum of N-hexyl-benzo[g]indole 80
Figure A. 65 DI-GC-MS spectrum of brominated N-hexyl-benzo[g]indole 81
Figure A. 66 DI-GC-MS spectrum of dimer of N-hexyl-benzo[g]indole.....81
Figure A. 67 Molar absorption coefficient plot of A-BTT in THF 82
Figure A. 68 Molar absorption coefficient plot of S-BTT in THF 82
Figure A. 69 Molar absorption coefficient plot of A-BTT-C6 in THF 83
Figure A. 70 Molar absorption coefficient plot of S-BTT-C6 in THF 83
Figure A. 71 Quantum yield report of A-BTT in CH_2Cl_2.....84
Figure A. 72 Quantum yield report of S-BTT in CH_2Cl_2 84
Figure A. 73 Quantum yield report of A-BTT-C6 in CH_2Cl_2.....85
Figure A. 74 Quantum yield report of S-BTT-C6 in CH_2Cl_2 85
Figure A. 75 Quantum yield report of A-BTT film 86
Figure A. 76 Quantum yield report of S-BTT film.....86
Figure A. 77 Quantum yield report of A-BTT-C6 film 87
Figure A. 78 Quantum yield report of S-BTT-C6 film.....87
Figure A. 79 One of mobility calculations of evaporated A-BTT film without annealing at 10 µm gap 88
Figure A. 80 One of mobility calculations of evaporated S-BTT film without annealing at 10 µm gap 89
Figure A. 81 One of mobility calculations of evaporated A-BTT film without annealing at 25 µm gap 90
Figure A. 82 One of mobility calculations of evaporated S-BTT film without annealing at 25 µm gap 91
Figure A. 83 One of mobility calculations of evaporated S-BTT film without annealing at 100 µm gap 92

จุฬาลงกรณ์มหาวิทยาลัย
Chulalongkorn University

CHAPTER 1
INTRODUCTION

1.1. Organic field-effect-transistor (OFET)

A field-effect transistor (FET) was patented in 1930 by Lilienfeld. The first electric-field-effect on the conductivity of organic thin film was measured by Kahng and co-workers in 1960 [1-3]. After that, there were some reports in the middle of 1980s; for instance, Ebisawa, Kudo, Koezuka and their co-workers independently prepared OFET devices based on polyacetylene, merocyanine, and polythiophene, respectively. The material variety and the concept of charge accumulation can be found in many review papers such as the report by Horowitz published in 1998 [4-9]. OFET consists of three electrodes (gate, source and drain), an insulating layer such as SiO_2, and a semiconductor thin film made of organic molecules. In FET, there are three types of operation mode, namely p-type and n-type and ambipolar type. In the p-channel transistor, to turn on the device, negative gate voltage needs to be applied; and then, holes (positive charge carriers) will be injected into the channel from source/drain electrodes. As a result, the mobile holes convey electricity from source to drain when drain bias is applied (**Figure 1.1**). On the other hand, in the n-channel transistor, positive gate voltage needs to be applied to turn on the device; then, the electrons (negative charge carriers) will be accumulated at the semiconductor/insulator interface. This will make the channel conducting again. In the case of ambipolar FET, both electrons and holes work as charge carriers, as the major carrier can be switched depending on the gate voltage. A good conductivity at the ON state can be obtained by larger carriers' mobility when the size of the FET is given.

OFET is being applied for inexpensive, large area, printable and bendable devices [10-12]. It has been already used as intelligent ink, identified tag, sensors and light emitting displays [13-16]. According to the molecular orbital theory, there are 2 important energy levels; namely HOMO (Highest Occupied Molecular Orbital) and LUMO (Lowest Unoccupied Molecular Orbital). HOMO is the highest energy level that contains electron(s) while LUMO is the lowest vacant energy level. Although hole

จุฬาลงกรณ์มหาวิทยาลัย
CHULALONGKORN UNIVERSITY

mobility in the Valence band (p-channel FET) and/or electron mobility in the Conduction band (n-channel FET) are important [17], other factors such as the contact resistance, ON/OFF ratio, and subthreshold swing are also important in practical use. Depending on the HOMO/LUMO levels of the molecules with respect to the work function of the electrodes, the injection barrier, or contact resistance, will be affected.

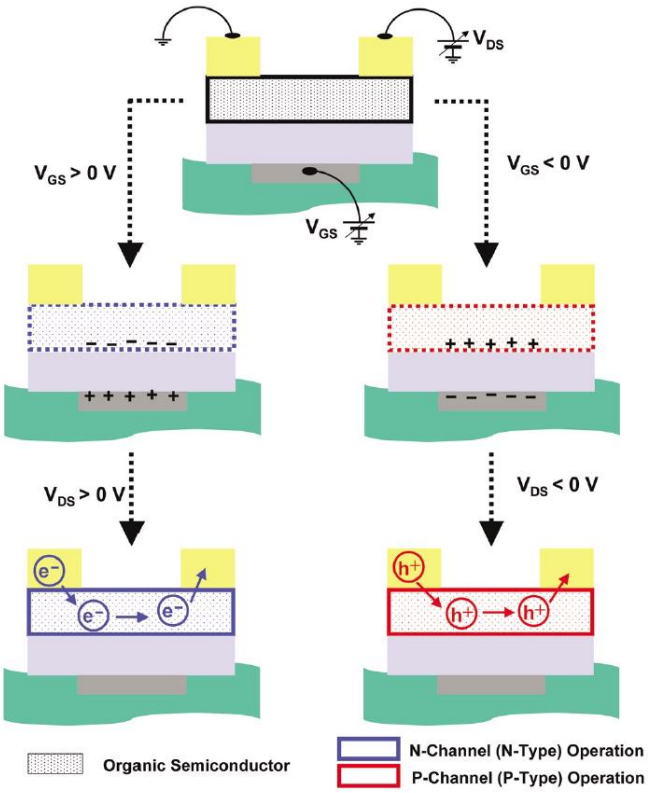

CHULALONGKORN UNIVERSITY

Figure 1.1 *Schematic of p- and n- transistor*

Before the application of gate voltage, HOMO and LUMO are located at certain energy levels. For p-channel FET, after applying a negative gate voltage, both HOMO and LUMO levels of the channel material are shifted up (**Figure 1.2c**). This will allow the energy level matching between HOMO and Fermi level of the electrodes when the hole carriers can flow into the FET channel. On the other hand, after applying a positive gate voltage, the HOMO and LUMO levels of n-type material are shifted down and then electron can flow into the channel [18, 19].

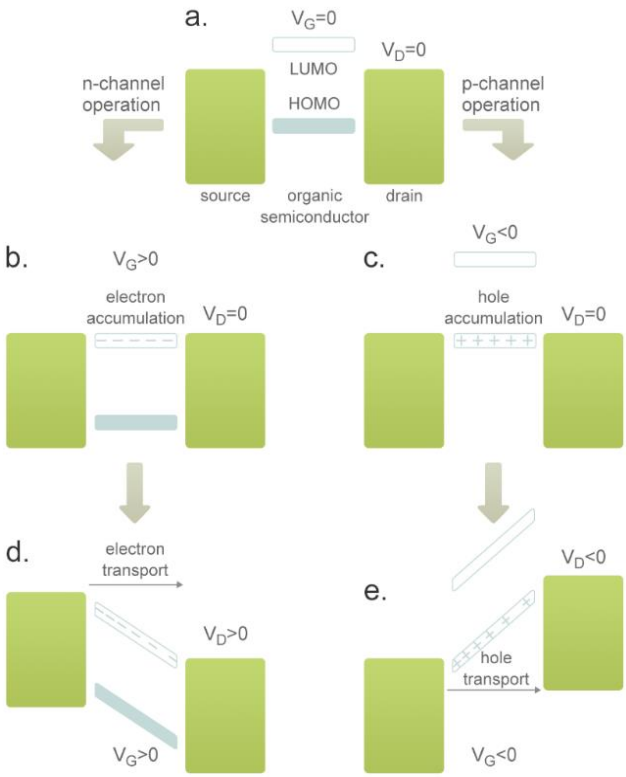

Figure 1.2 *(a) Idealized energy diagram of OFET at $V_G = V_D = 0$. (b) At $V_G > 0$ and $V_D = 0$ (c) At $V_G < 0$ and $V_D = 0$ (d) at $V_G > 0$ and $V_D > 0$ (e) at $V_G < 0$ and $V_D < 0$*

1.2. Band insulator

จุฬาลงกรณ์มหาวิทยาลัย
CHULALONGKORN UNIVERSITY

In a solid state, the electrons' energy becomes continuous to form energy bands. Valence band (VB) comprises HOMO, while conduction band (CB) comprises LUMO. If there is no doped carrier either in the VB nor CB, the solid becomes a semiconductor or an insulator (**Figure 1.3** [20]). If the band gap between VB and CB is much larger than room temperature, typically more than 4 eV, it is called an insulator because there is no thermally excited carrier. If there are intrinsic carriers in CB, the solid becomes a metal [21].

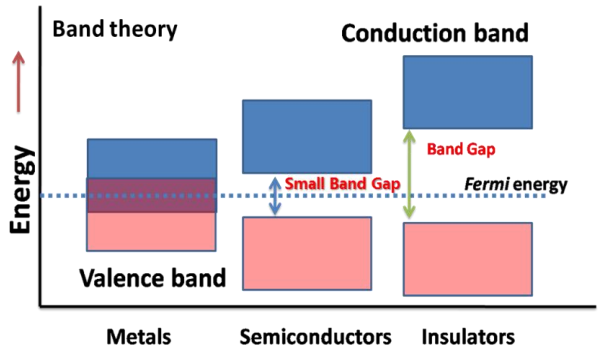

Figure 1.3 *Metal, semiconductor and insulator according to band theory*

1.3. Perylene

Among n-type organic semiconductors, one of the most brilliant materials is perylene-3,4,9,10-tetracarboxylic diimide derivatives (PTCDIs) [22]. PTCDIs are used not only in FET application but also as organic light emitting transistor (OLET) [23], inverter [24, 25], chemical sensor [26] and organic photovoltaic (OPV) [27] as they have shown high electron mobility [28-30] due to strong π-π interaction of perylene core (**Figure 1.4**).

จุฬาลงกรณ์มหาวิทยาลัย
Chulalongkorn University

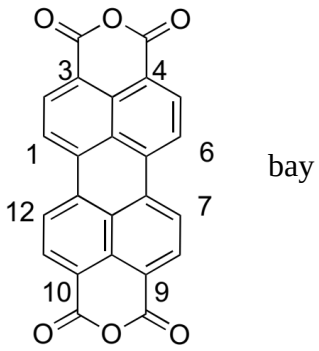

Figure 1.4 *Structure of perylene-3,4,9,10-tetracarboxylic dianhydride (PTCDA)*

To enhance the efficiency, self-assembled monolayers (SAMs) [31] and silsesquioxane copolymer [32] were employed as dielectric layer and the mobility values were found to be increased due to forming of a highly crystalline layer via hydrophobic interaction. Instead of forming SAMs on the substrate, *N*-alkyl perylene diimide compounds were synthesized acting as a long-alkyl-chain-attached molecule. The report revealed that strong hydrophobic interaction of long chain could prevent the migration of the first monolayer into bulk; as a result, electron mobility was enhanced after annealing (**Figure 1.5**) [33]. For instance, *N,N'*-ditridecyl PTCDI (PTCDI-C13) is an attractive molecule for air stable OFET [29] because of high electron mobility (2.1 cm^2/V s) after annealing (**Figure 1.6**) [22].

จุฬาลงกรณ์มหาวิทยาลัย
Chulalongkorn University

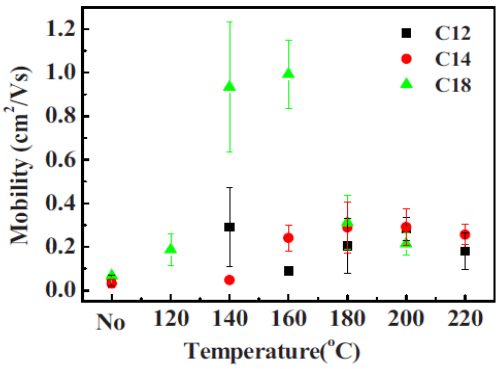

Figure 1.5 *Electron mobility of various PTCDI with thermal treatment*

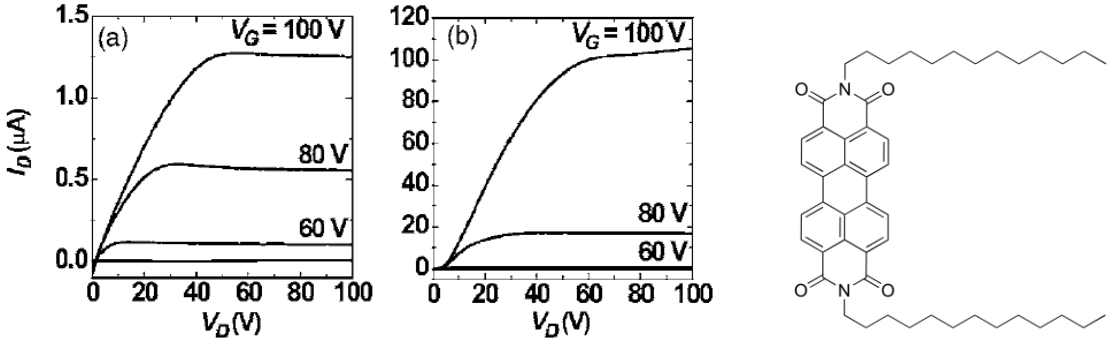

Figure 1.6 *I_d-V_d of 30 nm PTCDI-C13 film (a) before and (b) after annealing at 140 °C*

Basically, evaporation in high vacuum is employed to deposit those PTCDIs films because of their poor solubility, to result in films with several molecular layer thickness [34-36].

Perylene-3,4,9,10-tetracarboxylic diimide (PTCDI) was also used for preparing coronene derivatives. For instance, Wei Jiang and co-workers have successfully synthesized pyridyl-fused perylene bisimides in one pot. After Suzuki cross-coupling, the light was used to prepare core-extended perylene bisimides which their photophysical properties were performed in THF [37] (**Figure 1.7**).

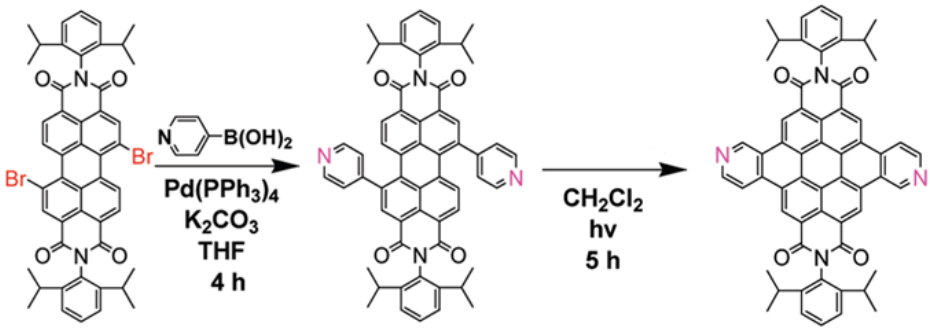

Figure 1.7 *Synthesis route for pyridyl-fused perylene bisimides*

1.4. Benzimidazole of perylene diimide derivatives

Benzimidazole derivatives were synthesized by condensation between 1,7-difluoro-perylene-3,4,9,10-tetracarboxylic dianhydride (DF-PTCDA) and 1,2-phenylenediamine; however, crude mixtures of regioisomers were purified by triple sublimation in a three-zone sublimation unit. The highest mobility was 6.2×10^{-5} cm^2/V s at 125ºC [38]. (**Figure 1.8**)

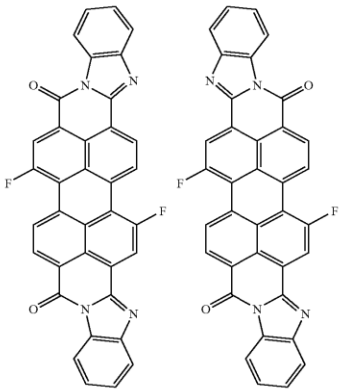

Figure 1.8 *Structure of benzimidazole derivatives in a patent*

In 1997, Heribert Quante and co-workers described absorption and emission properties of syn/anti 1,6,7,12-tetrakis(aryloxy)-3,4,9,10-perylenetetracarboxdiimide derivatives in dichloromethane at room temperature (**Figure 1.9**). This suggests that the introduction of the substituent on perylene core might improve the solubility [39].

จุฬาลงกรณ์มหาวิทยาลัย
CHULALONGKORN UNIVERSITY

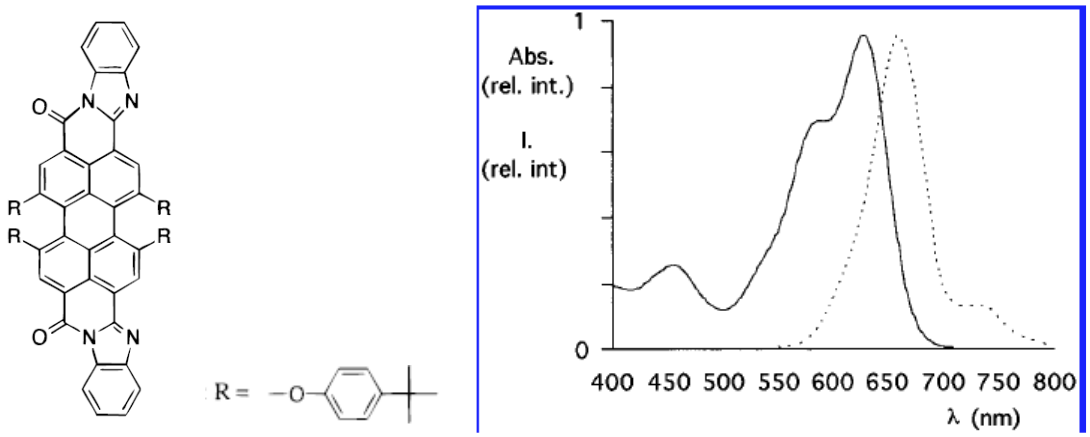

Figure 1.10 *Structure and normalzied absorption and emission spectrum of 1,6,7,12-tetrakis(aryloxy)-3,4,9,10-perylenetetracarboxdiimide derivatives*

Not only the aryloxy group but CF_3 moieties in bis(trifluoromethyl)-substituted-3,4,9,10-perylene tetracarboxylic bis(benzimidazole) regioisomers were also reported in terms of absorption and emission spectrum in dichloromethane. The author assumes that the introduction of bulky CF_3 moieties on perylene core might improve the solubility because of a possible twist of perylene core via intermolecular repulsion of steric CF_3 moieties [40]. (**Figure 1.10**)

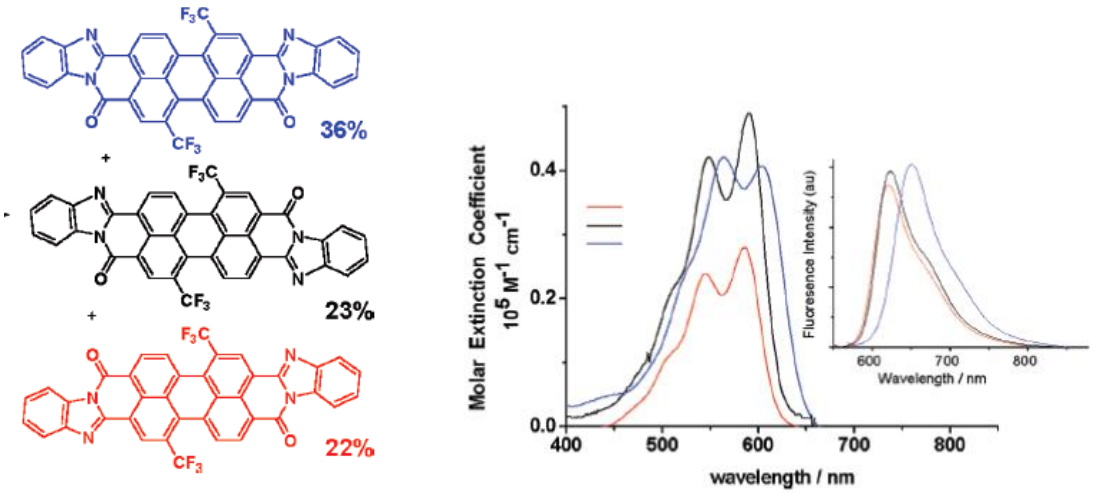

Figure 1.9 *Structure and normalzied absorption and emission spectrum of bis(trifluoromethyl)-substituted-3,4,9,10-perylene tetracarboxylic bis(benzimidazole) regioisomers*

Asymmetric soluble perylene imide benzimidazole was synthesized and liquid crystalline properties were found (**Figure 1.11**). The alkyl chain was decorated to alter solubility. Thus, UV absorption spectrum was revealed in $CHCl_3$ [41].

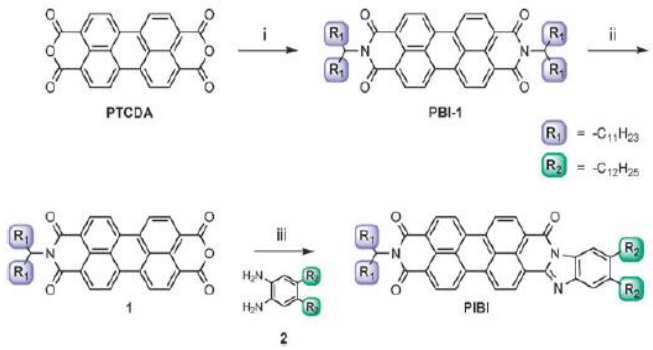

Figure 1.11 *Synthesis of asymmetric soluble perylene imide benzimidazole*

A thin film of perylenebis-benzimidazole was fabricated on polymer gate dielectric. The researchers found that the OFET performance was influenced by the gate dielectric. The highest mobility was 1.6 x 10^{-4} cm^2/V s on poly-benzocyclobutane gate dielectric (**Figure 1.12**). Nevertheless, the thermal evaporation process was conducted to coat perylenebis-benzimidazole layer which obstructed monolayer formation [42].

จุฬาลงกรณ์มหาวิทยาลัย

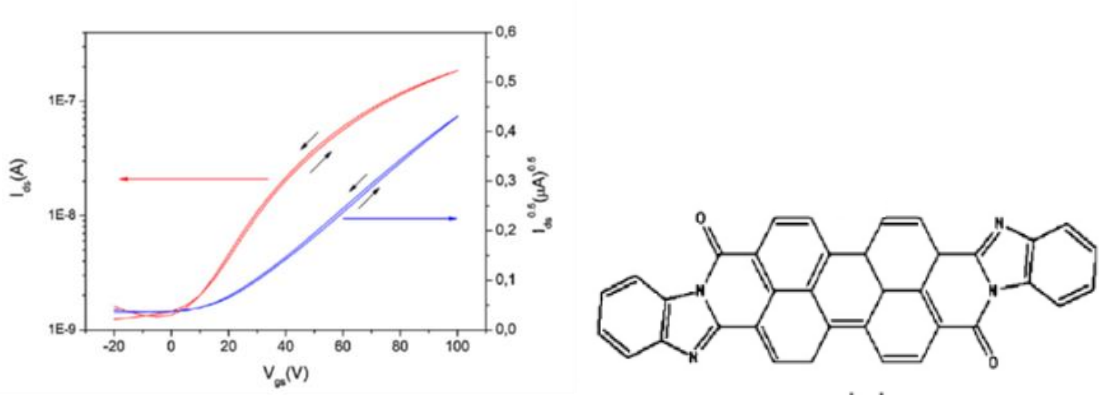

Figure 1.12 *I_d-V_g and $I_{d1/2}$-V_g characteristics of perylenebis-benzimidazole on benzocyclobutane*

1.5. Organic Light Emitting Diodes (OLEDs)

Organic light-emitting diodes (OLEDs) have been an interesting material used to create flat panel displays for past several years due to its advantages including large area fabrication, flexibility and light weight compare with other display technologies such as cathode ray tube (CRT), liquid crystal displays (LCD) and plasma displays (**Figure 1.13**) [43, 44].

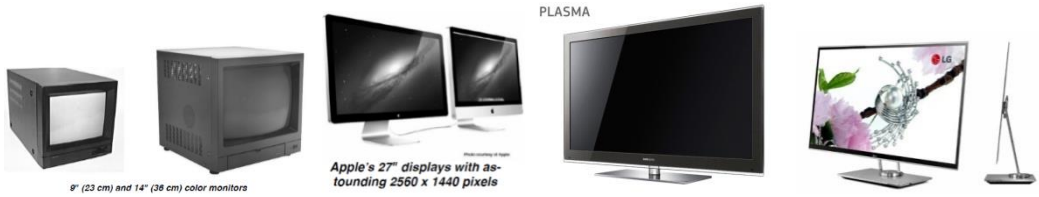

(a) *(b)* *(c)* *(d)*

Figure 1.13 *(a) CRT, (b) LCD, (c) plasma, and (d) OLED displays in computer monitor*

For instance, OLED display shows better quality in brightness and contrast than LCD displays (**Figure 1.14**) [45]. Light brightness, cost of production, the weight of device and energy consumption are important things to develop for the next generation of flat panel displays. Assuredly, OLEDs have been improved and developed to fulfill these requirements.

จุฬาลงกรณ์มหาวิทยาลัย

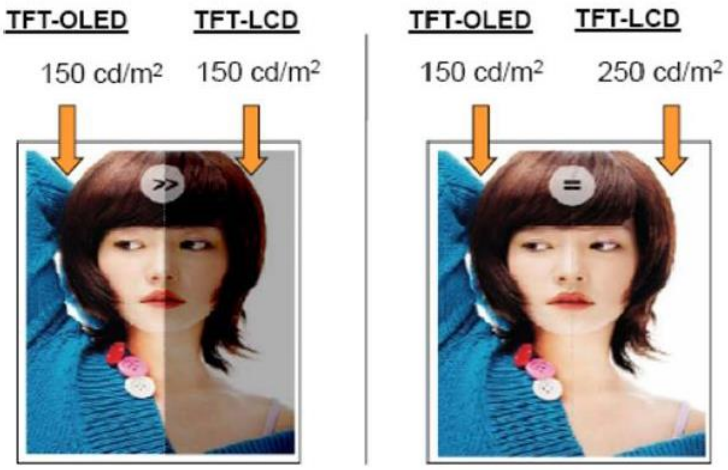

Figure 1.14 *Comparison of brightness and contrast between OLED and LCD display*

Generally, a single-layer OLED is made of a single emissive organic layer (EML) sandwiched between the cathode (Metal) and the anode (ITO); however, this device shows low quantum efficiency for photoluminescence. In order to enhance emission, hole transporting layer (HTL) was introduced to alter recombination of the hole and electron pairs (exciton pairs) at the interface which generates electroluminescence [46]. The radical cations typically form in hole transporting layer to carry holes and prevent electrons transfer to the other side of the electrode without recombination with holes.

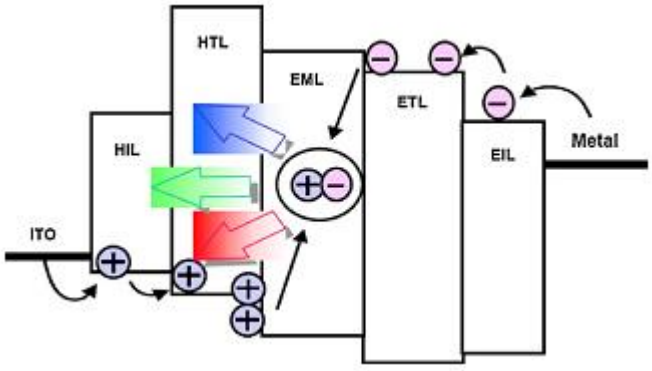

Figure 1.15 *Light-emitting mechanism in an OLED device (HIL = hole-injection layer; HTL = hole-transporting layer; EML = emissive layer; ETL = electron-transporting layer; EIL = electron-injection layer)*

จุฬาลงกรณ์มหาวิทยาลัย
Chulalongkorn University

The conventional hole materials are *N,N'*-diphenyl-*N,N'*-bis(1-naphthyl)-(1,1'-biphenyl)-4,4'-diamine (NPB) and *N,N'*-bis(3-methylphenyl)-*N,N'*-

TPD NPD

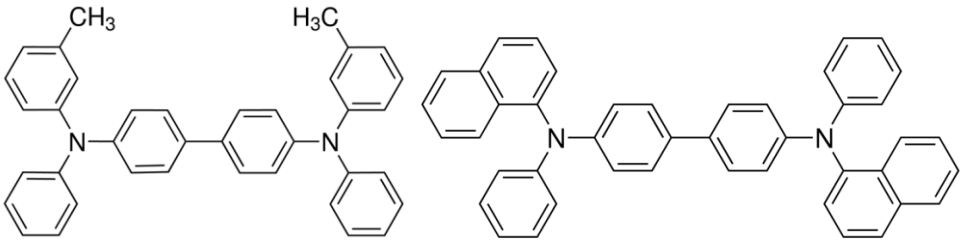

Figure 1.16 *Chemical structures of NPD and TPD*

bis(phenyl)benzidine (TPD); however, low glass transition temperature (T_g) of NPB and TPD (100 and 65^{o}C, respectively) can cause the poor morphology at high operating temperature. As a result, the device efficiency easily decays upon using [47-55].

1.6. Truxene and triazatruxene derivatives

Based on an extensive review of literature, it has been found that truxenes (10,15-dihydro-5*H*-diindeno[1,2-α;1',2'-*c*]-fluorene) and triazatruxenes (10,15-dihydro-5*H*-dihydro-5*H*-diindolo[3,2-a:3',2'-c]carbazole) are attractive materials for hole transporting and emissive layer in OLED application. For example, Ruksasorn and co-workers designed and synthesized two derivatives of carbazole with truxene showed high thermal stability (glass transition temperatures at 249 and 293°C, respectively) and excellent hole transporting property (12,000 cd m^{-2} at 12.0 V) [56].

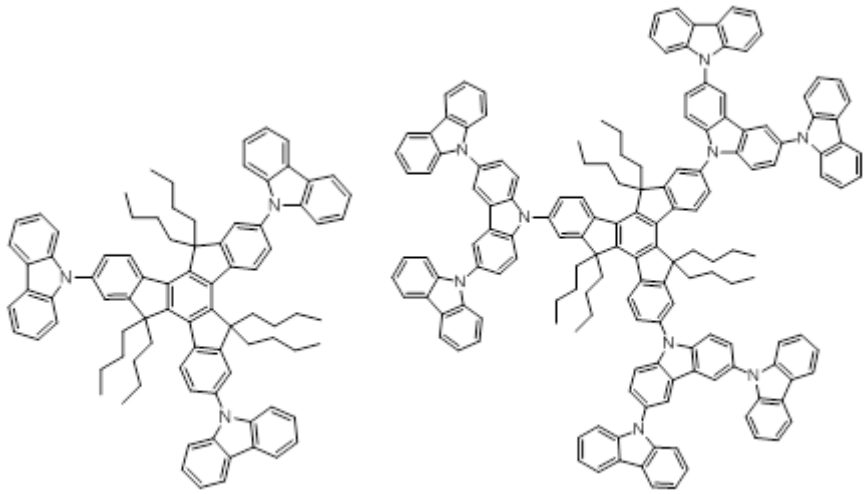

Figure 1.17 *Two derivatives of carbazole with truxene as a core structure*

Interestingly, spin coated film of truxene derivatives containing carbazole and pyrene moieties revealed excellent hole transporting property (maximum luminance 4.5 × 10^4 cd m^{-2} at 10.8 V) and good non-doped blue emissive layer (maximum luminance 8.0 × 10^3 cd m^{-2} at 9.6 V) [57].

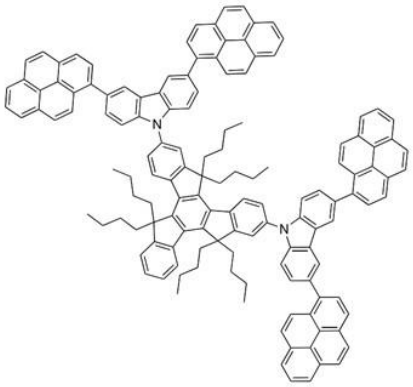

Figure 1.18 *Chemical structures of truxene derivatives with carbazole and pyrene moieties*

In 2012, Zhu and coworkers synthesized triazatruxene derivatives with substituent at 3, 8, 13 positions in five categories. Thermal properties of those compounds were investigated. Their T_d and T_m showed temperature measurement at 405^{o}C and 219-373^{o}C, respectively. However, T_g could not be observed for those compounds. Then, the optical properties were studied. They emitted blue light at 394-412 nm in solution and 416-461 nm in solid state, respectively. In addition, their quantum efficiencies were about 32-58% [58].

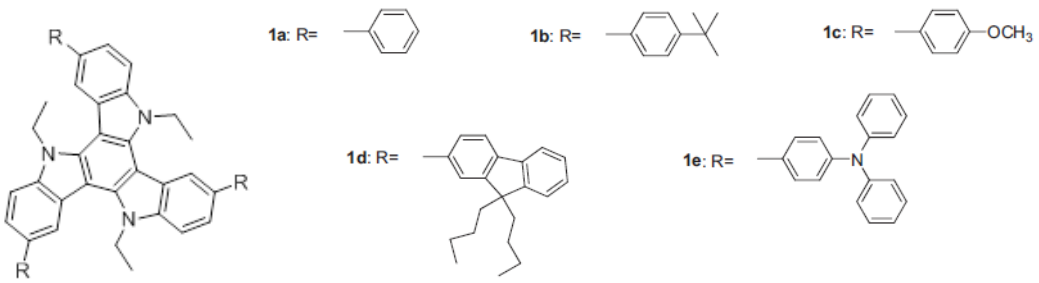

Figure 1.19 *Chemical structures of triazatruxene derivatives with substituent at 3, 8, 13 positions*

1.7. Coating techniques

Among several coating techniques, spin coating is an engaging solution-deposition process due to a good candidate for large area fabrication and economical

fabrication. Unlike solution-deposition process, molecular evaporation process requires high vacuum and large energy for heating.

There are plenty of solution-deposition processes such as dip coating, spin coating and drop casting. To coat the substrate, the compound needs to be dissolved in the solvent. After solvation, it will be coated by a variety of techniques.

For dip coating, the substrate is immersed in the solution and is lifted. This technique should be optimized by changing lifting speed and concentration of the solution. A monolayer was obtained in some cases [59, 60].

Many compounds such as 5T (heptathiophene) [61] and 7T [62] (septithiophene) were successfully coated by the spin coating method. Briefly speaking, the solution is dropped on the substrate and dried by spinning. This technique should be optimized by changing the spin speed, solvent and concentration of the solution.

About drop casting, the film is prepared by dropping the solution on the substrate and dried at ambient condition. This technique should be optimized by changing the solvent and concentration of the solution.

PTCDIs film has been prepared by the Langmuir-Blodgett (LB) technique. However, the preparation process was complicated, and it was not successful in forming a uniform layer [63]. Singh and co-workers synthesized *N,N'*-bis-(1-pentyl)hexyl-3,4,9,10-perylene diimide and fabricated thin films with its solution in chlorobenzene to measure FET properties, but spin-coated monolayer film was not obtained and mobility was only 5 x 10^{-4} cm^2/V s [64]. (**Figure 1.20**)

จุฬาลงกรณ์มหาวิทยาลัย
Chulalongkorn University

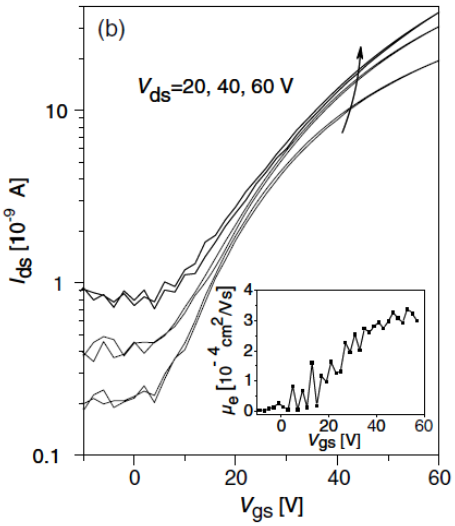

Figure 1.20 *I_d-V_g of spin-coated N,N'-bis-(1-pentyl)hexyl-3,4,9,10-perylene diimide film*

Recently, symmetrical pyrenyl triazatruxene containing benzyl moiety was spin coated in the formation of OLED devices; it as found that hole transporting property displayed three-times better than commercial hole transporting agent [65].

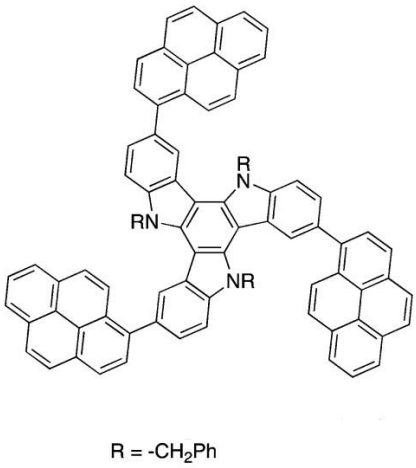

Figure 1.21 *Chemical structures of pyrenyl triazatruxene containing benzyl moiety*

1.8. Objectives

Currently, there are high demands of low-cost electronic devices. As an alternative class of optoelectronic materials, polyaromatic organic compounds have been quite useful due to their tunable structures and ease in fabrication using low-temperature solution processes. Perylene-3,4,9,10-tetracarboxylic dianhydride (PTCDA), has recently become an attractive scaffold for compounds used as the electrical modulator called organic field-effect transistor (OFET). In this work, PTCDA will be derivatized into novel benzimidazole analog with aryloxy substituents in order to enhance the solubility in the fabrication process. Moreover, the effects of the substituents at the aryloxy groups towards the photophysical properties will be investigated by experimentation. The charge transporting properties will also be examined after the materials are fabricated as OFET devices.

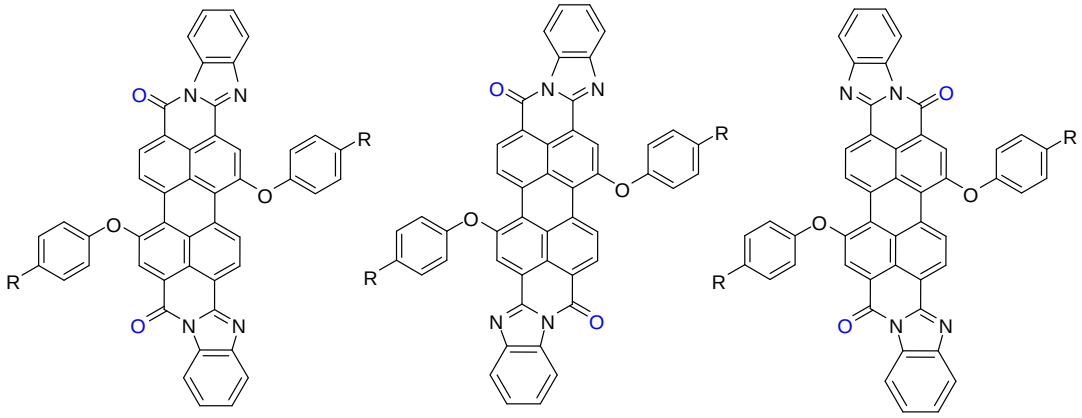

R = -Ph
= -4-Cl-C_6H_4
= 4-*t*-Bu-C_6H_4

Figure 1.22 *Target perylenebis-benzimidazole derivatives*

Based on the aforementioned studies, it can be seen that hole transporting properties of asymmetrical and symmetrical benzotriazatruxenes are not conclusive. We synthesized and characterized 4 benzotrizatruxene derivatives consisting of asymmetrical and symmetrical benzotriazatruxenes (**A-BTT and S-BTT**) without *N*-

substituted moiety and asymmetrical and symmetrical *N*-hexyl benzotriazatruxenes (**A-BTT-C6 and S-BTT-C6**). We also performed photophysical studies to analyze structural and electronic property of synthesized compounds. Finally, hole transporting performance of the spin-coated film was tested.

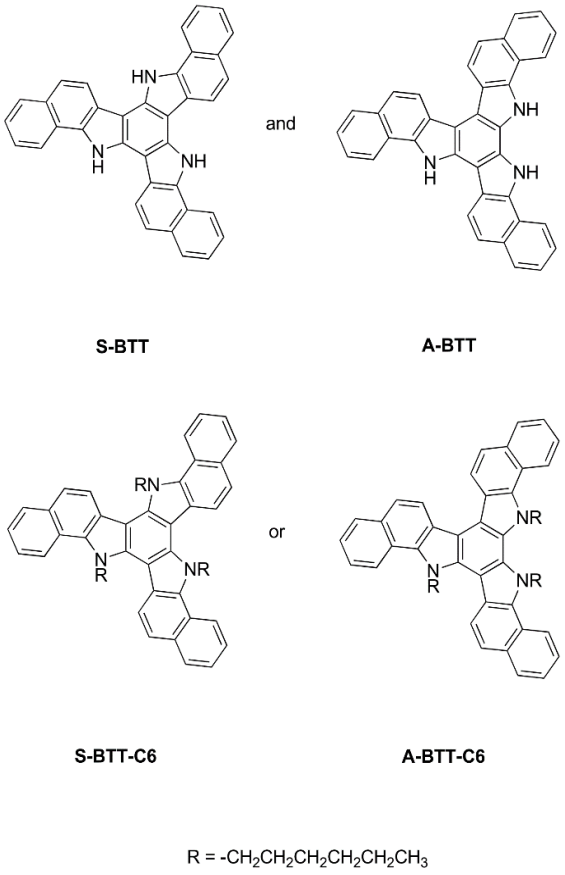

Figure 1.23 *Target molecules containing benzotriazatruxene*

CHAPTER 2
EXPERIMENTAL

2.1. Materials and instruments

Perylene-3,4,9,10-tetracarboxylic dianhydride, 1,7-dibromo-perylene-3,4,9,10-tetracarboxylic dianhydride (DB-PTCDA) and all phenol agents were purchased from Tokyo Chemical Industry (TCI, Japan). 1-aminotridecane, 1-aminohexane, aniline, propionic acid, tetrabutylammonium bromide, K_2CO_3, 1-octene, 0.5 M 9-BBN, 4,5-dibromo-1,2-phenylenediamine, 4,5-dimethyl-1,2-phenylenediamine, potassium iodide, tetrakistriphenylphosphine palladium(0) or $Pd(PPh_3)_4$, $PdCl_2$(dppf) and common solvent were purchased from WAKO Pure Chemical Industries (Japan). All commercially available chemicals were used without purification. P-doped Si substrates covered with a 300 nm-thick SiO_2 layer (SiO_2/Si) were cut into the size of 6 by 6 mm^2. The electrodes were patterned by photolithography. The Au/Ti electrodes were deposited by the sputtering method. The I-V characteristic study was conducted by 4200A-SCS parameter analyzer (Keithley). The temperature was regulated with LS336 temperature controller in combination with manual prober (Lake Shore Cryotronics). The morphology of the device surface was observed by DFM (dynamic force microscopy) while optical images for drop casted film were taken by polarized microscope (Nikon, Japan).

จุฬาลงกรณ์มหาวิทยาลัย
Chulalongkorn University

Regarding the benzotriazatruxene study, 1*H*-Benzo[g]indole was purchased from Sigma-Aldrich. Other chemical reagents and solvent were purchased from WAKO Pure Chemical Industries (Japan). All commercially available chemicals were used without purification. Thin layer chromatography (TLC) was performed on aluminium sheets precoated with silica gel (Merck Kiesegel 60 F_{254}) (Merck KgaA, Darmstadt, Germany). Column chromatography was performed on silica gel (Merck Kieselgel 60G) (Merck KGaA, Darmstadt, Germany). The ^{1}H NMR was determined on Varian Mercury NMR spectrophotometer (Varian, USA) at 400 MHz with chemical shifts reported as ppm in $CDCl_3$ and DMSO-d_6. The ^{13}C NMR was measured on Bruker Mercury NMR spectrophotometer (Bruker, Germany) equipped at 100 MHz with

chemical shifts reported as ppm in $CDCl_3$ and DMSO-d_6. Mass spectra were recorded on a Microflex MALDI-TOF mass spectrometer (Bruker Daltonics) using doubly recrystallized α-cyano-4-hydroxy cinnamic acid (CCA) and dithranol as a matrix. Absorption spectra were measured by a Varian Cary 50 UV-Vis spectrophotometer. The stock solutions of each compound were prepared in THF at 10^{-3} – 10^{-5} M, then diluted to more than 5 different concentrations. To obtain the accurate result, all absorbances should not exceed 1.0 because it gives a non-linear effect on Beer's law, $A= \varepsilon bc$ which A is absorbance, ε is absorption coefficient and c is concentration. The absorption coefficient (ε) was obtained from the slope of the calibration curve between concentration and absorbance. The λ_{max} was chosen from the wavelength that provides the highest absorbance. Fluorescence spectra were obtained from a Varian Cary Eclipse spectrofluorometer. Absolute quantum yields were measured using the FLS980 spectrometer (Edinburgh Instrument).

2.2. Synthesis

Bromination of perylene-3,4,9,10-tetracarboxylic dianhydride

Perylene-3,4,9,10-tetracarboxylic dianhydride (1.64 g; 4.18 mmol) was dissolved in 15 mL of concentrated H_2SO_4. After that, the solution was stirred for 1 hour at ambient temperature; and then, Iodine (0.78 g; 3.08 mmol) was added and the solution was heated at 85ºC for 1 hour. Next, liquid bromine (1.50 mL; 29.28 mmol) was swiftly dropped and heated at 110ºC for 2 days. To precipitate the product, the reaction mixture was added into the ice; the crude product was separated by suction filtration and dried with the water bath. The product was used without purification in the next step.

จุฬาลงกรณ์มหาวิทยาลัย
Chulalongkorn University

1,7-dibromo-*N,N'*-diphenyl-3,4,9,10-perylenetetracarboxylic diimide (DB-PTCDI-PH)

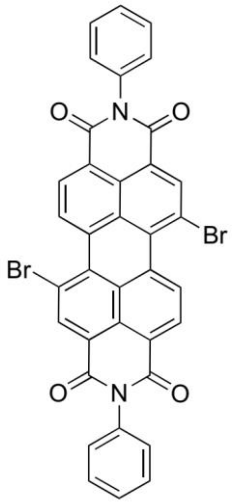

To synthesize DB-PTCDI-C13, a procedure described in literatures [66, 67] was modified. Crude brominated perylene-3,4,9,10-tetracarboxylic dianhydride (0.53 g; 0.95 mmol) and aniline (0.60 mL; 3.18 mmol) was blended with 15 ml of propionic acid. The suspension was refluxed overnight then poured into the ice bath. The crude product was filtrated by suction filtration, and column chromatography (dichloromethane: hexane 4:1) was conducted to obtain the red powder of **DB-PTCDI-PH** (28%). ^{1}H NMR ($CDCl_3$, 400 MHz): δ = 9.56 (d, *J* = 8.0 Hz, 2H), 8.98 (s, 2H), 8.78 (d, *J* = 8.0 Hz, 2H), 7.65 – 7.49 (m, 6H), 7.35 (d, *J* = 7.0 Hz, 4H) ppm.

1,6,7-tribromo-*N,N'*-diphenyl-3,4,9,10-perylenetetracarboxylic diimide (TB-PTCDI-PH)

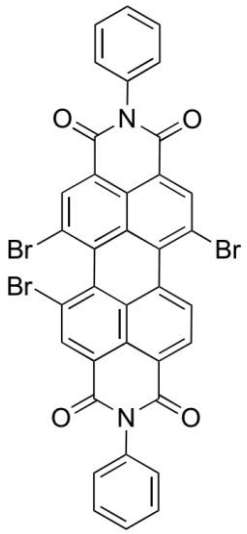

The procedure liked DB-PTCDI-PH. The red powder was obtained (4%). ^{1}H NMR ($CDCl_3$, 400 MHz) δ = 9.50 (d, *J* = 8.2 Hz, 1H), 8.97 (s, 1H), 8.89 (d, *J* = 0.6 Hz, 2H), 8.79 (d, *J* = 8.1 Hz, 1H), 7.64 – 7.51 (m, 6H), 7.38 – 7.31 (m, 4H) ppm.

1,7-di(4-methoxyphenoxy)-*N,N'*-diphenyl-3,4,9,10-perylenetetracarboxylic diimide (DM-PTCDI-PH)

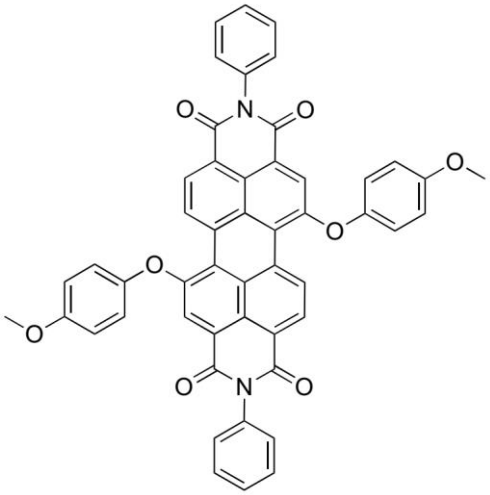

Synthesized DB-PTCDI-PH (0.06 g; 0.08 mmol), 4-methoxy phenol (0.11 g; 0.88 mmol) and potassium carbonate (0.11 g; 0.77 mmol) was heated in 8 ml of NMP for 1 day. The reaction bottle was cooled down to room temperature. After that, 1 M HCl (20 mL) was added then filtrated to obtain black powder. The crude product was purified by column chromatography on silica gel (dichloromethane: hexane = 6:1). The purple powder was obtained (38%). ^{1}H NMR ($CDCl_3$, 400 MHz) δ = 9.66 (d, *J* = 9.9 Hz, 2H), 8.63 (d, *J* = 8.2 Hz, 2H), 8.28 (s, 2H), 7.52 – 7.38 (m, 7H), 7.24 (d, *J* = 7.9 Hz, 3H), 7.07 (d, *J* = 7.0 Hz, 4H), 6.91 (d, *J* = 14.2 Hz, 4H), 3.79 (d, *J* = 14.6 Hz, 6H) ppm.

1,7-di(4-methoxyphenoxy)-3,4,9,10-perylenetetracarboxylic dianhydride (DM-PTCDA)

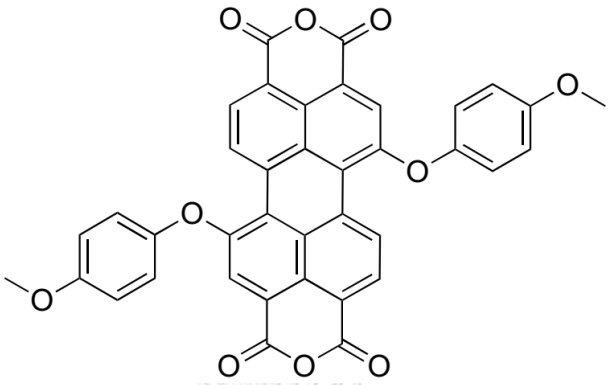

DM-PTCDI-PH (1.13 g; 1.29 mmol) and potassium hydroxide (0.25 g; 4.53 mmol) were dispersed in tert-butyl alcohol (20 mL). The reaction mixture was refluxed, and acetic acid per 2 N HCl (30 mL) was slowly added into the reaction mixture and heated at 90ºC. To generate anhydride moieties, the mixture was heated at 45ºC overnight then extracted by chloroform (100 mL) which was dried by anhydrous $MgSO_4$. The organic phase was evaporated to obtain a crude product.

B-octyl-9-BBN (9-octyl-9-borabicyclo[3.3.1]nonane)

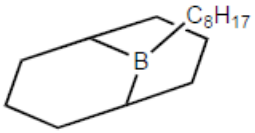

1-octene (1.40 g, 12.50 mmol) was added in 6 ml dried THF. At 0ºC, 25 mL 0.5 M 9-BBN in THF (1.52 g, 12.50 mmol) was added into the solution. Next, the reaction mixture was stirred at room temperature for 6 hours. The product was used in the next step without purification.

4,5-dioctyl-1,2-phenylenediamine

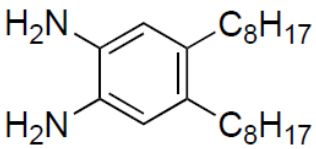

4,5-dibromo-1,2-phenylenediamine (1.56 g, 5.85 mmol), crude B-octyl-9-BBN and 10 mL 3 M NaOH was dissolved in 12 mL THF under argon atmosphere. Next, $PdCl_2$(dppf) (0.26 g, 0.35 mmol, 6 mol%) was added into the reaction mixture. The reaction was refluxed at 70°C for 16 hours. After that, 40 mL hexane was added for dilution then 5 mL 30% H_2O_2, 50 ml brine. Dry over anhydrous $MgSO_4$. The crude was obtained after evaporation which was purified by column chromatography on silica gel (dichloromethane: ethyl acetate 4:1). The black oil was obtained (37%); APCI-LC-MS *cal* 332.57 *found* [332] [M].

Dibromo perylene benzimidazole containing octyl groups

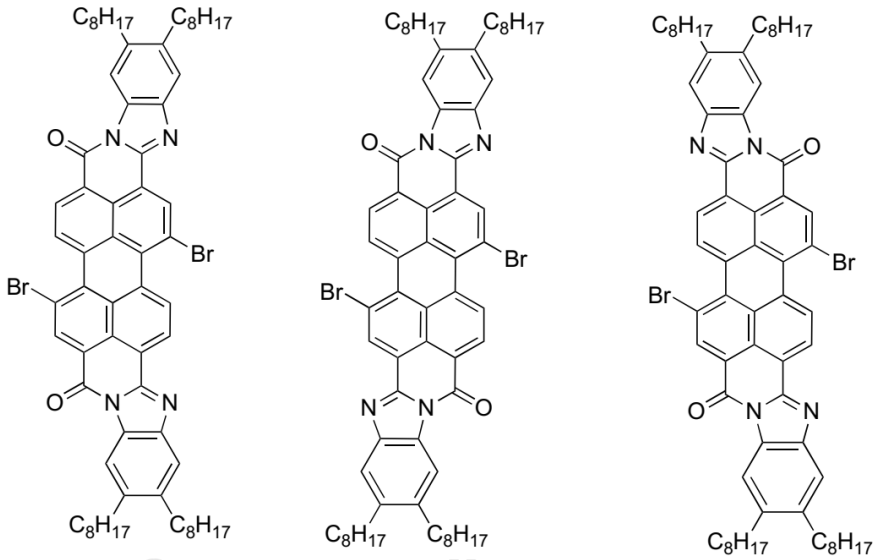

Chulalongkorn University

1,7-dibromo-perylene-3,4,9,10-tetracarboxylic dianhydride (DB-PTCDA; 0.64 g; 1.17 mmol), 4,5-dioctyl-1,2-phenylenediamine (1.17 g; 3.51 mmol) was mixed with acetic acid (4.00 mL) and NMP (16.00 mL). The suspension was heated 120°C for 3 days. To quench the reaction, cold water was added to collected by suction filtration. MeOH washing was performed to purify the product briefly. The characterization will be explained in results and discussion.

Dibromo perylene benzimidazole containing methyl groups (reaction was in acetic acid)

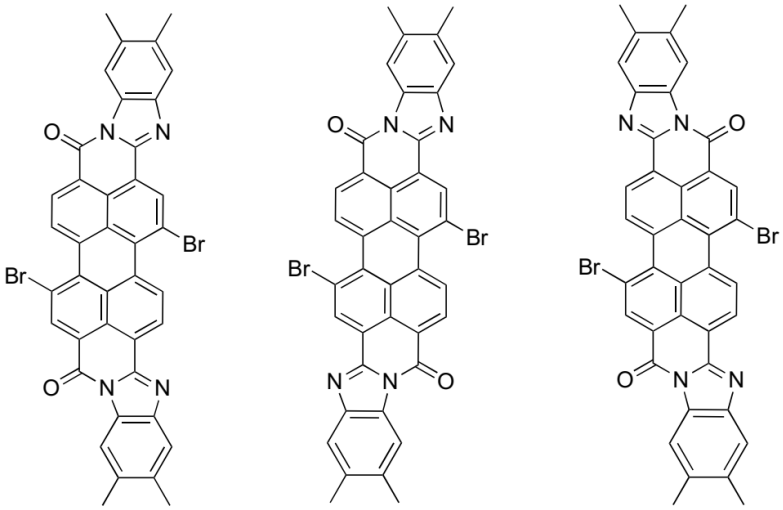

1,7-dibromo-perylene-3,4,9,10-tetracarboxylic dianhydride (DB-PTCDA; 0.20 g; 0.37 mmol), 4,5-dimethyl-1,2-phenylenediamine (0.20 g; 1.48 mmol) was mixed with acetic acid (1.00 mL) and NMP (4.00 mL). The suspension was heated 120^{o}C for 1 day. To quench the reaction, cold water was added to collected by suction filtration. MeOH washing was performed to purify the product (71%) briefly. The characterization will be explained in results and discussion.

Dibromo perylene benzimidazole containing methyl groups (reaction was in propionic) (DB-BP-C1)

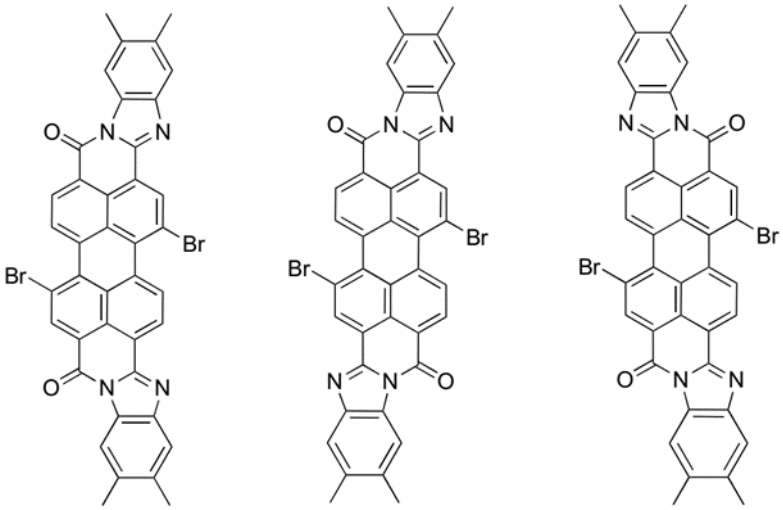

1,7-dibromo-perylene-3,4,9,10-tetracarboxylic dianhydride (DB-PTCDA; 1.17 g; 2.13 mmol), 4,5-dimethyl-1,2-phenylenediamine (1.17 g; 8.61 mmol) was mixed

with propionic acid (40.00 mL). The mixture was refluxed for 1 day. To quench the reaction, cold water was added to collected by suction filtration. MeOH washing was performed to purify the product (91%) used without purification. MALDI-TOF MS: *cal*. 750.44 *found* 751.00 [M].

1,7-di(4-*t*-butyl-phenoxy)-perylene benzimidazole containing methyl groups (DTP-BP-C1)

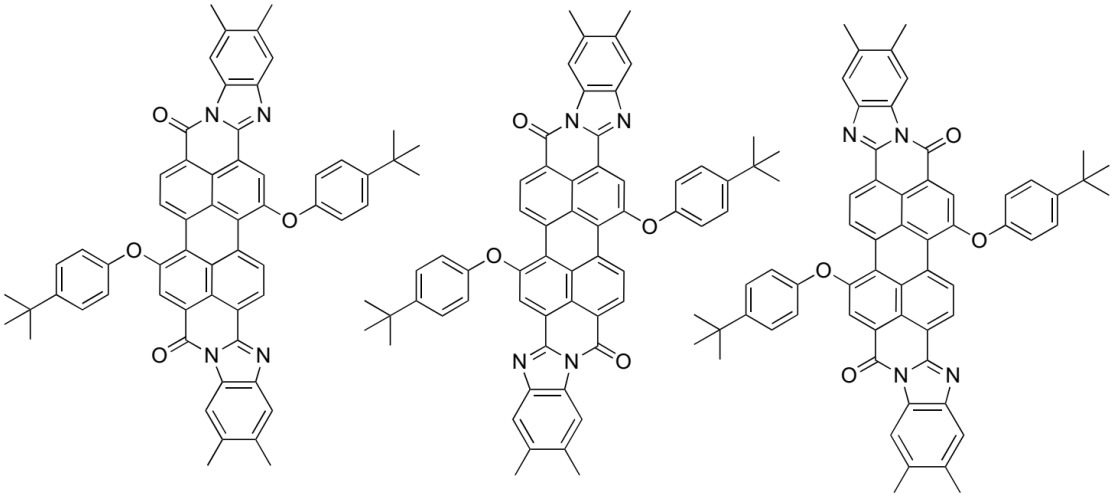

DB-BP-C1 (0.35 g; 0.46 mmol), potassium carbonate (0.38 g; 2.77 mmol) and 4-tert-butyl phenol (0.28 g; 1.85 mmol) was dissolved in 50 mL of NMP. The reaction was heated at 100^{o}C for 1 day. After cooling down to ambient temperature, 1 M HCl (100.00 mL) was added. The crude was obtained by suction filtration. We dried **DTP-BP-C1** at room temperature. The purple powder (87%) was characterized by LC-MS. APCI-LC-MS: *cal.* 889.05 *found* 889 [M].

จุฬาลงกรณ์มหาวิทยาลัย
Chulalongkorn University

Dimethyl-4,4'-(perylene benzimidazole-1,7-diylbis(oxy))dibenzoate containing methyl groups (DAP-BP-C1)

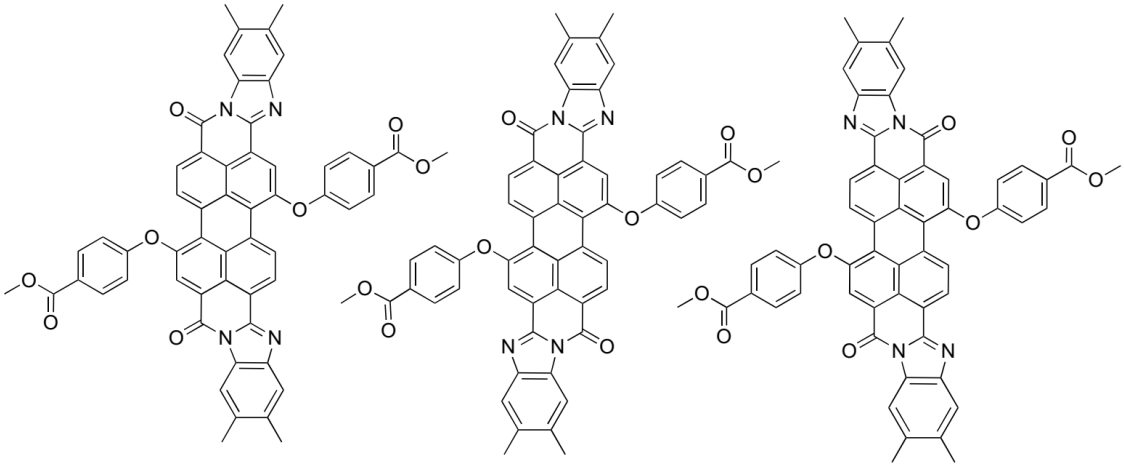

DB-BP-C1 (1.05 g; 1.40 mmol), potassium carbonate (3.10 g; 22.42 mmol) and methyl-4-hydroxy benzoate (1.70 g; 11.21 mmol) was dissolved in 150 ml of NMP. The reaction was heated at 120^{o}C for 2 days. After cooling down to ambient temperature, 1 M HCl (300.00 mL) was added. The crude was obtained by suction filtration. We dried **DAP-BP-C1** at room temperature. The purple powder (98%) was characterized by LC-MS. The characterization will be explained in results and discussion.

1,7-diphenoxy-perylene benzimidazole containing methyl groups (DP-BP-C1)

จุฬาลงกรณ์มหาวิทยาลัย
Chulalongkorn University

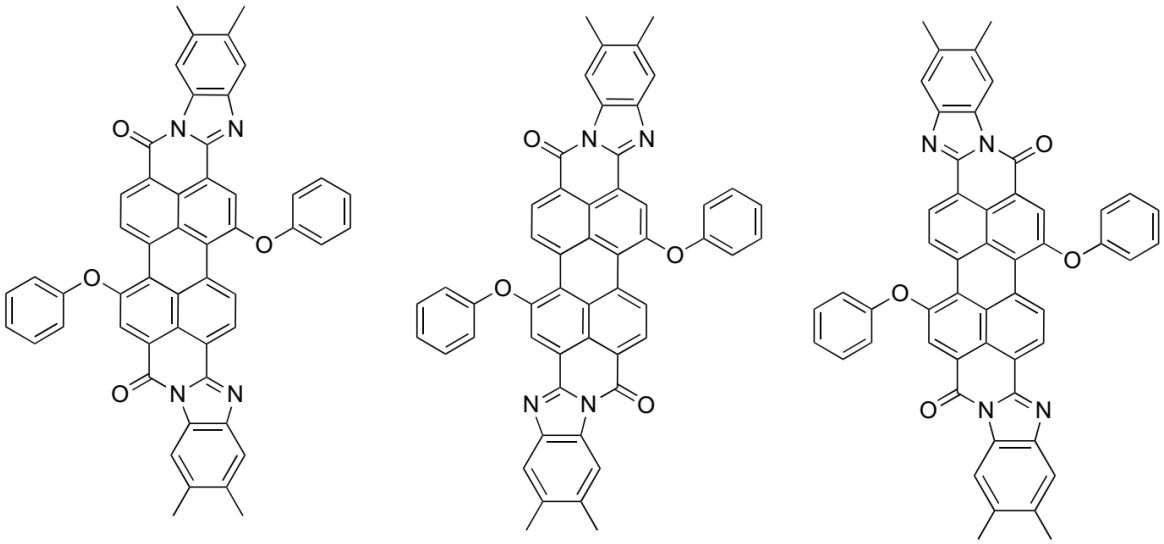

DB-BP-C1 (1.01 g; 1.35 mmol), potassium carbonate (2.98 g; 21.54 mmol) and phenol (1.01 g; 10.77 mmol) was dissolved in 150 mL of NMP. The reaction was heated at 120^{o}C for 2 days. After cooling down to ambient temperature, 1 M HCl (300.00 mL) was added. The crude was obtained by suction filtration with washing by water. We dried **DP-BP-C1** at room temperature. The purple powder (quantitative yield) was characterized by LC-MS. APCI-LC-MS: *cal*. 776.83 *found* 777 [M].

6,13-dihydro-5*H*-benzo[*i*]benzo[6,7]indolo[2,3-*a*]benzo[6,7]indolo[2,3-*c*]carbazole (A-BTT) and 12,19-dihydro-5*H*-benzo[*i*]benzo[6,7]indolo[3,2-*a*]benzo[6,7]indolo[3,2-*c*]carbazole (S-BTT)

จุฬาลงกรณ์มหาวิทยาลัย
Chulalongkorn University

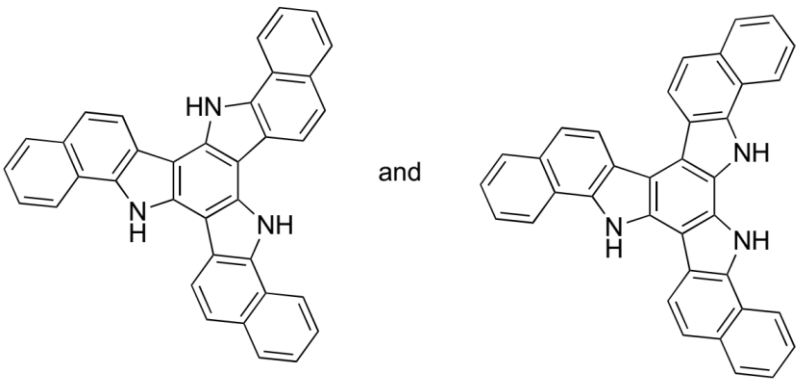

S-BTT and **A-BTT**

The procedure in literature was modified [68]. Benzo[g]indole (0.30 g; 1.80 mmol) was dissolved in acetonitrile (4.20 mL; approx. 0.43 M). *N*-bromosuccinimide (0.64 g; 3.61 mmol) was gradually added in solution in 15 minutes. After that, the reaction solution was stirred at room temperature for 3 hours. The dark green suspension was filtrated. The solid crude was washed with acetonitrile. The green powder was obtained which was used in the next step without purification.

The green powder was dispersed in methanol (9.02 mL; approx. 0.2 M). Triethylamine (3.27 ml; 23.44 mmol) and formic acid (0.88 mL; 23.44 mmol) were slowly dropped in reaction, respectively. While the reaction was heating at 65°C, 10% palladium on activated carbon (0.02 g; 0.18 mmol) was added. The reaction was refluxed for 30 minutes. The hot solution was filtrated with Celite and washed with dichloromethane (100 mL). The organic phase was washed with 1 M hydrochloric acid. The anhydrous sodium sulfate was added for drying. The crude was evaporated via evaporator. In order to purify symmetric and asymmetric benzo triazatruxene, column chromathography was carried out with mobile phase (hexane: ethyl acetate; 4:1) to give dark green solid of symmetrical product (R_f = 0.45; 5%) and black solid of asymmetrical product (R_f = 0.25; 7%). For **A-BTT**, ^{1}H NMR ([D_6]-DMSO, 400 MHz): δ = 12.39 (s, 1H, N_{arom}-H), 12.34 (s, 1H, N_{arom}-H), 12.22 (s, 1H, N_{arom}-H), 9.31 (d, *J* = 8.7 Hz, 1H, aromatic H), 9.18 (d, *J* = 8.2 Hz, 1H, aromatic H), 9.01 (dd, *J* = 8.8, 4.6 Hz, 2H, aromatic H), 8.53 (t, *J* = 7.7 Hz, 2H, aromatic H), 8.20 – 8.11 (m, 3H, aromatic H), 7.90 (dd, *J* = 14.0, 8.7 Hz, 3H, aromatic H), 7.76 (dt, *J* = 15.0, 7.3 Hz, 3H, aromatic H), 7.60 (dt, *J* = 21.8, 7.2 Hz, 3H, aromatic H) ppm and ^{13}C NMR ([D_6]-DMSO, 400 MHz): δ = 133.6, 133.2, 133.1, 130.8, 130.6, 130.4, 130.1, 128.7, 128.5, 128.5, 128.2, 125.8, 125.0, 124.9, 124.82, 124.76, 124.1, 122.4, 122.1, 121.9, 121.8, 121.6, 121.42, 121.39, 121.2, 120.8, 119.59, 119.57, 119.4, 118.6, 118.5, 117.7, 113.9, 110.2, 107.0, 103.6 ppm and MALDI-TOF MS (*m/z*): calc.: (495.17 [$C_{36}H_{21}N_3$]); found: (494.620 [M^+]). For **S-BTT**, ^{1}H NMR ([D_6]-DMSO, 400 MHz): δ = 12.26 (s, 1H, N_{arom}-H), 9.28 (d, *J* = 8.6 Hz, 1H, aromatic H), 9.17 (d, *J* = 8.4 Hz, 1H, aromatic H), 8.14 (d, *J* = 8.1 Hz, 1H, aromatic H), 7.91 (d, *J* = 8.6 Hz, 1H, aromatic H), 7.73 (t, *J* = 7.5 Hz, 1H, aromatic H), 7.58 (t, *J* = 7.4 Hz, 1H, aromatic H) ppm, ^{13}C NMR ([D_6]-DMSO, 400 MHz): δ = 133.0, 131.8,

จุฬาลงกรณ์มหาวิทยาลัย
Chulalongkorn University

130.4, 128.4, 125.1, 124.1, 122.4, 121.6, 120.9, 119.7, 117.7, 103.6 ppm and MALDI-TOF MS (*m/z*): calc.: (495.17 [$C_{36}H_{21}N_3$]); found: (494.731 [M^+]).

5,6,13-trihexyl-6,13-dihydro-5H-benzo[i]benzo[6,7]indolo[2,3-a]benzo[6,7]indolo[2,3-c]carbazole (A-BTT-C6)

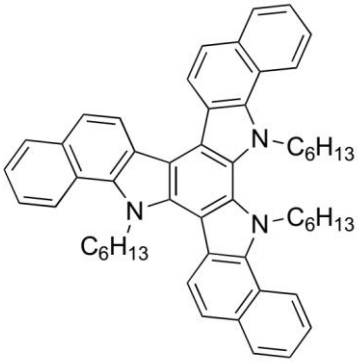

A-BTT-C6

To prepare alkylated compound, **A-BTT** (0.03 g; 0.06 mmol) and potassium hydroxide (0.06 g; 1.16 mmol) was added in DMF (0.33 mL). After that, the solution was stirred for 30 minutes; and then, 1-bromohexane (0.04 mL; 0.32 mmol) was added and stirred overnight. Next, reaction mixture was poured in water. The suspension was extracted by ethyl acetate and dried by anhydrous sodium sulfate. The organic phase was evaporated to obtain as crude which was purified by column chromathography (hexane:ethyl acetate; 1:19). The light green solid was obtained (90%). ^{1}H NMR ($CDCl_3$, 400 MHz,): δ = 9.14 (d, *J* = 8.7 Hz, 1H, aromatic H), 9.07 (d, *J* = 8.6 Hz, 1H, aromatic H), 8.74 – 8.67 (m, *J* = 5.9 Hz, 3H, aromatic H), 8.66 (d, *J* = 8.6 Hz, 1H, aromatic H), 8.13 (d, *J* = 4.9 Hz, 3H, aromatic H), 7.94 (t, *J* = 7.1 Hz, 3H, aromatic H), 7.72 (dd, *J* = 14.9, 7.8 Hz, 3H, aromatic H), 7.59 (dt, *J* = 13.8, 7.0 Hz, 3H, aromatic H), 5.40 – 5.17 (m, 6H), 1.36 – 1.11 (m, 5H), 0.77 (d, *J* = 2.3 Hz, 7H), 0.70 (dd, *J* = 8.7, 5.2 Hz, 5H), 0.65 (d, *J* = 6.2 Hz, 4H), 0.59 – 0.51 (m, 2H), 0.47 (d, *J* = 3.5 Hz, 6H), 0.41 (d, *J* = 6.2 Hz, 4H). ^{13}C NMR ($CDCl_3$, 400 MHz): δ = 129.2, 129.1, 125.6, 125.5, 124.6, 124.5, 124.1, 122.3, 122.1, 52.6, 52.3, 51.0, 30.9, 30.7, 30.3, 29.7, 27.6, 26.0,

25.9, 25.8, 22.1, 22.0, 21.2, 13.5 ppm and MALDI-TOF MS (*m/z*): calc.: (747.46 [$C_{54}H_{57}N_3$]); found: (747.801 [M^+]).

5,12,19-trihexyl-12,19-dihydro-5*H*-benzo[*i*]benzo[6,7]indolo[3,2-*a*]benzo[6,7]indolo[3,2-*c*]carbazole (S-BTT-C6)

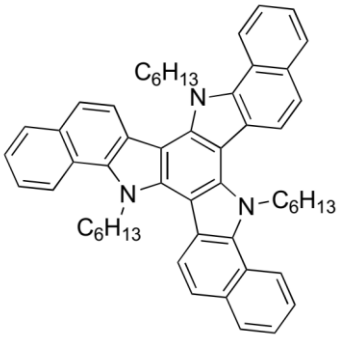

S-BTT-C6

To prepare alkylated compound, **S-BTT** (0.04 g; 0.08 mmol) and potassium hydroxide (0.09 g; 1.61 mmol) was added in DMF (0.50 mL). After that, the solution was stirred for 30 minutes; and then, 1-bromohexane (0.07 mL; 0.48 mmol) was added and stirred overnight. Next, reaction mixture was poured in water. The suspension was extracted by ethyl acetate and dried by anhydrous sodium sulfate. The organic phase was evaporated to obtain as crude which was purified by column chromathography (hexane:ethyl acetate; 1:19). The light green solid was obtained (41%).^{1}H NMR ($CDCl_3$, 400 MHz,): δ = 8.67 (d, *J* = 8.4 Hz, 3H, aromatic H), 8.58 (d, *J* = 8.7 Hz, 3H, aromatic H), 8.09 (d, *J* = 7.7 Hz, 3H, aromatic H), 7.88 (d, *J* = 8.6 Hz, 3H, aromatic H), 7.72 – 7.67 (m, 3H, aromatic H), 7.55 (t, *J* = 7.1 Hz, 3H, aromatic H), 5.36 (t, *J* = 7.1 Hz, 6H), 1.33 – 1.28 (m, 6H), 0.73 (dd, *J* = 7.9, 4.3 Hz, 12H), 0.61 – 0.55 (m, 6H), 0.44 (t, *J* = 6.9 Hz, 9H). ^{13}C NMR ($CDCl_3$, 400 MHz): δ = 131.5, 129.1, 125.6, 124.1, 122.4, 122.0, 121.5, 52.43, 37.1, 31.4, 30.8, 30.2, 30.0, 29.7, 28.6, 25.8, 21.9, 13.5 ppm and MALDI-TOF MS (*m/z*): calc.: (747.46 [$C_{54}H_{57}N_3$]); found: (748.030 [M^+]).

จุฬาลงกรณ์มหาวิทยาลัย
Chulalongkorn University

***N*-ethyl benzo[g]indole**

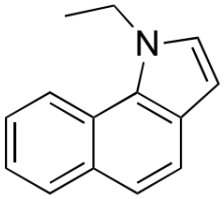

Benzo[g]indole (0.40 g; 2.39 mmol) and potassium hydroxide (0.40 g; 7.16 mmol) was mixed in DMF (2.50 mL). To synthesized alkylated product, 1-bromoethane (0.36 mL; 4.77 mmol) was dropped and stirred at room temperature for 4 hours. The crude was diluted with ethyl acetate (100 mL) and washed with water. Next, it was dried over anhydrous sodium sulfate. Evaporated organic phase was kept as crude which was purified by column chormathography (hexane: ethyl acetate; 9:1). The clear colorless solution was achieved (86%). DI-GC-MS: *cal*. 195.26 *found* 195 [M].

***N, N, N*-triethyl-benzotriazatruxene (S-BTT-C2) via *N*-ethyl benzo[g]indole**

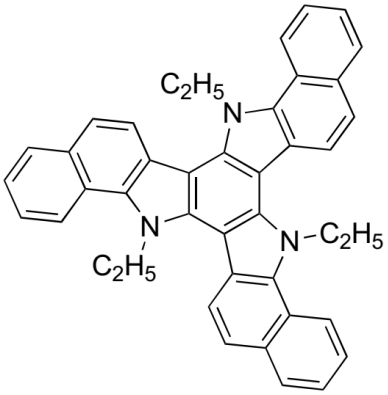

N-ethyl benzo[g]indole (0.40 g; 2.05 mmol) was dissolved in acetonitrile (4.78 mL; approx. 0.43 M). *N*-bromosuccinimide (0.73 g; 4.11 mmol) was gradually added in solution in 15 minutes. After that, the reaction solution was stirred at room temperature for 3 hours. The dark green suspension was filtrated. The solid crude was washed with acetonitrile. The green powder was obtained which was used in the next step without purification.

The green powder was dispersed in methanol (10.27 mL; approx. 0.2 M). Triethylamine (3.73 mL; 26.70 mmol) and formic acid (1.01 mL; 26.70 mmol) were slowly dropped in reaction, respectively. While the reaction was heating at 65^{o}C, 10%

palladium on activated carbon (0.02 g; 0.20 mmol) was added. The reaction was refluxed for 30 minutes. The hot solution was filtrated with Celite and washed with dichloromethane (100 mL). The organic phase was washed with 1 M hydrochloric acid. The anhydrous sodium sulfate was added for drying. The crude was evaporated via the evaporator. In order to purify, column chromatography was carried out with mobile phase (hexane: dichloromethane; 3:1) to give yellow solid of symmetric product (1%).

_N_-hexyl benzo[g]indole

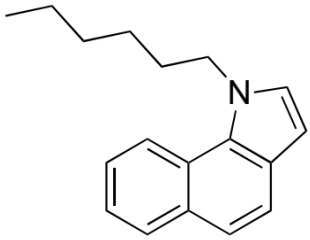

Benzo[g]indole (0.31 g; 1.83 mmol) and potassium hydroxide (0.31 g; 5.49 mmol) was mixed in DMF (2.00 mL). To synthesized alkylated product, 1-bromohexane (0.51 mL; 3.66 mmol) was dropped and stirred at room temperature for 4 hours. The crude was diluted with ethyl acetate (100 mL) and washed with water. Next, it was dried over anhydrous sodium sulfate. Evaporated organic phase was kept as crude which was purified by column chormathography (hexane: ethyl acetate; 10:1). The clear colorless solution was achieved (88%). DI-GC-MS: *cal*. 251.37 *found* 251 [M].

จุฬาลงกรณ์มหาวิทยาลัย
CHULALONGKORN UNIVERSITY

_N, N, N_-trihexyl-benzotriazatruxene (S-BTT-C6) via _N_-hexyl benzo[g]indole

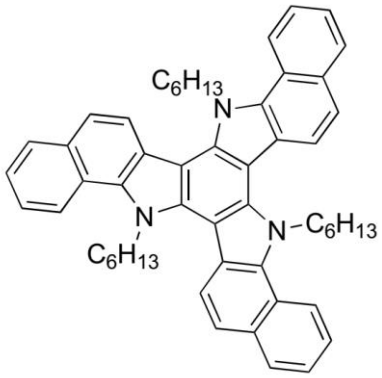

N-hexyl benzo[g]indole (0.30 g; 1.18 mmol) was dissolved in acetonitrile (2.75 mL; approx. 0.43 M). *N*-bromosuccinimide (0.42 g; 2.36 mmol) was gradually added in solution in 15 minutes. After that, the reaction solution was stirred at room temperature for 3 hours. The dark green solution was evaporated. The crude was diluted with dichloromethane and extracted with 1 M sodium thiosulfate. The green solution was dried over anhydrous sodium sulfate which was used in the next step without purification.

The green solution was dispersed in methanol (5.91 mL; approx. 0.2 M). Triethylamine (2.14 mL; 15.37 mmol) and formic acid (0.58 mL; 15.37 mmol) were slowly dropped in reaction, respectively. While the reaction was heating at 65^{o}C, 10% palladium on activated carbon (0.01 g; 0.12 mmol) was added. The reaction was refluxed for 30 minutes. The hot solution was filtrated with Celite and washed with dichloromethane (100 mL). The organic phase was washed with 1 M hydrochloric acid. The anhydrous sodium sulfate was added for drying. The crude was evaporated via evaporator. The yellow oil was received. The characterization will be explained in results and discussion.

2.3. OFET evaluation

2.3.1. OFET fabrication

จุฬาลงกรณ์มหาวิทยาลัย
Chulalongkorn University

For spin coating process, each synthesized compound (1 mg) was dissolved in toluene containing 1% THF (1 mL). After sonication, the solution was spin coated on a SiO_2/Si substrate with the rate of 1500 rpm. Next, the coated substrate was heated for annealing under argon atmosphere. All spin-coated devices were prepared in this manner. (**Figure 2.24**)

Drop cast film was prepared in a similar manner. After sonication, the solution was dropped and dried at room temperature on bare SiO_2/Si. The annealing process was conducted under argon atmosphere.

In order to coat the compound by evaporation process, substrates were loaded in the vacuum chamber. At 10^{-6} Torr, the compound tube was heated and deposited on the SiO_2/Si substrates. The annealing was again conducted to facilitate the charge

transfer process.

2.3.2. OFET performance investigation

The mobility (μ) was obtained from drain current (I_d) and gate voltage (V_g) plots. First, the normalized conductivity (σ) can be calculated by drain current, electrode gap length (L) and width of the electrode (W; 0.1 cm) using this equation:

$$\sigma = I_d * \frac{L}{W} \quad \text{(eq. 1)}$$

After plotting of conductivity dependence on the gate voltage, the mobility in linear regime is given by,

$$\mu = \frac{d}{\varepsilon_0 \varepsilon'} * \frac{d\sigma}{dV_g} \quad \text{(eq. 2)}$$

The mobility can be also calculated in saturation regime if the I_d-V_d plot shows saturation regime. The mobility is given by,

$$\mu = \frac{d}{\varepsilon_0 \varepsilon'} * 2 * \frac{L}{W} * \left(\frac{dI_d^{1/2}}{dV_g}\right)^2 \quad \text{(eq. 3)}$$

where d is the thickness of SiO_2 insulating layer (300 nm), ε_0 is vacuum permittivity of electric constant (8.85×10^{-12} F/m) and ε is relative permittivity of SiO_2 (3.9).

จุฬาลงกรณ์มหาวิทยาลัย
Chulalongkorn University

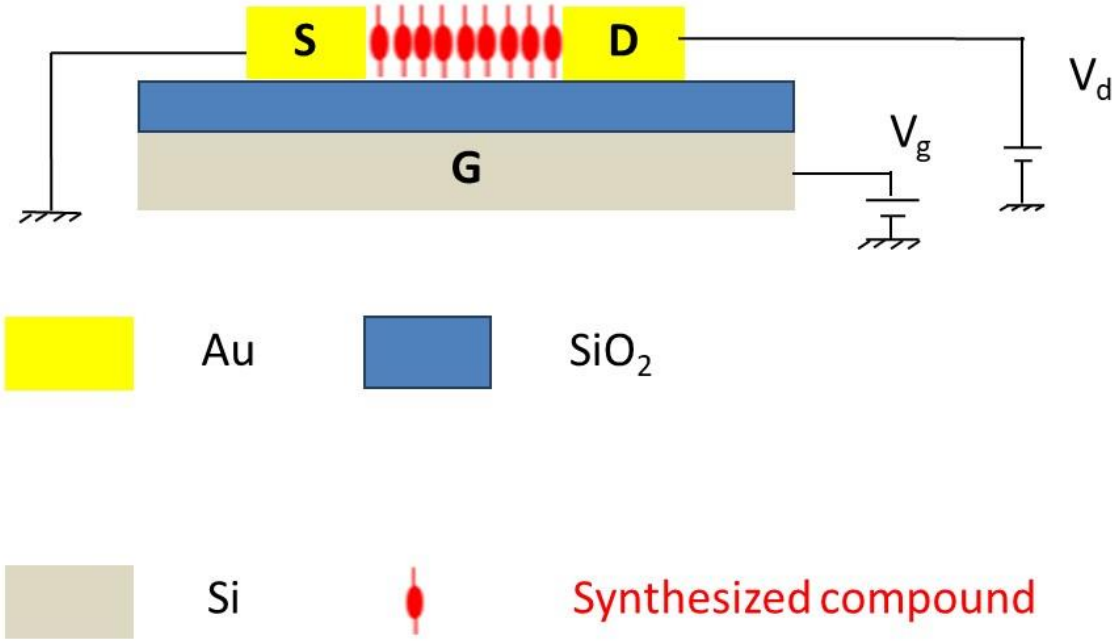

Figure 2.24 *Device scheme for OFET investigation*

2.4. OLED evaluation

2.4.1. OLED fabrication

จุฬาลงกรณ์มหาวิทยาลัย
Chulalongkorn University

To clean a substrate, ultrasonic treatment in detergent was conducted with an indium tin oxide (ITO) glass substrate (purchased from Kintec Company); and then, the substrate was washed in deionized water and acetone, respectively. After that, the substrate was dried at 100^{o}C in a vacuum oven. A 40 nm of PEDOT: PSS hole injection layer was spin-coated on top of patterned ITO substrate with the rate of 5000 rpm for 30 s and dried at 100^{o}C for 15 min under vacuum. Next, all HTL film was coated on top of PEDOT: PSS layer by spin-coating $CHCl_3$: toluene (2:1) solution of our synthesized compounds (2% w/v) with the rate of 2500 rpm for 30 s and dried at 120^{o}C for 15 min at ambient condition. Then spin-coated substrate was placed into vacuum evaporator (Mini-SPECTROS 100 from Kurt J. Lesker company) under based pressure around 10^{-6} mbar. The emitting layer (EML) and electron transporting layer (ETL) were

deposited from alumina crucibles with the rate of 0.5-1.0 nm s^{-1}. Alq_3 was used as emitting layer (EML) and electron transporting layer (ETL) for hole transporting efficiency investigation. Last, a 0.5 nm thick LiF and a 95 nm thick aluminium layer was deposited to be acted as the cathode. The thickness of LiF, aluminium and Alq_3 layers were monitored and recorded by quartz oscillator thickness meter.

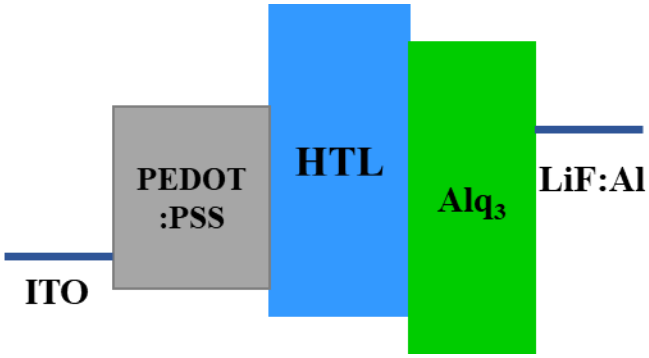

Figure 2.25 *Illustration of our fabricated devices*

2.4.2. OLED performance investigation

The device performance was conducted under M. E. Thomson's protocol. Calculated external quantum efficiencies were reported to evaluate device performance. Current density-voltage-luminescence (*J-V-L*) characteristics were carried out with source meter (Keithley 2400) and power meter (Newport 1835C) which equipped with calibrated silicon photodiode (Newport 818-UV/CM). The EL spectra were obtained by multichannel spectrometer (Ocean Optics USB4000). All measurements were undertaken under ambient condition at room temperature.

All device measurements were conducted in an OLED closed box at room temperature. When we applied voltage, the record of currents, brightness and EL spectra were obtained at the same time to provide the current density–voltage–luminance (*J-V-L*) characteristics and EL spectra. The turn-on voltage was defined at the brightness of 1 cd/m^2. The current density was calculated as the following formula (1):

$$J = \frac{I}{A} \qquad (1)$$

which I (mA) is the current and A (cm^2) is the pixel active area of the device. The luminous efficiency of the device was calculated as the following formula (2):

$$\eta_{lum} = \frac{L}{J} \quad (2)$$

which, L (cd/m^2) is the luminance and J (mA/cm^2) is the current density.

The quantum efficiency of a device can be categorized into two categories; internal and external quantum efficiencies.

Internal quantum efficiency (IQE) The total number of generated photons inside the device per electron-hole pair injected into the device was shown in this value. It is represented by η_{int}. Regard to OLEDs, the internal quantum efficiency in the case of fluorescent materials is given by (OIDA 2002)

$$\eta_{int} = \gamma\, \eta_s \Phi_f\,, \quad (3)$$

where γ is the fraction of injected charges that produce excitons called the charge balance factor, η_s is the fraction of singlet excitons called singlet exciton efficiency and Φ_f is the fraction of energy which is released from the material as light called the quantum efficiency of fluorescence.

External quantum efficiency (EQE**)** This is defined as the total number of photons emitted from the device per electron-hole pair injected into the device. It is represented by η_{ext}. The external quantum efficiency is related to the internal quantum efficiency and is given by (OIDA 2002)

$$\eta_{ext} = R_e\, \eta_{int}, \quad (4)$$

where R_e is the extraction or outcoupling efficiency representing the number of photons emitted from the device per number of photons generated in the device.

Power Efficiency

The luminous efficacy (power efficiency) is the lumen output per input electrical power. As you can see, The unit is in lumen per watt (lm/W) or candela per ampere (cd/A). It is represented by η_p.

CHAPTER 3
RESULTS AND DISCUSSION

3.1. Synthesis and characterization of benzimidazole perylene derivatives via hydrolysis

First, perylene-3,4,9,10-tetracarboxylic dianhydride was brominated with liquid bromine in concentrated sulfuric acid **(Figure 3.26)**. However, the crude product was poorly soluble in common organic solvent such as chloroform so the NMR characterization could not be performed. The brominated crude product was used without purification in the imidization step with propionic acid. Unlike the brominated product, the imidized product with bromine moieties was easily dissolved in common organic solvents such as chloroform and toluene; after purification, we discovered that the imidized products consisted of 1,7-dibromo-*N,N'*-diphenyl-3,4,9,10-perylenetetracarboxylic diimide **(DB-PTCDI-PH)** and 1,6,7-tribromo-*N,N'*-diphenyl-3,4,9,10-perylenetetracarboxylic diimide **(TB-PTCDI-PH).** The percentage yields of brominated compounds are 28% and 4%, respectively. The ^{1}H-NMR characterization was displayed in **Figure A. 43 and 44**, respectively.

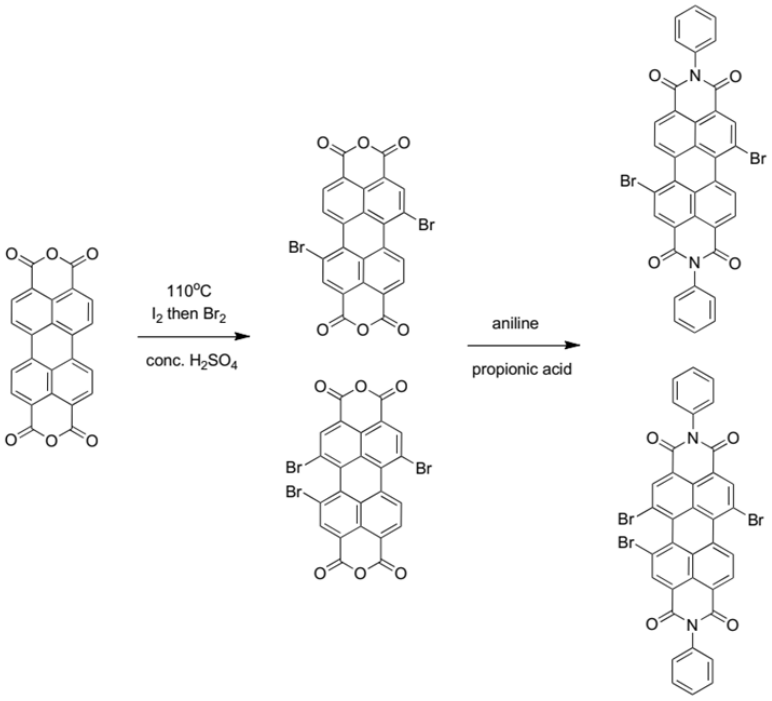

Figure 3.26 *Bromination and imidization of perylene*

To achieve the benzimidazole target molecules, the attempt for nucleophilic substitution reaction was conducted with 4-methoxy phenol in basic condition using

potassium carbonated as a base **(Figure 3.27)**. The ^{1}H-NMR characterization was displayed in **Figure A. 45.** Moreover, the solution color in chloroform was changed into purple; generally, the **DB-PTCDI-PH** solution was orange color. This result thus suggested that the aryloxy groups directly affect the conjugation and electronic property of the molecule. In comparison with **DB-PTCDI-PH,** the singlet proton NMR of perylene core is shifted from 9.00 ppm to 8.25 ppm in **DM-PTCDI-PH,** aryloxy substituted compound. The substituted **(DM-PTCDI-PH)** was successfully obtained (38%).

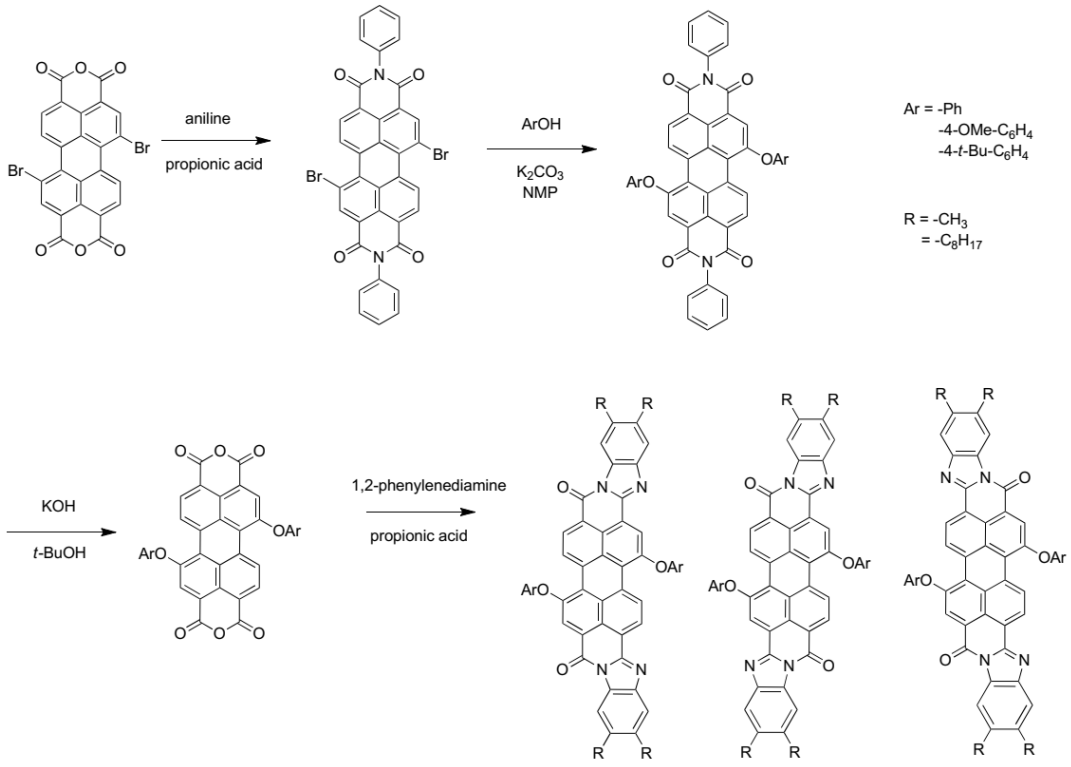

Figure 3.27 *Synthesis strategy of benzimidazole perylene via hydrolysis*

Unfortunately, 1,7-di(4-methoxyphenoxy)-3,4,9,10-perylenetetracarboxylic dianhydride **(DM-PTCDA)** was not obtained via hydrolysis in refluxed tert-butanol **(Figure 3.27)**. The TLC indicated only the unreacted starting material**.** Attempt to use freshly prepared sodium t-butoxide for the reaction also failed to provide the hydrolysis product. Regrettably, **DM-PTCDA** was also not achieved. The synthesis of

benzimidazole perylene derivatives via hydrolysis was not accomplished due to the failure in hydrolysis step.

3.2. Synthesis and characterization of benzimidazole perylene derivatives via brominated perylene benzimidazole

The synthesis of perylene benzimidazole derivatives is described in the experimental part **(Figure 3.28**). A red powder of 1,7-dibromo-perylene-3,4,9,10-tetracarboxylic dianhydride (**DB-PTCDA**) was refluxed in propionic acid with 4,5-dimethyl or 4,5-dioctyl of 1,2-phenylenediamine to obtained dibromo perylene

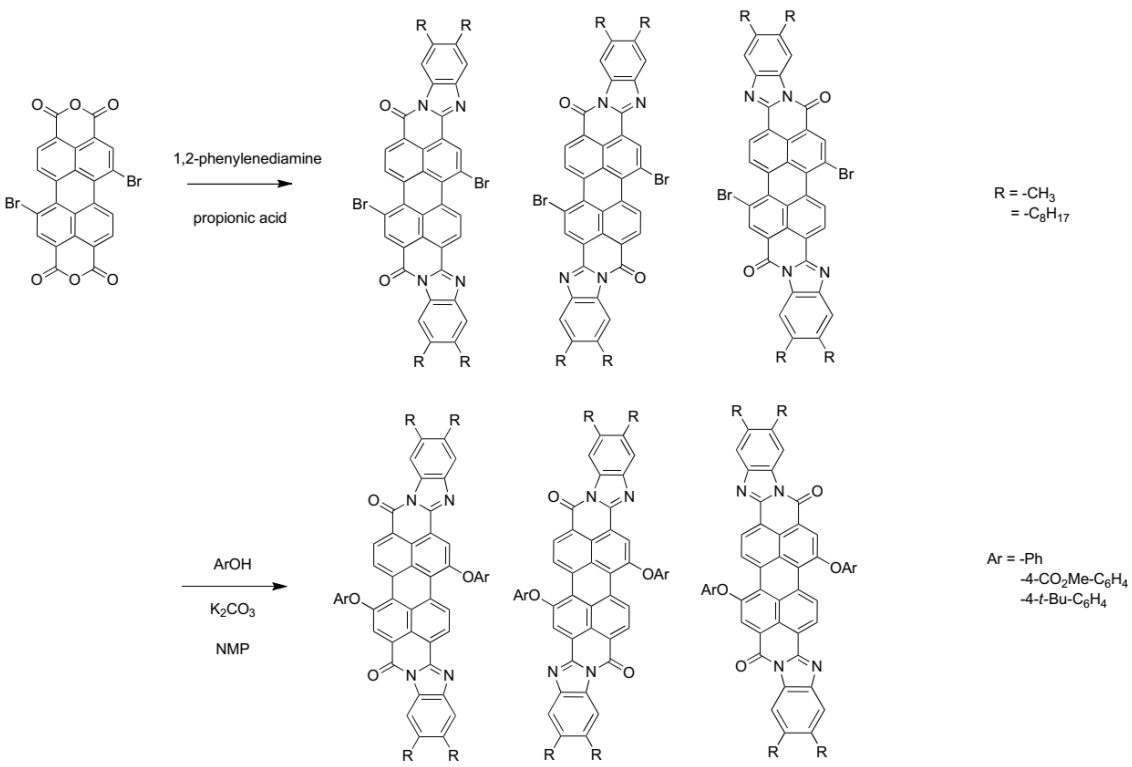

Figure 3.28 *Synthesis of perylene benzimidazole derivatives via brominated perylene benzimidazole*

benzimidazole containing methyl groups and octyl groups. The crude product was changed into purple powder which might be an effect of extension conjugation at N-C-N position in benzimidazole ring.

As a result, the reaction with propionic acid was better since the anhydride

region in FTIR was diminished which again confirmed the success of imidization (**Figure 3.29**). However, there was an obstacle in the purification process as the products were poorly soluble in common organic solvents such as dichloromethane. Although toluene was recommended in pieces of literature to be used as solvent for crystallization; our perylene benzimidazole derivatives were poorly soluble.

จุฬาลงกรณ์มหาวิทยาลัย
Chulalongkorn University

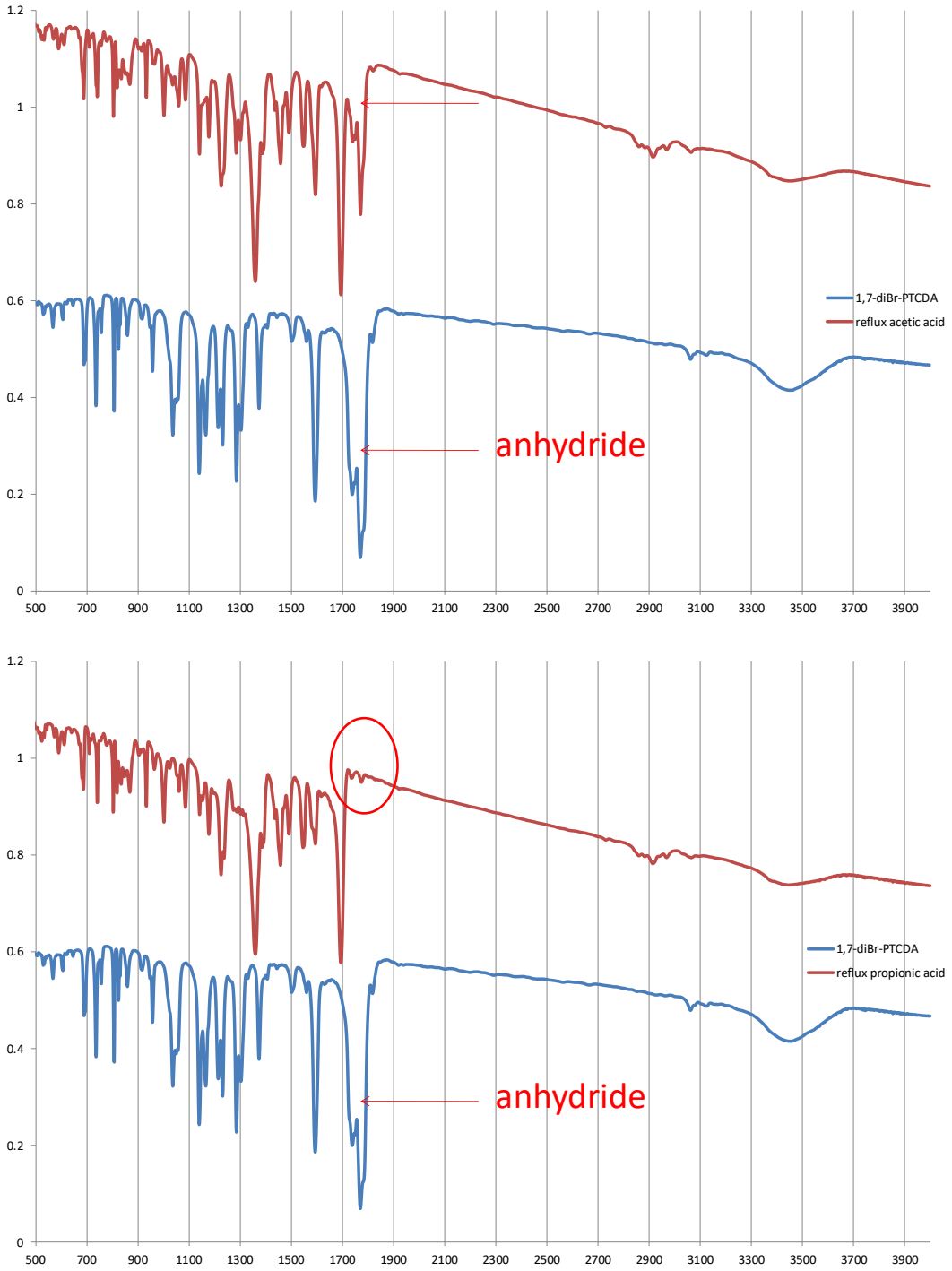

Figure 3.29 *FTIR results (wavenumber (cm-1) and transmittance) of reaction in (top) acetic acid (bottom) propionic acid (red line: product; blue line:* ***PTCDA****)*

Besides, the compounds were miscible in acidic solvent such as trichloroacetic acid in toluene (1:8 v/v). We tried trichloroacetic acid in toluene solution as mobile

phase for TLC. The results seemed that the synthesized dibromo perylene benzimidazole derivatives can move in such condition. After that, the silica on TLC had suddenly broken apart the aluminum substrate. Additionally, the recovery of our compounds in solution seemed to be not successful as the solubility of compounds were poor. Hence, it was hard to purify by column chromatography and crystallization. At last, the 1,7-dibromo perylene benzimidazole containing methyl groups was applied in the next step without purification (**Figure A. 46**).

To establish the target benzimidazole perylene, the variety of phenol was reacted with 1,7-dibromo perylene benzimidazole containing methyl groups in NMP and potassium carbonate. After that, each crude was checked by APCI-LC-MS mass spectrometer (**Figure A. 47-49**). From the results, we found that all synthesized products were favorable outcome.

The author attempted to dissolve the synthesized crude perylenebis-benzimidazole (**Figure 3.30**). Unfortunately, this mixture was highly insoluble in toluene and dichloromethane. The result exhibited that the author has successfully synthesized the target compound, however, the purification could not be conducted by column chromatography with silica gel and alumina gel due to poor solubility. As a result, synthesized perylenebis-benzimidazole cannot be used as an n-type semiconductor for OFET application, especially by solution-deposition fabrication.

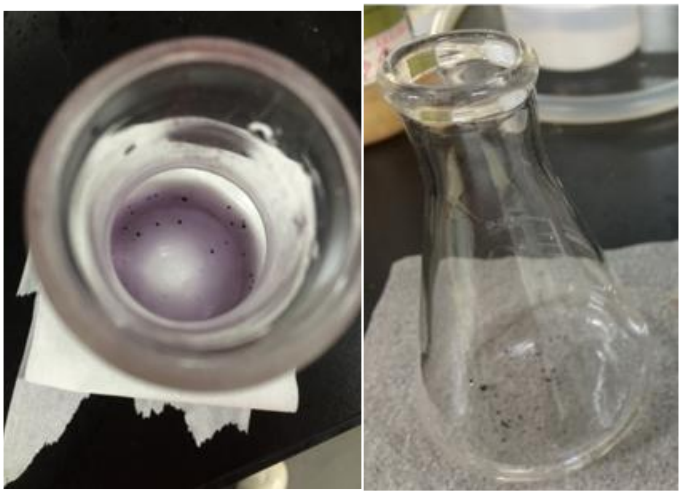

Figure 3.30 *Solubility of synthesized perylene-benzimidazole regioisomers in methylenechloride (left) toluene (right)*

3.3. Synthesis and characterization of benzotriazatruxene derivatives

Synthesis of our four target molecules consisting of **A-BTT, S-BTT, A-BTT-C6** and **S-BTT-C6** were disclosed in this context. To acquire **A-BTT** and **S-BTT,** reaction optimization was explained in Toworakajohnkun and co-workers' report [68]. Regarding the first step, the cyclotrimerization products were generated by *N*-bromosuccinimide (NBS) in acetonitrile as in **Figure 3.31**. This reaction was stirred at room temperature for 3 hours; after that, the precipitated was filtrated and debrominated in the next step without purification by palladium catalyst [69]. Our yield for **A-BTT** and **S-BTT** are 7% and 5%, respectively. The characterization results were shown in **Figure A. 50-55.** These poor yields might be attributed to the addition of NBS procedure and reaction temperature.

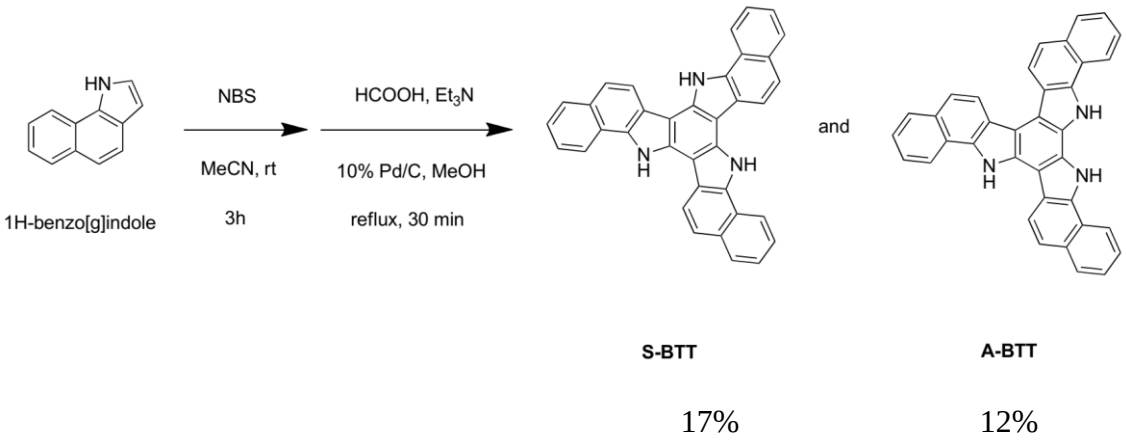

Figure 3.31 *Synthesis of A-BTT and S-BTT*

This cyclotrimerization is exothermic process; it provides the poor yield at low temperature. Our controlled room temperature was 20^{o}C which might be the obstacle for the cyclotrimerization process. Nevertheless, this procedure is conducted with a safer reagent such as NBS; this trimerization conventionally prepared with a toxic reagent such as liquid bromine [70]. **A-BTT** and **S-BTT** have poor solubility in toluene. To increase the solubility, we designed **A-BTT-C6** and **S-BTT-C6** containing hexyl moiety. At first, we produced *N*-hexyl derivatives via cyclotrimerization of 1-ethyl-1*H*-benzo[g]indole (DI-GC-MS in **Figure A. 62**) and 1-hexyl-1*H*-benzo[g]indole (DI-GC-

MS in **Figure A. 2.23**) with NBS (**Figure 3.32**). For ethyl moieties, **S-BTT-C2** was provided but low yield (1%) without asymmetrical product (DI-GC-MS in **Figure A. 63**). According to cyclotrimerization via NBS, benzotriazatruxene containing hexyl group was not afforded; after purification, 33% brominated 1-hexyl-1*H*-benzo[g]indole and 6% of dimer were taken place due to steric repulsion (**Figure A. 65 and 66**).

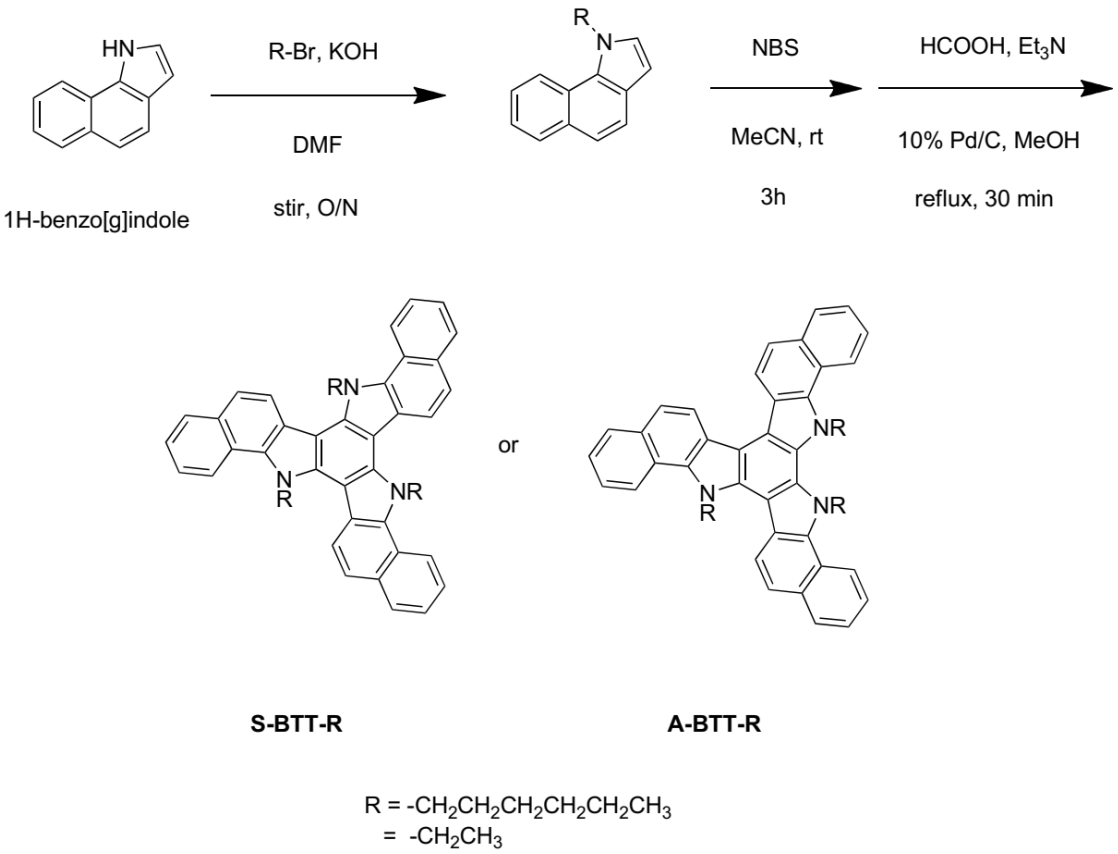

Figure 3.32 *Synthesis of N,N,N-trialkyl benzotriazatruxene via N-alkyl-1H-benzo[g]indole*

A-BTT and **S-BTT** were alkylated with potassium hydroxide and 1-bromohexane to obtain **A-BTT-C6** and **S-BTT-C6** in moderate yields of 90-41% (**Figure 3.33**). The characterization of **A-BTT-C6** and **S-BTT-C6** were displayed in an appendix (**Figure A. 56-61**). The solubility of **A-BTT-C6** and **S-BTT-C6** is better in common organic solvent; for example, their solubilities in toluene are highly soluble. Hexyl groups could show a disorder in the crystal structure. The molecular π-core seems to be twisted to avoid steric repulsion between hexyl and truxene moieties making the solubility better for **A-BTT-C6** and **S-BTT-C6**.

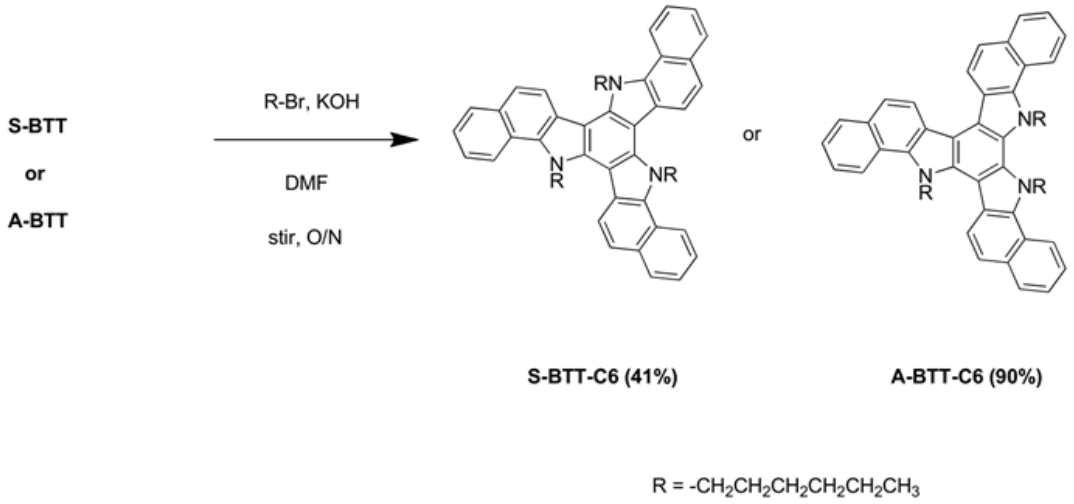

Figure 3.33 *Synthesis of A-BTT-C6 and S-BTT-C6*

3.4. Thermal characterization of benzotriazatruxene derivatives

The Differential Scanning Calorimetry (DSC) was utilized for measuring their glass transition temperature (T_g), melting temperature (T_m), and crystal temperature (T_c). The results show in **Figure 3.34** which obtained from DSC measurements on the second heating cycle with a heating rate of 10°C per minute under ambient atmosphere. **S-BTT-C6** showed excellent thermal stability due to their high pi-stack, hydrophobic interaction and aromaticity. Only benzotriazatruxene without alkyl group **(S-BTT and A-BTT)** did not observe due to their extremely high crystallinity. However, in conclusion of this topic, all our synthesized compounds could be claimed as higher glass transition temperature than TPD (65°C) which have been used as common hole transporting material in OLED application. These thus suggested that the molecules hardly decompose when the compounds are used in high thermal process or long time using.

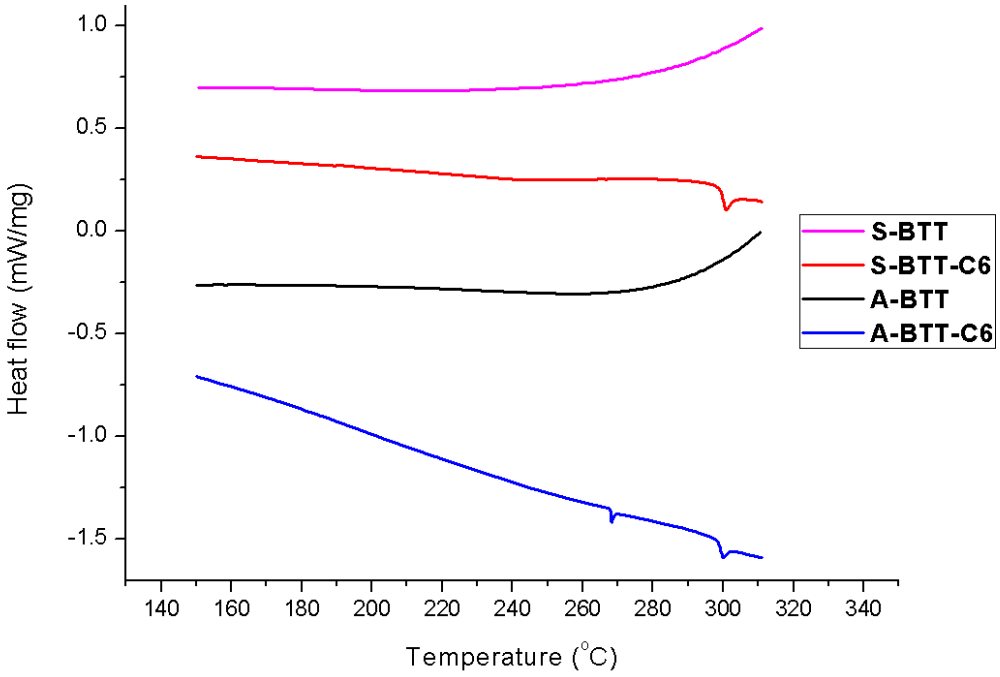

Figure 3.34 *DSC thermograms of A-BTT, S-BTT, A-BTT-C6 and S-BTT-C6*

จุฬาลงกรณ์มหาวิทยาลัย
Chulalongkorn University

3.5. Photophysical properties of benzotriazatruxene derivatives

The photophysical properties of all triazatruxenes were investigated in terms of maximum absorption wavelengths (λ_{max}^{abs}), molar absorption coefficients (log ε) and maximum emission wavelengths (λ_{max}^{em}) in solution. Regarding fluorescent quantum yield (QY), both solution and solid state were conducted to evaluate the emission efficiency and demonstrate the emission as an emissive film. All results were summarized in **Table 3.1**. The absorption and emission spectra of all compounds were exhibited in **Figure 3.35** and **3.36**. In THF solution, the maximum absorption wavelengths of **A-BTT** and **S-BTT** were 330 and 318 nm, respectively. The logarithm molar absorption coefficients of **A-BTT** and **S-BTT** were 3.92 (**Figure A. 67**) and 3.88 (**Figure A. 68**), respectively.

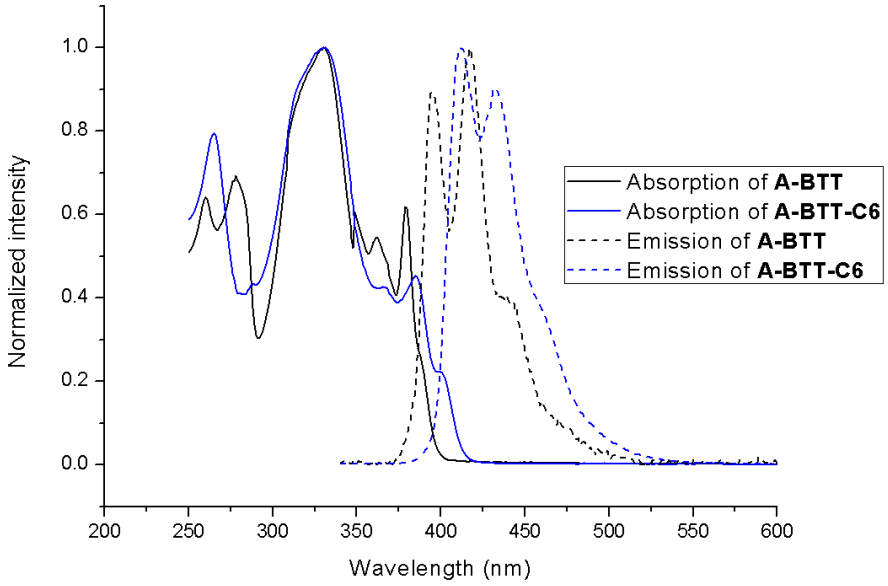

Figure 3.35 *Absorption and emission spectra of A-BTT and A-BTT-C6 in THF*

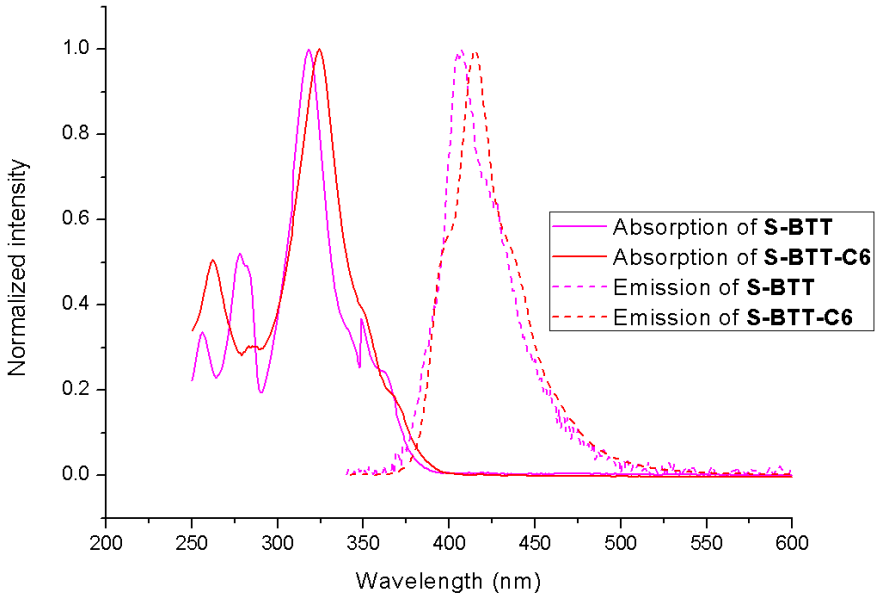

Figure 3.36 *Absorption and emission spectra of S-BTT and S-BTT-C6 in THF*

As regards *N*-hexyl derivatives, the maximum absorption wavelengths of **A-BTT-C6** and **S-BTT-C6** were 331 and 324 nm, respectively. These results were similar to **A-BTT** and **S-BTT**. In other words, the introduction of hexyl moiety slightly affects the electronic states, the energy level of the ground state and excited state, of the compounds. The logarithm molar absorption coefficients (m^{-1} cm^{-1}) of **A-BTT-C6** and **S-BTT-C6** were 4.35 (**Figure A. 69**) and 4.21 (**Figure A. 70**), respectively. For *N*-hexyl derivatives, the decreasing of crystallinity could occur and result in the enhancement of molar absorption coefficients directly associated with the self-quenching effect. For emission, the similar maximum emission wavelengths within the range of 407-417 nm. This small bathochromic shift compared to symmetric benzotriazatruxenes (**S-BTT** and **S-BTT-C6**) in both asymmetric benzotriazatruxenes (**A-BTT** and **A-BTT-C6**) affected by small radiative decay from their locally excited states.

From the fluorescent quantum yield in solution phase, the decoration of hexyl moieties in both symmetric and asymmetric benzotriazatruxenes influenced the emission efficiencies; for example, the quantum yield of **S-BTT-C6** is 13.5% (**Figure A. 74**) while that of **S-BTT** is 3.2% (**Figure A. 72**). We thus believe that the -NH group is highly responsive for these observed results since the hexyl group is inert moiety for inter- and intramolecular interaction such as hydrogen bonding and protonation. In addition, the decreasing of crystallinity, relating to self-quenching absorption, might be the reason for ameliorated emission efficiencies by mean of hexyl moiety. The **A-BTT-C6** solution especially emitted the highest quantum yield (QY = 20.1%; **Figure A. 73**) over **S-BTT-C6** (QY = 13.5%). According to vibrational and rotational relaxation, **S-BTT-C6** containing C_3-symmetric point group might be attributed to the larger rotational relaxation. In comparison with asymmetric triazatruxene containing hexyl group (**A-BTT-C6**), the less relaxation might be the reason for higher emission efficiency; moreover, asymmetric nature pattern might exhibit increasing of the reflection at the edge [71] and light-extraction efficiency (LEE) [72, 73]. For thin film, all emission films were totally diminished because the bond rotation and molecular relaxation were restricted in the solid state. Consequently, we firstly planned to fabricate this compound as an emissive layer (EML); as the previous mention, all compounds were not able to fabricate as EML.

จุฬาลงกรณ์มหาวิทยาลัย
Chulalongkorn University

Table 3.1 *Photophysical and electrochemical properties of A-BTT, S-BTT, A-BTT-C6 and S-BTT-C6*

Cpd	λ_{max}^{abs} [nm] (log ε [M^{-1} cm^{-1}])	λ_{max}^{em} [nm]	QY[c] (%)		*Exp.* E_g[d] (eV)	*Cal.* E_g[e] (eV)	HOMO (eV)[e]	LUMO (eV)[e]
	Solution[a]	Solution[b]	Solution	Film				
A-BTT	330 (3.92)	417	1.0	0.0	3.10	3.79	-4.84	-1.04
S-BTT	318 (3.88)	407	3.2	0.0	3.18	3.99	-4.88	-0.88
A-BTT-C6	331 (4.35)	411	20.1	0.7	2.99	3.67	-4.83	-1.16
S-BTT-C6	324 (4.21)	415	13.5	0.0	3.14	3.90	-4.83	-0.93

[a]measured in THF. [b]measured in THF and excited at 330 nm. [c]Absolute quantum yield. [d]estimated from the onset of the absorption spectra ($E_g = 1240/\lambda_{onset}$) in eV. [e]optimized using B3LYP/6-31G(d,p) modeled by Polarizable Continuum Model (PCM) method using GAUSSIAN09 by Dr. Supawadee Namuangruk (NANOTEC, Thailand).

3.6. FET properties of benzotriazatruxene derivatives

Each benzotriazatruxene derivatives was dissolved in 1% THF-containing toluene and the solution was used for spin coating and drop casting, solution-deposition process. After annealing for 1 hour, DFM (Dynamic force microscope) image of benzotriazatruxene derivatives displayed rough surface textures partially containing three-dimensional islands. All results are summarized in **Table 3.2** The mobility values were extremely low or could not be obtained. Generally, annealing and substrate modified with SAM (self-assembled monolayer) are known to be improved in terms of

mobility and surface roughness; however, the situation could not be improved. All measurements showed the same result; for instance, the relationship between drain current (I_d) and gate voltage (V_g) of spin-coated **S-BTT-C6** film with annealing was presented at 10 μm gap in **Figure 3.37**. Especially, **S-BTT-C6** devices were fabricated with and without annealing at 1500 rpm and 4500 rpm; in addition, devices with drop casting method, performed with **S-BTT-C6**, showed no FET behavior.

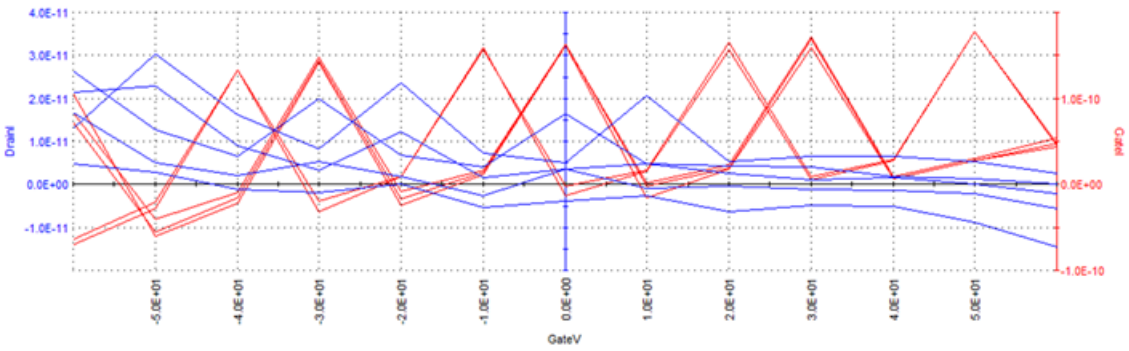

Figure 3.37 *Example of failed result (I_d-V_g characteristic) such as from spin-coated S-BTT-C6*

จุฬาลงกรณ์มหาวิทยาลัย
Chulalongkorn University

Table 3.2 *Annealing temperature for 1 hour and SAM effect on DFM image of benzotriazatruxene films via the solution-deposition process (thickness is below the image)*

Method	Compound	Annealing	DFM	FET

Spin 1500 rpm on bare substrate	**A-BTT**	-	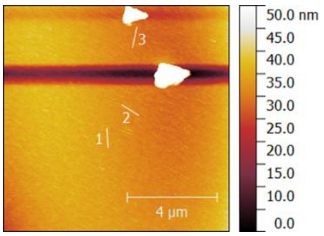 1.0-2.0 nm	No conductivity
Spin 1500 rpm on bare substrate	**A-BTT**	60°C	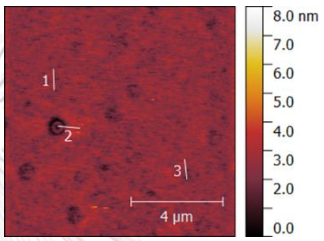 1.0-2.0 nm	No conductivity
Spin 1500 rpm on bare substrate	**A-BTT**	90°C	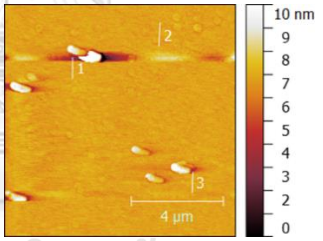 3.0-4.0 nm	No conductivity
Spin 1500 rpm on bare substrate	**A-BTT**	120°C	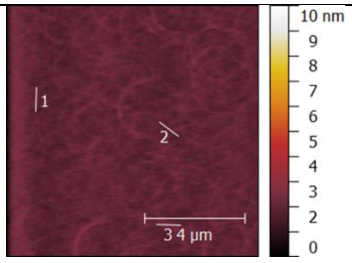 0.6-0.8 nm	No conductivity

จุฬาลงกรณ์มหาวิทยาลัย
Chulalongkorn University

Spin 1500 rpm on bare substrate	**S-BTT**	-	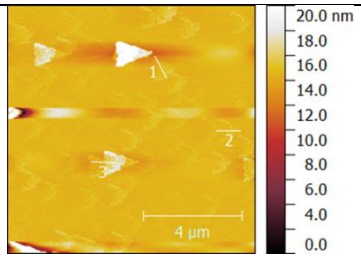 2.0-3.0 nm	No conductivity
Spin 1500 rpm on bare substrate	**S-BTT**	60°C	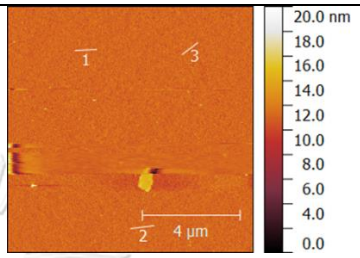 1.0 nm	No conductivity
Spin 1500 rpm on bare substrate	**S-BTT**	90°C	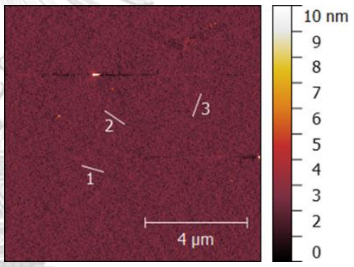 1.0-1.5 nm	No conductivity
Spin 1500 rpm on bare substrate	**S-BTT**	120°C	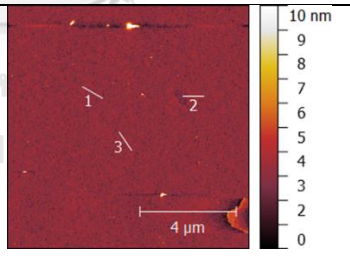 1.0-1.5 nm	No conductivity
Spin 4500 rpm on bare substrate	**S-BTT**	-	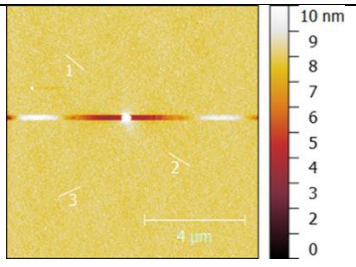 0.5-1.0 nm	No conductivity

จุฬาลงกรณ์มหาวิทยาลัย
Chulalongkorn University

Spin 4500 rpm on bare substrate	**S-BTT**	60ºC	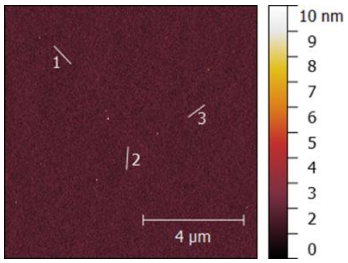 0.2-0.8 nm	No conductivity
Spin 4500 rpm on bare substrate	**S-BTT**	90ºC	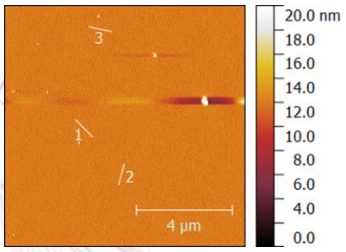 0.2-1.0 nm	No conductivity
Spin 4500 rpm on bare substrate	**S-BTT**	120ºC	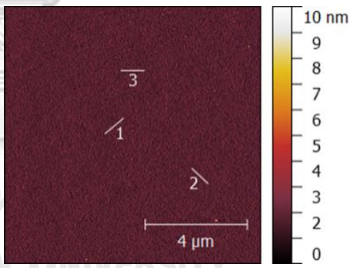 0.5-1.0 nm	No conductivity
Spin 1500 rpm on SAM substrate	**S-BTT**	-	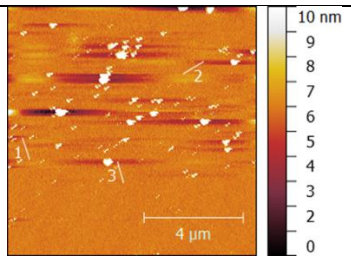 0.2-2.0 nm	No conductivity

จุฬาลงกรณ์มหาวิทยาลัย
Chulalongkorn University

Spin 1500 rpm on SAM substrate	**S-BTT**	60ºC	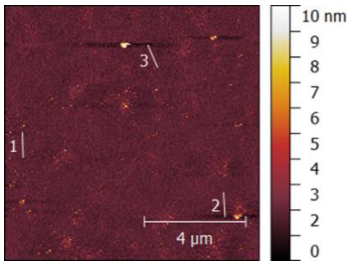 0.5-1.0 nm	No conductivity
Spin 1500 rpm on SAM substrate	**S-BTT**	90ºC	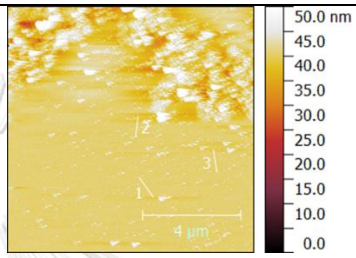 1.0-3.0 nm	No conductivity
Spin 1500 rpm on SAM substrate	**S-BTT**	120ºC	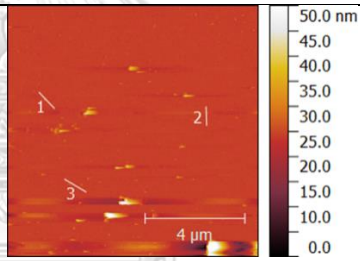 2.0-3.0 nm	No conductivity
Drop on bare substrate	**S-BTT**	-	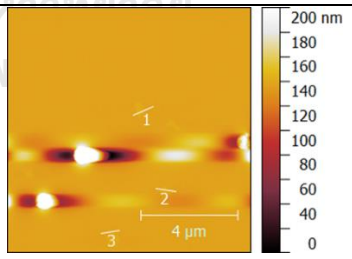	No conductivity
Drop on bare substrate	**S-BTT**	60ºC	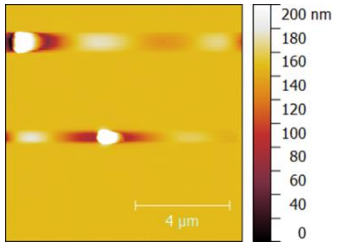	No conductivity

จุฬาลงกรณ์มหาวิทยาลัย
Chulalongkorn

Drop on bare substrate	**S-BTT**	90°C	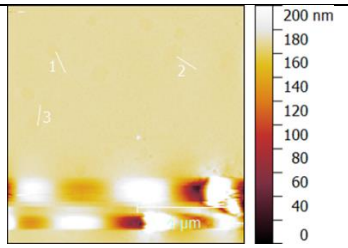 2.0-4.0 nm	No conductivity
Drop on bare substrate	**S-BTT**	120°C	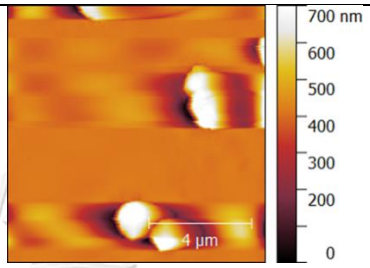	No conductivity

Unlike solution-deposition process, the DFM morphology characterization of the evaporated film is also displayed in **Figure 3.38.** This is performed at the center of the substrate **A-BTT** and **S-BTT** without annealing. The result found that roughness on the film was changed from the rough with the three-dimension island to smooth without three-dimension island molecular steps. It means that rough surface in spin-coated film, a result from amorphous-like crystallization during solvent evaporation, was changed by fabrication process. Hence, fabrication process can influence molecular ordering as displayed in images.

จุฬาลงกรณ์มหาวิทยาลัย
Chulalongkorn University

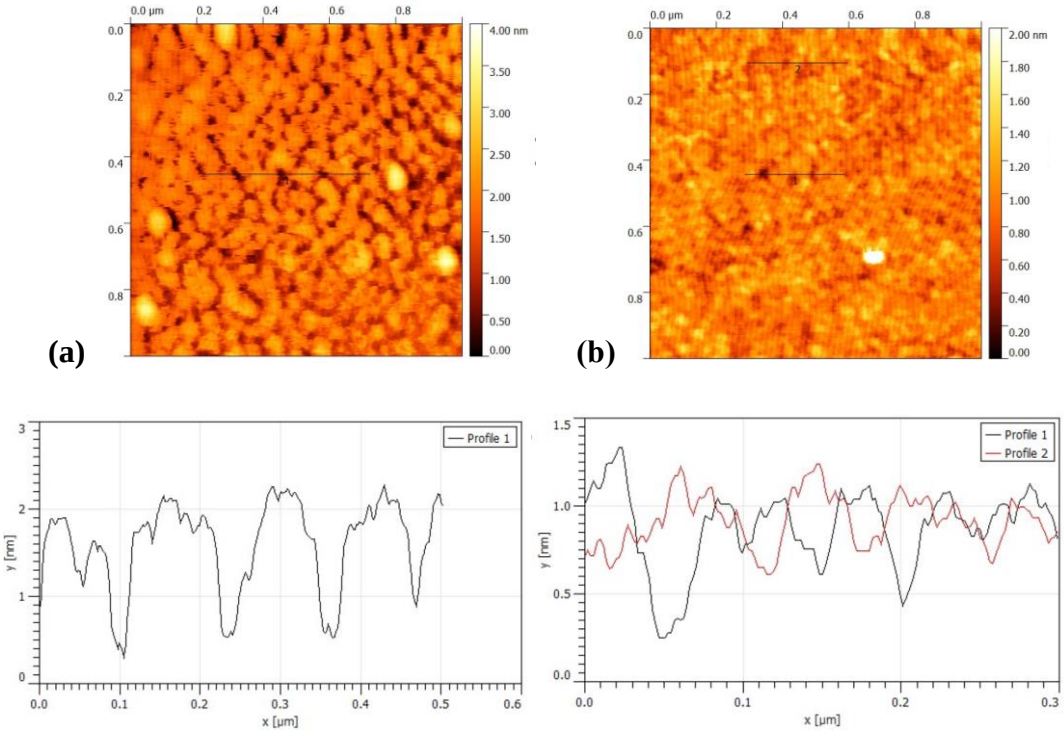

Figure 3.38 *DFM images of (a) A-BTT and (b) S-BTT without annealing of evaporated film*

จุฬาลงกรณ์มหาวิทยาลัย
CHULALONGKORN UNIVERSITY

The FET performance of evaporated film on SiO_2 (300 nm)/Si substrate was measured in a vacuum chamber. The I_d - V_d characteristic of typical **A-BTT** and **S-BTT** films are shown in **Figure 3.39**. Judging from the fact that negative V_g enhances I_d, p-type FET behavior was confirmed. The mobility was tabulated in **Table 3.3** and calculated in **Figure A. 79-83**. The highest hole mobility was calculated at 1.62 x 10^{-5} cm^2 V^{-1} s^{-1} (averaged value for three samples) from linear regime without annealing as **Table 3.3**.

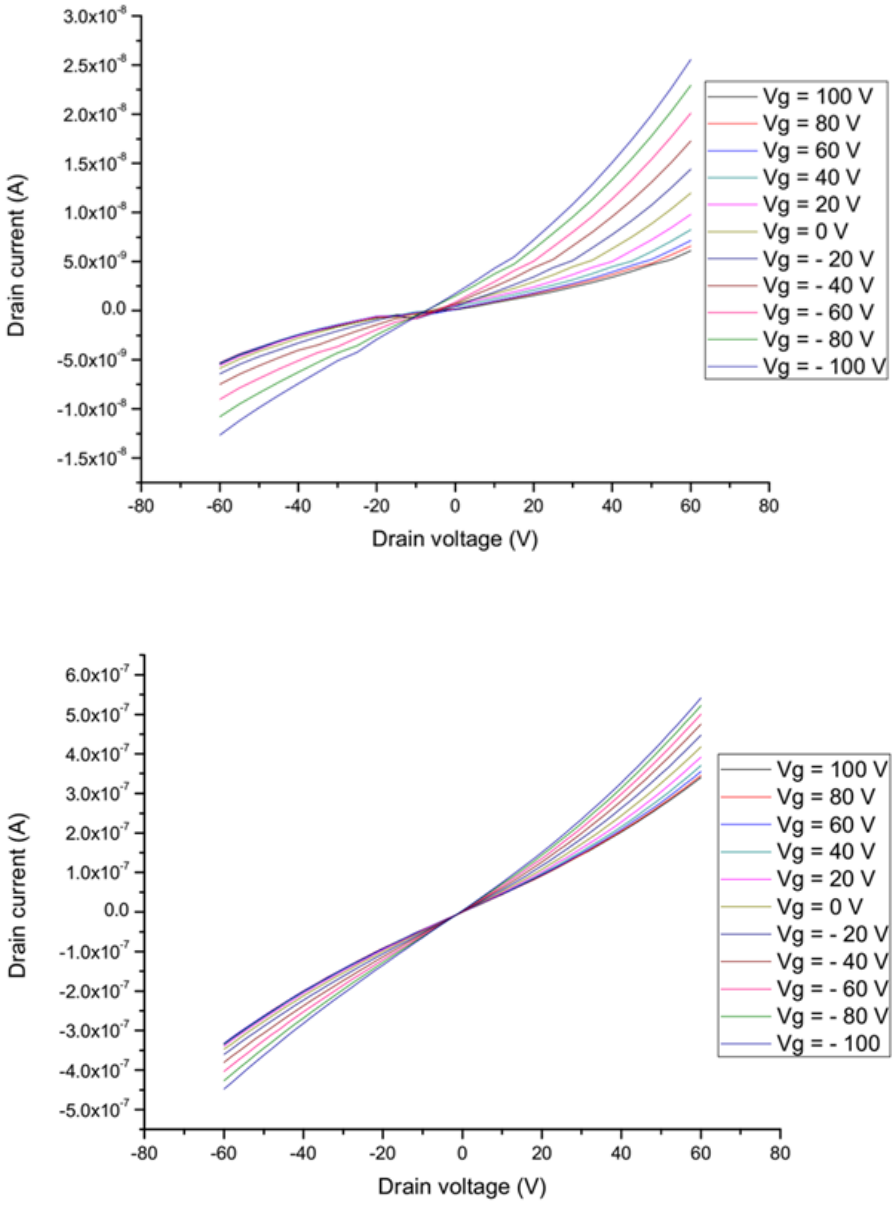

Figure 3.39 *Electrical characterization (top) A-BTT, (bottom) S-BTT of evaporated sample without annealing.*

The results concluded that FET mobility was significantly influenced by fabrication process. The higher electron mobility was obtained from evaporated **S-BTT** device than evaporated **A-BTT** device since C_3-symmetric point group in **S-BTT** might be attributed to this rotational relaxation in hole hopping which drastically related to low reorganization energy. However, both compounds containing -NH moieties partially suppressed the hole mobility. Therefore, FET properties of benzotriazatruxene derivatives were successfully investigated; nonetheless, their hole mobility values were mediocre. They are hard to be good candidates for hole mobility material.

Table 3.3 *Summary of mobility values for evaporated A-BTT and S-BTT on bare substrates*

Compound	10 µm ($cm^2 V^{-1} s^{-1}$)	25 µm ($cm^2 V^{-1} s^{-1}$)	100 µm ($cm^2 V^{-1} s^{-1}$)
A-BTT	2.74×10^{-6} ($\pm 1.47 \times 10^{-7}$)	4.28×10^{-6} ($\pm 2.34 \times 10^{-7}$)	NA
S-BTT	1.62×10^{-5} ($\pm 3.26 \times 10^{-6}$)	1.86×10^{-5} ($\pm 1.53 \times 10^{-6}$)	2.66×10^{-5} ($\pm 1.11 \times 10^{-5}$)

จุฬาลงกรณ์มหาวิทยาลัย
CHULALONGKORN UNIVERSITY

NA stands for Not Available. The values in parentheses are standard deviations.

3.7. Hole transporting properties of benzotriazatruxene derivatives in OLEDs

To investigate hole-transporting properties, multi-layer OLED devices with the structure of ITO/PEDOT: PSS/HTL/Alq_3/LiF: Al (**Figure 3.40**) were fabricated with **A-BTT** (device 1), **S-BTT** (device 2), **A-BTT-C6** (device 3) and **S-BTT-C6** (device 4) as the HTL. In comparison with commercial hole transporting material, TPD was

fabricated in the same manner (device 5). All devices were composed of ITO as the anode, the LiF: Al as the cathode and Alq_3 as the light-emitting and electron-transporting layers. As tabulated in **Table 3.4**, the results indicated that device 3 and device 4 with **A-BTT-C6** and **S-BTT-C6** emitted the green color of Alq_3 (528 nm) excepts device 1 and device 2 with **A-BTT** and **S-BTT** because -NH group is highly sensitive for these observed results as hexyl group is inert moiety for inter- and intramolecular interaction such as hydrogen bonding and protonation. In addition, the increasing of crystallinity, which is proportional to self-quenching absorption, might be the reason for inadequate emission efficiencies for **A-BTT** and **S-BTT**. However, all results of our devices thus indicated that benzotriazatruxenes containing alkyl group (*i.e*. hexyl) could potentially be used as a hole transporting layer (HTL) in OLED.

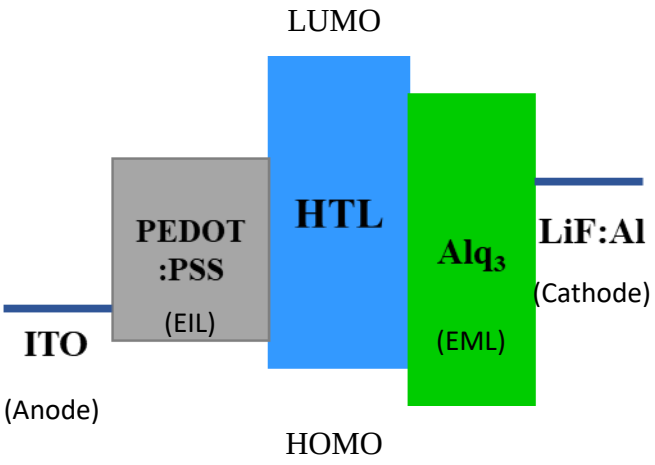

Figure 3.40 *Illustration of our fabricated devices*

The voltage-luminance and voltage-current density characteristics of the devices are shown in **Figure 3.41** and summarized in **Table 3.4**. Device 4 exhibited the best performance with a maximum luminance of 5,481 cd m^{-2} at 13.6 V, a turn-on voltage of 2.6 V and external efficiency of 0.61% which is better than **TPD**, a commercially available HTL. This is possibly attributed to the fact that device 4 has charge balance better than the other three devices due to a small energy barrier between **S-BTT-C6** and ITO. Moreover, it should be suggested that **S-BTT-C6** containing C_3-symmetric point group might be attributed to this rotational relaxation in hole hopping which drastically related to low reorganization energy. In comparison with asymmetric

triazatruxene containing hexyl group (**A-BTT-C6**), the alternative greater relaxation process might be taken place in solid states for poor emission efficiency, indicated a maximum luminance of 3,953 cd m-^{2} at 15.4 V, a turn-on voltage of 5.1 V and external efficiency of 0.57%. Additionally, symmetric compounds could exhibit prominent emission intensity owing to smaller energy loss in transition process and their molecular robustness [74, 75]. Not only symmetry of the molecule but the blocking of the excited electrons from the cathode to anode also might be the reason for the better hole transporting property as LUMO level of **S-BTT-C6** is higher than **A-BTT-C6** (**Table 3.1**). Therefore, hole transporting efficiencies of these compounds depend on the symmetry of the molecule and substituent at *N*-position which can be related to rotational relaxation and their crystallinities, respectively.

Table 3.4 *Electroluminescent properties of device 1-5*

Device	HTL	EML	V_{on}[a]	L_{max}[b]	J_{max}[c]	PE[d]	% EQE[e]	λ[f]

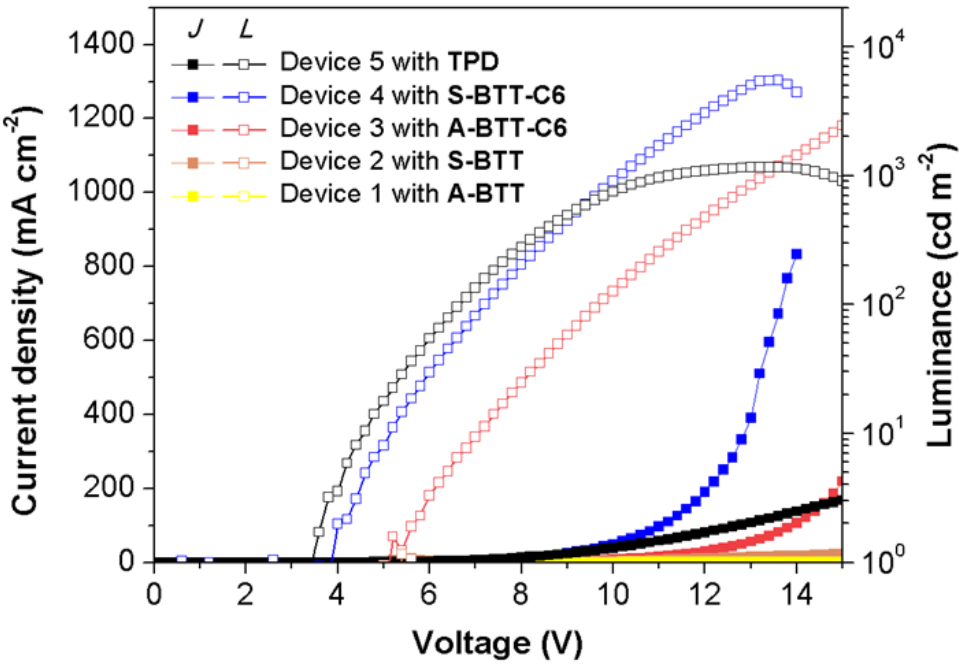

Figure 3.41 *Current density and luminance vs. voltage (J-V-L) characteristic of device 1-5*

1	**A-BTT**	Alq_3	N/A	N/A	N/A	N/A	N/A	N/A
2	**S-BTT**	Alq_3	N/A	N/A	18	N/A	N/A	N/A
3	**A-BTT-C6**	Alq_3	5.1	3953 (15.4)	1098	0.61 (6.0)	0.57 (10.8)	528
4	**S-BTT-C6**	Alq_3	2.6	5481 (13.6)	833	3.55 (3.0)	0.61 (9.6)	528
5	**TPD**	Alq_3	3.4	1161 (13.4)	186	1.62 (4.2)	0.90 (4.4)	534

N/A = Not available

[a]Turn-on voltage (V). [b]Maximum luminance (cd m^{-2}) (at applied potential V). [c]Current density (mA cm^{-2}). [d]Photoluminuous efficacy (lm W^{-1}) (at applied potential V) [e]External efficiency (%) (at applied potential V). [f]Maximum emission wavelength (nm).

จุฬาลงกรณ์มหาวิทยาลัย
CHULALONGKORN UNIVERSITY

CHAPTER 4
CONCLUSIONS

Unfortunately, the development of n-type FET is not successful for perylene-benzimidazole derivatives because of their own poor solubility. The purification and solution-deposition process could not be conducted. Unlike benzimidazole, four derivatives of symmetrical and asymmetrical benzotriazatruxene with and without a hexyl substituent at the *N*-position were synthesized from the commercially available 1*H*-benzo[g]indole and subjected to a comparative evaluation of the photophysical and hole transporting properties. All benzotriazatruxene derivatives were dissolved easily in common organic solvents. However, FET efficiencies of annealing and non-annealing devices composing of **A-BTT** and **S-BTT** film were almost unable to be measured because of their severe morphology of the fabricated film as shown in DFM image.

On the other hand, as HTL in OLED, the results revealed that their quantum efficiencies and hole transporting properties were exclusively depended on substituent at the *N*-position of benzotriazatruxenes. The compound without a hexyl group (**A-BTT** and **S-BTT**) exhibited the poor quantum yield, while those compounds with hexyl group or alkyl groups (**A-BTT-C6** and **S-BTT-C6**) possessed high quantum efficiencies and also hole transporting properties. It was proposed that quantum yields of these compounds strongly depend on the self-quenching of exciton from fluorophores benzotriazatruxene. Furthermore, C_3-symmetric point group slightly affect quantum yield. The compound without C_3-symmetric point group (**A-BTT-C6**) exhibited the high quantum yield due to smaller rotational relaxation and their packing pattern. Unlike quantum yield, compound containing C_3-symmetric point group (**S-BTT-C6**) showed the superior hole transporting property with maximum luminance of 5,481 cd m^{-2} at 13.6 V and a low turn-on voltage of 2.6 V.

จุฬาลงกรณ์มหาวิทยาลัย
Chulalongkorn University

REFERENCES

1. Edgar, L.J., *Method and apparatus for controlling electric currents*. 1930, Edgar, Lilienfeld Julius: United States.
2. Kahng, D. Silicon-silicon dioxide field induced surface devices. the Solid State Device Research Conf., Pittsburgh, PA. June 1960. (1960).
3. Yamashita, Y. Organic semiconductors for organic field-effect transistors. Science and Technology of Advanced Materials. 10 *(*2), (2009): p. 024313.
4. Ebisawa, F.;Kurokawa, T. and Nara, S. Electrical properties of polyacetylene/polysiloxane interface. Journal of Applied Physics. 54 *(*6), (1983): p. 3255-3259.
5. Kudo, K.;Yamashina, M. and Moriizumi, T. Field Effect Measurement of Organic Dye Films. Japanese Journal of Applied Physics. 23 *(*Part 1, No. 1), (1984): p. 130-130.
6. Koezuka, H.;Tsumura, A. and Ando, T. Field-effect transistor with polythiophene thin film. Synthetic Metals. 18 *(*1), (1987): p. 699-704.
7. Tsumura, A.;Koezuka, H. and Ando, T. Polythiophene field-effect transistor: Its characteristics and operation mechanism. Synthetic Metals. 25 *(*1), (1988): p. 11-23.
8. Horowitz, G. Organic Field-Effect Transistors. Advanced Materials. 10 *(*5), (1998): p. 365-377.
9. Sun, Y.;Liu, Y. and Zhu, D. Advances in organic field-effect transistors. Journal of Materials Chemistry. 15 *(*1), (2005): p. 53-65.
10. Murphy, A.R. and Fréchet, J.M.J. Organic Semiconducting Oligomers for Use in Thin Film Transistors. Chemical Reviews. 107 *(*4), (2007): p. 1066-1096.
11. Allard, S.;Forster, M.;Souharce, B.;Thiem, H. and Scherf, U. Organic Semiconductors for Solution-Processable Field-Effect Transistors (OFETs). Angewandte Chemie International Edition. 47 *(*22), (2008): p. 4070-4098.
12. Anthony, J.E. The Larger Acenes: Versatile Organic Semiconductors. Angewandte Chemie International Edition. 47 *(*3), (2008): p. 452-483.
13. Katz, H.E.;Hong, X.M.;Dodabalapur, A. and Sarpeshkar, R. Organic field-effect transistors with polarizable gate insulators. Journal of Applied Physics. 91 *(*3), (2002): p. 1572-1576.
14. Subramanian, V.;Chang, P.C.;Lee, J.B.;Molesa, S.E. and Volkman, S.K. Printed organic transistors for ultra-low-cost RFID applications. IEEE Transactions on Components and Packaging Technologies. 28 *(*4), (2005): p. 742-747.
15. Dodabalapur, A. Organic and polymer transistors for electronics. Materials Today. 9 *(*4), (2006): p. 24-30.
16. Muccini, M. A bright future for organic field-effect transistors. Nature Materials. 5 *(*8), (2006): p. 605-613.
17. Facchetti, A. Semiconductors for organic transistors. Materials Today. 10 *(*3), (2007): p. 28-37.
18. Weimer, P.K. The TFT A New Thin-Film Transistor. Proceedings of the IRE. 50 *(*6), (1962): p. 1462-1469.
19. Fan, Y., *Fabrication and operation of monolayer Mott FET at room temperature*. 2017.

20. . https://nirajchawake.wordpress.com/2014/10/20/semiconductors-why-%E2%88%86e%E2%89%A43-2-ev/.
21. Mott, N.F. and Peierls, R. Discussion of the paper by de Boer and Verwey. Proceedings of the Physical Society. 49 (4S), (1937): p. 72-73.
22. Tatemichi, S.;Ichikawa, M.;Koyama, T. and Taniguchi, Y. High mobility n-type thin-film transistors based on N,N′ -ditridecyl perylene diimide with thermal treatments. Applied Physics Letters. 89 (11), (2006): p. 112108.
23. Capelli, R.;Amsden, J.J.;Generali, G.;Toffanin, S.;Benfenati, V.;Muccini, M.;Kaplan, D.L.;Omenetto, F.G. and Zamboni, R. Integration of silk protein in organic and light-emitting transistors. Organic Electronics. 12 (7), (2011): p. 1146-1151.
24. Jeong, Y.J.;Jang, J.;Nam, S.;Kim, K.;Kim, L.H.;Park, S.;An, T.K. and Park, C.E. High-performance organic complementary inverters using monolayer graphene electrodes. ACS Appl Mater Interfaces. 6 (9), (2014): p. 6816-24.
25. Oh, J.-D.;Kim, J.-W.;Kim, D.-K. and Choi, J.-H. Low-voltage organic transistors and inverters using HfOx dielectrics. Organic Electronics. 30, (2016): p. 131-135.
26. Wu, N.;Wang, C.;Bunes, B.R.;Zhang, Y.;Slattum, P.M.;Yang, X. and Zang, L. Chemical Self-Doping of Organic Nanoribbons for High Conductivity and Potential Application as Chemiresistive Sensor. ACS Appl Mater Interfaces. 8 (19), (2016): p. 12360-8.
27. Hsiao, Y.S.;Liao, Y.H.;Chen, H.L.;Chen, P. and Chen, F.C. Organic Photovoltaics and Bioelectrodes Providing Electrical Stimulation for PC12 Cell Differentiation and Neurite Outgrowth. ACS Appl Mater Interfaces. 8 (14), (2016): p. 9275-84.
28. Horowitz, G.;Kouki, F.;Spearman, P.;Fichou, D.;Nogues, C.;Pan, X. and Garnier, F. Evidence for n-type conduction in a perylene tetracarboxylic diimide derivative. Advanced Materials. 8 (3), (1996): p. 242-245.
29. Malenfant, P.R.L.;Dimitrakopoulos, C.D.;Gelorme, J.D.;Kosbar, L.L.;Graham, T.O.;Curioni, A. and Andreoni, W. N-type organic thin-film transistor with high field-effect mobility based on a N,N′ -dialkyl-3,4,9,10-perylene tetracarboxylic diimide derivative. Applied Physics Letters. 80 (14), (2002): p. 2517-2519.
30. Chesterfield, R.J.;McKeen, J.C.;Newman, C.R.;Ewbank, P.C.;da Silva Filho, D.A.;Brédas, J.-L.;Miller, L.L.;Mann, K.R. and Frisbie, C.D. Organic Thin Film Transistors Based on N-Alkyl Perylene Diimides: Charge Transport Kinetics as a Function of Gate Voltage and Temperature. The Journal of Physical Chemistry B. 108 (50), (2004): p. 19281-19292.
31. Cheng, H.;Huai, J.;Cao, L. and Li, Z. Novel self-assembled phosphonic acids monolayers applied in N-channel perylene diimide (PDI) organic field effect transistors. Applied Surface Science. 378, (2016): p. 545-551.
32. Kang, W.;An, G.;Kim, M.J.;Lee, W.H.;Lee, D.Y.;Kim, H. and Cho, J.H. Ladder-Type Silsesquioxane Copolymer Gate Dielectrics for High-Performance Organic Transistors and Inverters. The Journal of Physical Chemistry C. 120 (6), (2016): p. 3501-3508.
33. Jeon, H.-G.;Hattori, J.;Kato, S.;Oguma, N.;Hirata, N.;Taniguchi, Y. and Ichikawa, M. Thermal treatment effects on N-alkyl perylene diimide thin-film

transistors with different alkyl chain. Journal of Applied Physics. 108 *(*12), (2010): p. 124512.

34. Jang, J.;Nam, S.;Chung, D.S.;Kim, S.H.;Yun, W.M. and Park, C.E. High Tg Cyclic Olefin Copolymer Gate Dielectrics for N,N′ -Ditridecyl Perylene Diimide Based Field-Effect Transistors: Improving Performance and Stability with Thermal Treatment. Advanced Functional Materials. 20 *(*16), (2010): p. 2611-2618.
35. Kim, S.H.;Jang, M.;Kim, J.;Choi, H.;Baek, K.-Y.;Park, C.E. and Yang, H. Complementary photo and temperature cured polymer dielectrics with high-quality dielectric properties for organic semiconductors. Journal of Materials Chemistry. 22 *(*37), (2012): p. 19940-19947.
36. Roh, J.;Lee, J.;Kang, C.-m.;Lee, C. and Jung, B.J. Air stability of PTCDI-C13-based n-OFETs on polymer interfacial layers. physica status solidi (RRL) – Rapid Research Letters. 7 *(*7), (2013): p. 469-472.
37. Jiang, W.;Li, Y.;Yue, W.;Zhen, Y.;Qu, J. and Wang, Z. One-Pot Facile Synthesis of Pyridyl Annelated Perylene Bisimides. Organic Letters. 12 *(*2), (2010): p. 228-231.
38. Konemann, M.M., DE), Osswald, Peter (Wain, DE), Schmidt, Rudiger (Paderborn, DE), Wurthner, Frank (Hochberg, DE),, *FLUORINATED RYLENETETRACARBOXYLIC ACID DERIVATIVES AND USE THEREOF*. 2009, BASF AKTIENGESELLSCHAFT (Ludwigshafen, DE): United States.
39. Quante, H.;Geerts, Y. and Müllen, K. Synthesis of Soluble Perylenebisamidine Derivatives. Novel Long-Wavelength Absorbing and Fluorescent Dyes. Chemistry of Materials. 9 *(*2), (1997): p. 495-500.
40. Yuan, Z.;Xiao, Y.;Li, Z. and Qian, X. Efficient Synthesis of Regioisomerically Pure Bis(trifluoromethyl)-Substituted 3,4,9,10-Perylene Tetracarboxylic Bis(benzimidazole). Organic Letters. 11 *(*13), (2009): p. 2808-2811.
41. Wicklein, A.;Kohn, P.;Ghazaryan, L.;Thurn-Albrecht, T. and Thelakkat, M. Synthesis and structure elucidation of discotic liquid crystalline perylene imide benzimidazole. Chemical Communications. 46 *(*13), (2010): p. 2328-2330.
42. Tozlu, C.;Erten-Ela, S.;Singh, T.B.;Sariciftci, N.S. and İçli, S. Comparative study of arylene bisimides substituted with imidazole side group for different dielectrics on the OFET application. Synthetic Metals. 172, (2013): p. 5-10.
43. Geffroy, B.;le Roy, P. and Prat, C. Organic light-emitting diode (OLED) technology: materials, devices and display technologies. Polymer International. 55 *(*6), (2006): p. 572-582.
44. Weiss, D.S. and Abkowitz, M. Advances in Organic Photoconductor Technology. Chemical Reviews. 110 *(*1), (2010): p. 479-526.
45. Zhu, F., in *Symposium on Sustainability Driven Innovative Technologies*. 2009.
46. Gustafsson, G.;Cao, Y.;Treacy, G.M.;Klavetter, F.;Colaneri, N. and Heeger, A.J. Flexible light-emitting diodes made from soluble conducting polymers. Nature. 357 *(*6378), (1992): p. 477-479.
47. Giro, G.;Cocchi, M.;Di Marco, P.;Di Nicolò, E.;Fattori, V.;Kalinowski, J. and Ghedini, M. The role played by cell configuration and layer preparation in LEDs based on hydroxyquinoline metal complexes and a triphenyl-diamine derivative (TPD). Synthetic Metals. 102 *(*1), (1999): p. 1018-1019.

48. Ko, C.-W. and Tao, Y.-T. 9,9-Bis{4-[di-(p-biphenyl)aminophenyl]}fluorene: a high Tg and efficient hole-transporting material for electroluminescent devices. Synthetic Metals. 126 *(*1), (2002): p. 37-41.
49. Chen, C.-H.;Shen, W.-J.;Jakka, K. and Shu, C.-F. Synthesis and characterization of spiro(adamantane-2,9′ -fluorene)-based triaryldiamines: thermally stable hole-transporting materials. Synthetic Metals. 143 *(*2), (2004): p. 215-220.
50. Ren, X.;Alleyne, B.D.;Djurovich, P.I.;Adachi, C.;Tsyba, I.;Bau, R. and Thompson, M.E. Organometallic Complexes as Hole-Transporting Materials in Organic Light-Emitting Diodes. Inorganic Chemistry. 43 *(*5), (2004): p. 1697-1707.
51. Fang, Q.;Xu, B.;Jiang, B.;Fu, H.;Zhu, W.;Jiang, X. and Zhang, Z. A novel fluorene derivative containing four triphenylamine groups: Highly thermostable blue emitter with hole-transporting ability for organic light-emitting diode (OLED). Synthetic Metals. 155 *(*1), (2005): p. 206-210.
52. Son, S.-H.;Yun, J.-J.;Oh, G.-C.;Jung, S.-Y.;Kim, Y.-K.;Kuhta, A.V.;Olkhovik, V.K.;Sasnouski, G. and Han, E.-M. Electroluminescence characteristics of a novel biphenyl derivative with benzoxazole for organic light-emitting diodes. Current Applied Physics. 5 *(*1), (2005): p. 75-78.
53. Zhi-feng, Z.;Zhen-bo, D.;Dong, G.;Chun-jun, L. and Peng, L. Improved performance of organic light-emitting devices with 2-(4-biphenyl)-5-(4-butylphenyl)-1,3,4-oxadiazole. Displays. 26 *(*3), (2005): p. 133-136.
54. Kao, P.-C.;Chu, S.-Y.;You, Z.-X.;Liou, S.J. and Chuang, C.-A. Improved efficiency of organic light-emitting diodes using CoPc buffer layer. Thin Solid Films. 498 *(*1), (2006): p. 249-253.
55. Sharma, A.;Singh, D.;Makrandi, J.K.;Kamalasanan, M.N.;Shrivastva, R. and Singh, I. Fabrication and characterization of OLED with Mg complex of 5-chloro-8-hydroxyquinoline as emission layer. Materials Chemistry and Physics. 108 *(*2), (2008): p. 179-183.
56. Raksasorn, D.;Namuangruk, S.;Prachumrak, N.;Sudyoadsuk, T.;Promarak, V.;Sukwattanasinitt, M. and Rashatasakhon, P. Synthesis and characterization of hole-transporting star-shaped carbazolyl truxene derivatives. RSC Advances. 5 *(*89), (2015): p. 72841-72848.
57. Wongsilarat, C.;Namuangruk, S.;Prachumrak, N.;Sudyoadsuk, T.;Promarak, V.;Sukwattanasinitt, M. and Rashatasakhon, P. Solution processed blue-emitting and hole-transporting materials from truxene-carbazole-pyrene triads. Organic Electronics. 57, (2018): p. 352-358.
58. Zhu, T.;He, G.;Chang, J.;Zhao, D.;Zhu, X. and Zhu, H. The synthesis, photophysical and electrochemical properties of a series of novel 3,8,13-substituted triindole derivatives. Dyes and Pigments. 95 *(*3), (2012): p. 679-688.
59. Li, L.;Gao, P.;Schuermann, K.C.;Ostendorp, S.;Wang, W.;Du, C.;Lei, Y.;Fuchs, H.;Cola, L.D.;Müllen, K. and Chi, L. Controllable Growth and Field-Effect Property of Monolayer to Multilayer Microstripes of an Organic Semiconductor. Journal of the American Chemical Society. 132 *(*26), (2010): p. 8807-8809.
60. Jang, J.;Nam, S.;Im, K.;Hur, J.;Cha, S.N.;Kim, J.;Son, H.B.;Suh, H.;Loth, M.A.;Anthony, J.E.;Park, J.-J.;Park, C.E.;Kim, J.M. and Kim, K. Highly Crystalline Soluble Acene Crystal Arrays for Organic Transistors: Mechanism of

จุฬาลงกรณ์มหาวิทยาลัย
CHULALONGKORN UNIVERSITY

Crystal Growth During Dip-Coating. Advanced Functional Materials. 22 *(*5), (2012): p. 1005-1014.

61. Chen, H.;Dong, S.;Bai, M.;Cheng, N.;Wang, H.;Li, M.;Du, H.;Hu, S.;Yang, Y.;Yang, T.;Zhang, F.;Gu, L.;Meng, S.;Hou, S. and Guo, X. Solution-Processable, Low-Voltage, and High-Performance Monolayer Field-Effect Transistors with Aqueous Stability and High Sensitivity. Advanced Materials. 27 *(*12), (2015): p. 2113-2120.
62. Defaux, M.;Gholamrezaie, F.;Wang, J.;Kreyes, A.;Ziener, U.;Anokhin, D.V.;Ivanov, D.A.;Moser, A.;Neuhold, A.;Salzmann, I.;Resel, R.;de Leeuw, D.M.;Meskers, S.C.J.;Moeller, M. and Mourran, A. Solution-Processable Septithiophene Monolayer Transistor. Advanced Materials. 24 *(*7), (2012): p. 973-978.
63. Doherty, W.J.;Simmonds, A.G.;Mendes, S.B.;Armstrong, N.R. and Saavedra, S.S. Molecular Ordering in Monolayers of an Alkyl-Substituted Perylene-Bisimide Dye by Attenuated Total Reflectance Ultraviolet—Visible Spectroscopy. Applied Spectroscopy. 59 *(*10), (2005): p. 1248-1256.
64. Singh, T.B.;Erten, S.;Günes, S.;Zafer, C.;Turkmen, G.;Kuban, B.;Teoman, Y.;Sariciftci, N.S. and Icli, S. Soluble derivatives of perylene and naphthalene diimide for n-channel organic field-effect transistors. Organic Electronics. 7 *(*6), (2006): p. 480-489.
65. Techajaroonjit, T.;Namuangruk, S.;Prachumrak, N.;Promarak, V.;Sukwattanasinitt, M. and Rashatasakhon, P. Synthesis, characterization, and hole-transporting properties of pyrenyl N-substituted triazatruxenes. RSC Advances. 6 *(*61), (2016): p. 56392-56398.
66. Huang, C.;Barlow, S. and Marder, S.R. Perylene-3,4,9,10-tetracarboxylic Acid Diimides: Synthesis, Physical Properties, and Use in Organic Electronics. The Journal of Organic Chemistry. 76 *(*8), (2011): p. 2386-2407.
67. Choppawa, T.;Sukwattanasinitt, M.;Sahasithiwat, S.;Ruangpornvisuti, V. and Rashatasakhon, P. Substituent effect on quantum efficiency in 4-aryloxy-N-(2′,6′-diisopropylphenyl)-1,8-naphthalimides: Experimental and computational investigations. Dyes and Pigments. 109, (2014): p. 175-180.
68. Toworakajohnkun, N.;Sukwattanasinitt, M. and Rashatasakhon, P. N-Bromosuccinimide mediated synthesis of triazatruxenes from indoles. Tetrahedron Letters. 58 *(*43), (2017): p. 4149-4152.
69. Gómez-Lor, B. and Echavarren, A.M. Synthesis of a Triaza Analogue of Crushed-Fullerene by Intramolecular Palladium-Catalyzed Arylation. Organic Letters. 6 *(*17), (2004): p. 2993-2996.
70. Franceschin, M.;Ginnari-Satriani, L.;Alvino, A.;Ortaggi, G. and Bianco, A. Study of a Convenient Method for the Preparation of Hydrosoluble Fluorescent Triazatruxene Derivatives. European Journal of Organic Chemistry. 2010 *(*1), (2010): p. 134-141.
71. Ko, M.-D.;Rim, T.;Kim, K.;Meyyappan, M. and Baek, C.-K. High efficiency silicon solar cell based on asymmetric nanowire. Scientific Reports. 5, (2015): p. 11646.
72. Szenes, A., Bánhelyi, B., Csendes, T. et al. Enhancing Diamond Fluorescence via Optimized Nanorod Dimer Configurations. Plasmonics. 13, (2018): p. 1977.

73. Chen, C.-J.;Yao, J.;Zhu, W.;Chao, J.-H.;Shang, A.;Lee, Y.-G. and Yin, S. Ultrahigh light extraction efficiency light emitting diodes by harnessing asymmetric obtuse angle microstructured surfaces. Optik. 182, (2019): p. 400-407.
74. Liu, J. and Zhang, G.-h. The Synthesis and Study on Optical Characteristics of the Asymmetrical Polymerizable Fluorescent Brighteners. International Journal of Polymeric Materials and Polymeric Biomaterials. 60 *(*2), (2010): p. 199-211.
75. Oh, S.H.;Kim, B.G.;Yun, S.J.;Maheswara, M.;Kim, K. and Do, J.Y. The synthesis of symmetric and asymmetric perylene derivatives and their optical properties. Dyes and Pigments. 85 *(*1), (2010): p. 37-42.

จุฬาลงกรณ์มหาวิทยาลัย
CHULALONGKORN UNIVERSITY

APPENDIX

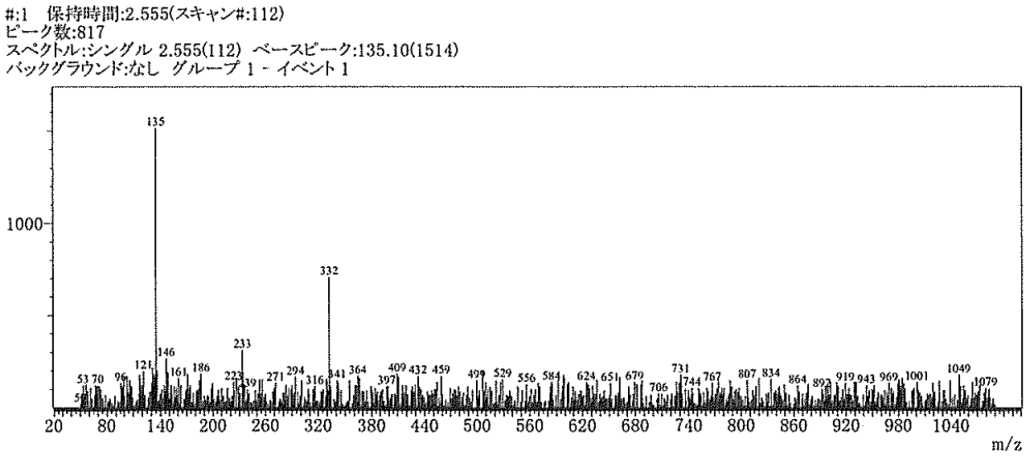

Figure A. 42 *GC-MS spectrum of 4,5-dioctyl-1,2-phenylene diamine*

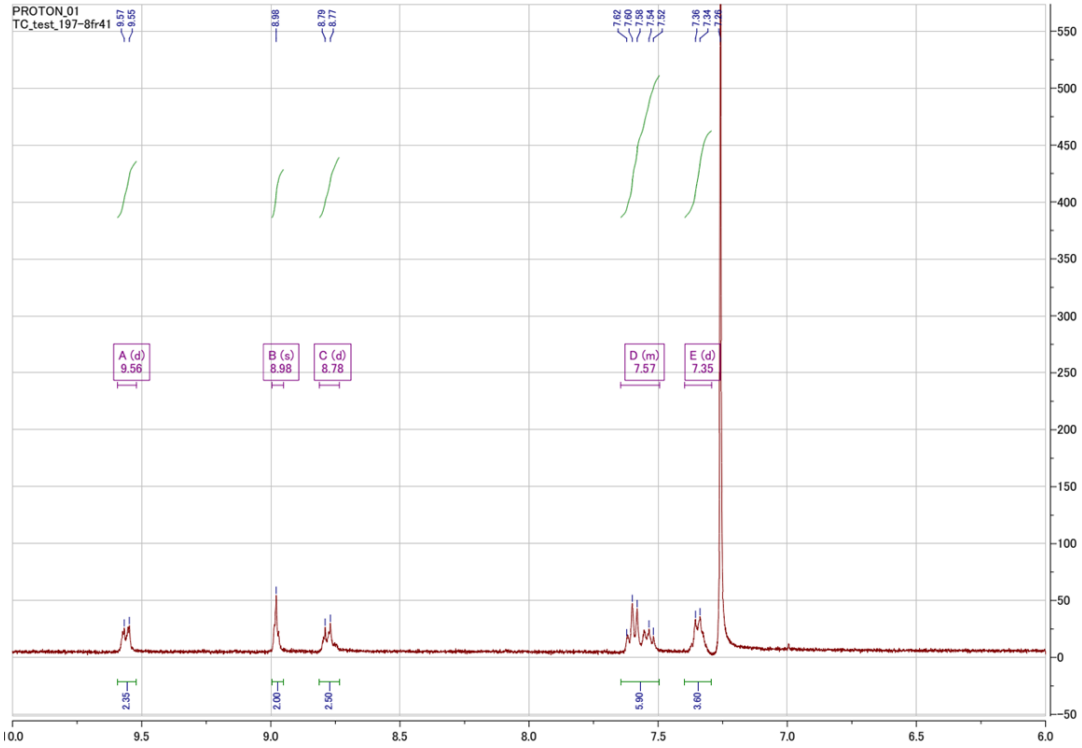

Figure A. 43 *^{1}H-NMR spectrum of 1,7-dibromo-N,N-diphenyl-perylene-3,4,9,10-tetracarboxylic diimide (DB-PTCDI-PH)*

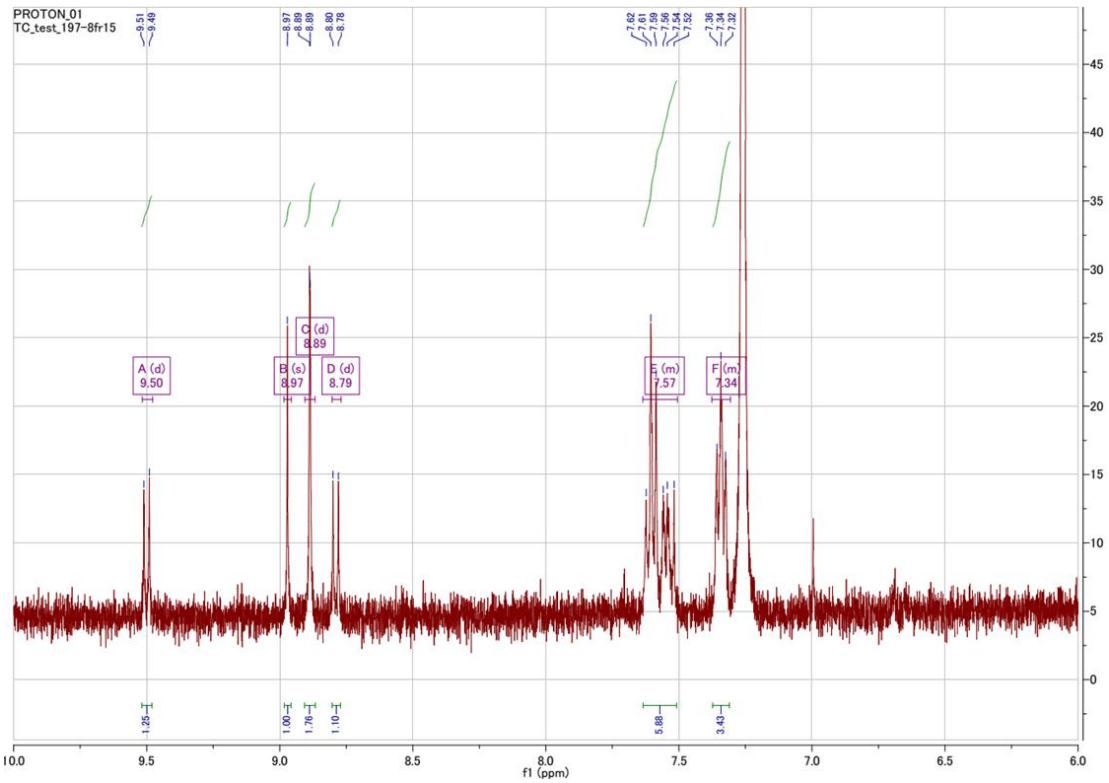

Figure A. 44 *^{1}H-NMR spectrum of 1,6,7-tribromo-N,N-diphenyl-perylene-3,4,9,10-tetracarboxylic diimide (TB-PTCDI-PH)*

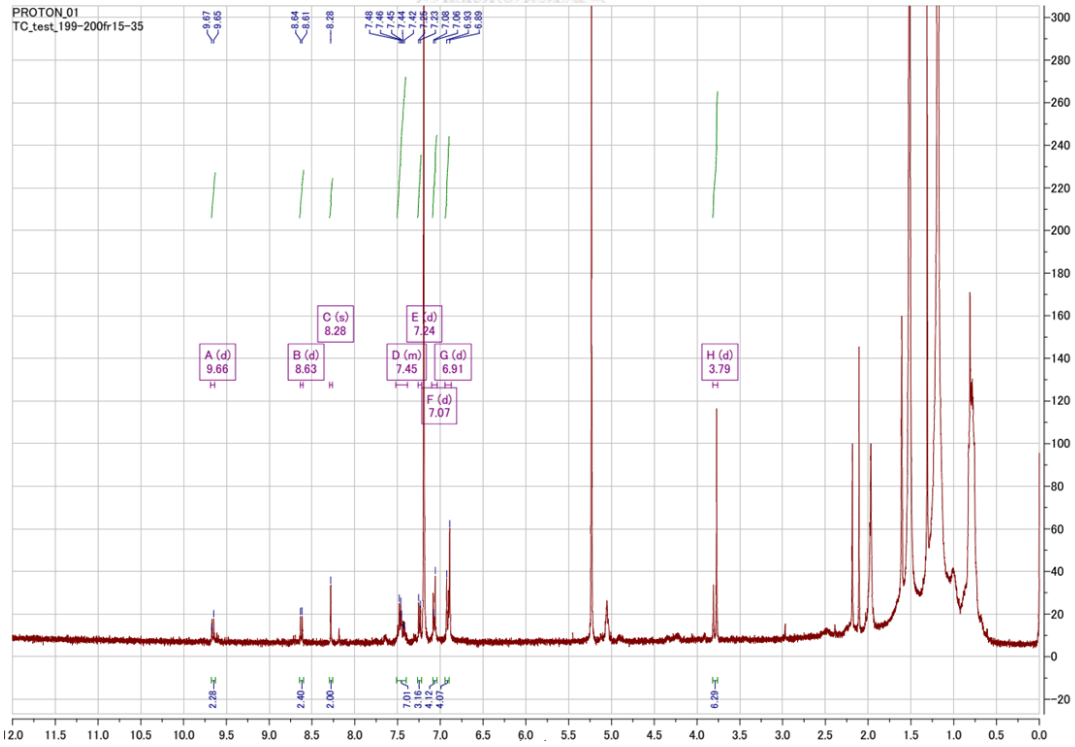

Figure A. 45 *^{1}H-NMR spectrum of 1,7-di(4-methoxy-phenoxy)-N,N-diphenyl-perylene-3,4,9,10-tetracarboxylic diimide (DM-PTCDI-PH)*

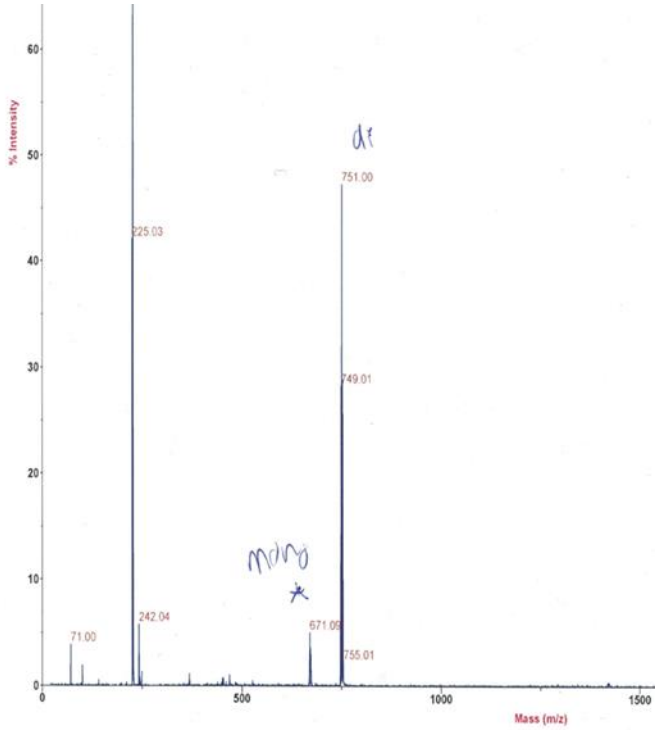

Figure A. 46 *MALDI-TOF mass spectrum of DB-BP-C1*

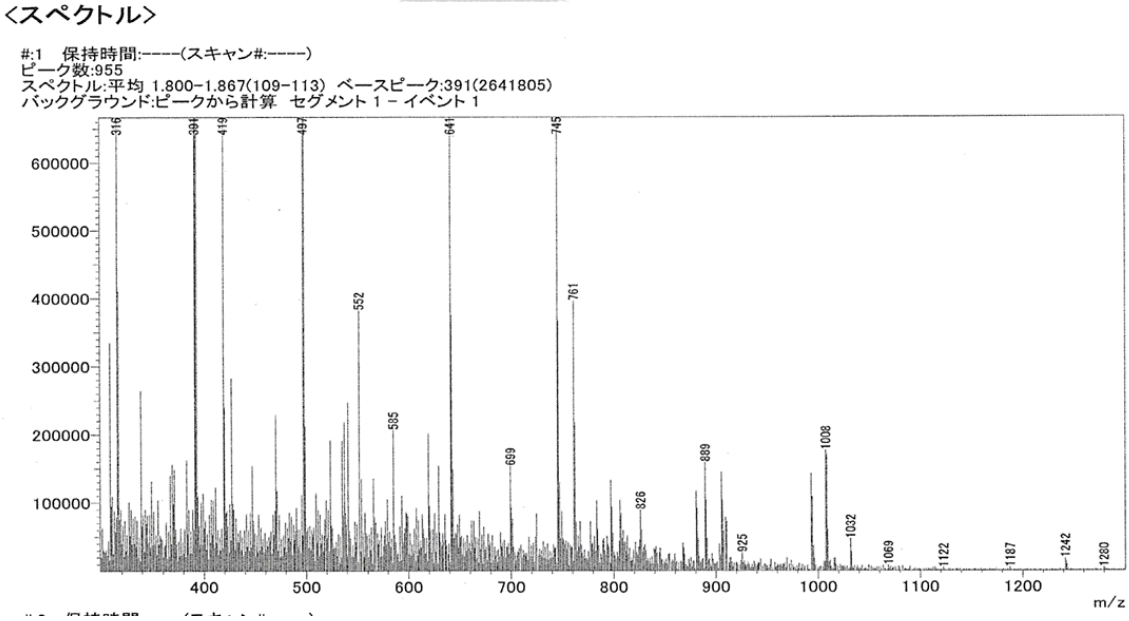

Figure A. 47 *LC-MS mass spectrum of DTP-BP-C1*

<スペクトル>

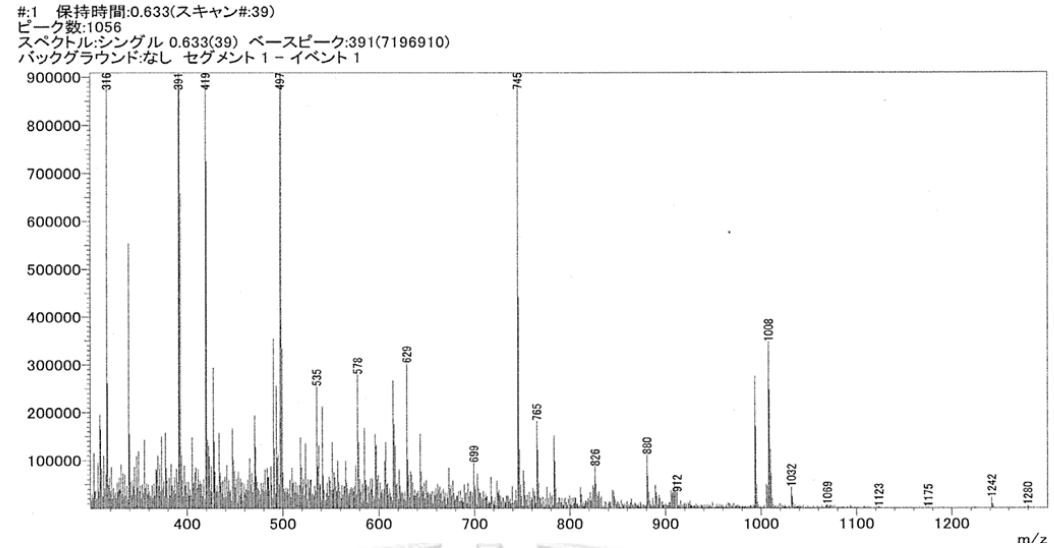

Figure A. 48 *LC-MS mass spectrum of DAP-BP-C1*

<スペクトル>

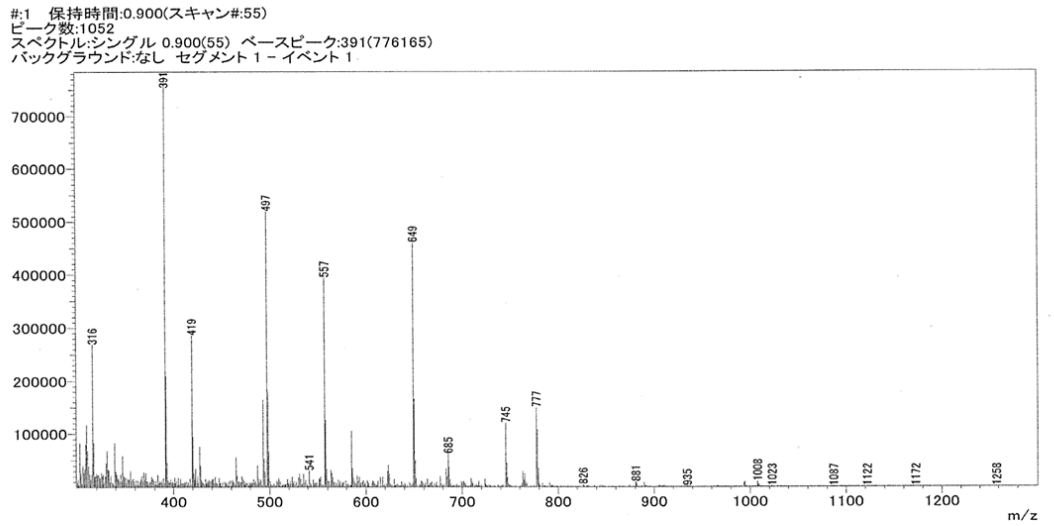

Figure A. 49 *LC-MS mass spectrum of DP-BP-C1*

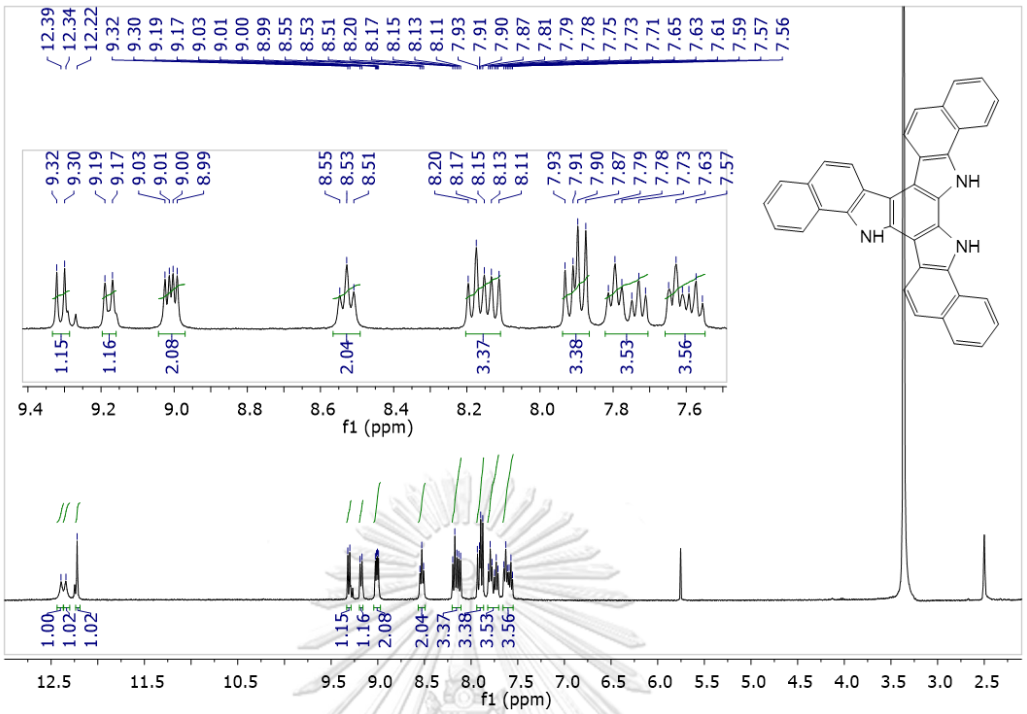

Figure A. 50 *^{1}H-NMR spectrum of 6,13-dihydro-5H-benzo[i]benzo[6,7]indolo[2,3-a]benzo[6,7]indolo[2,3-c]carbazole (A-BTT)*

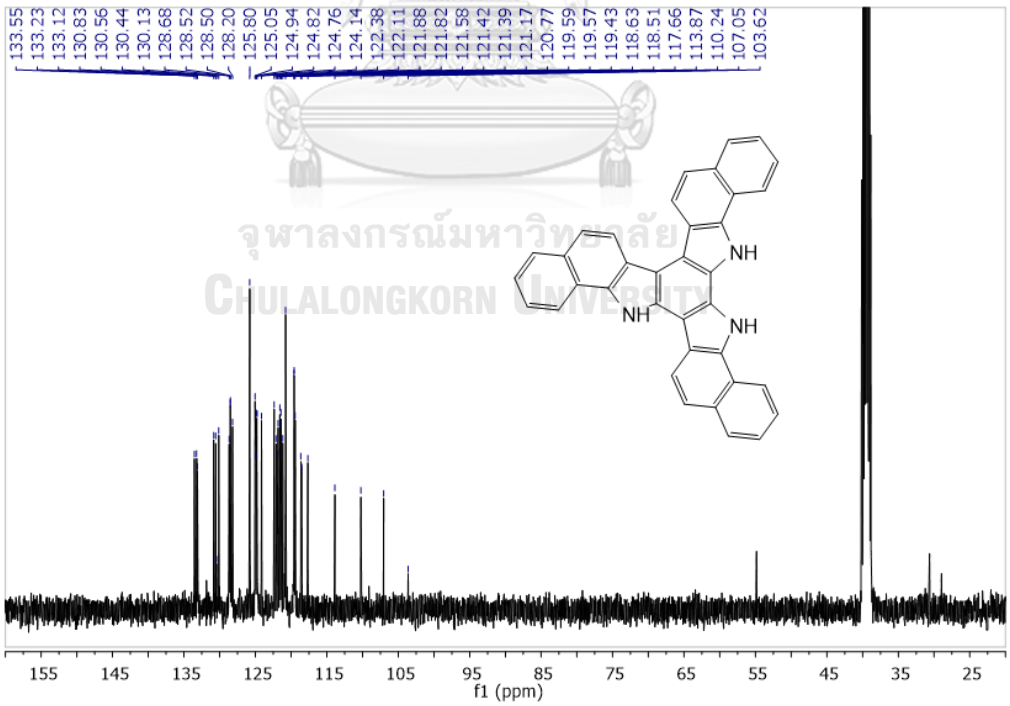

Figure A. 51 *^{13}C-NMR spectrum of 6,13-dihydro-5H-benzo[i]benzo[6,7]indolo[2,3-a]benzo[6,7]indolo[2,3-c]carbazole (**A-BTT**)*

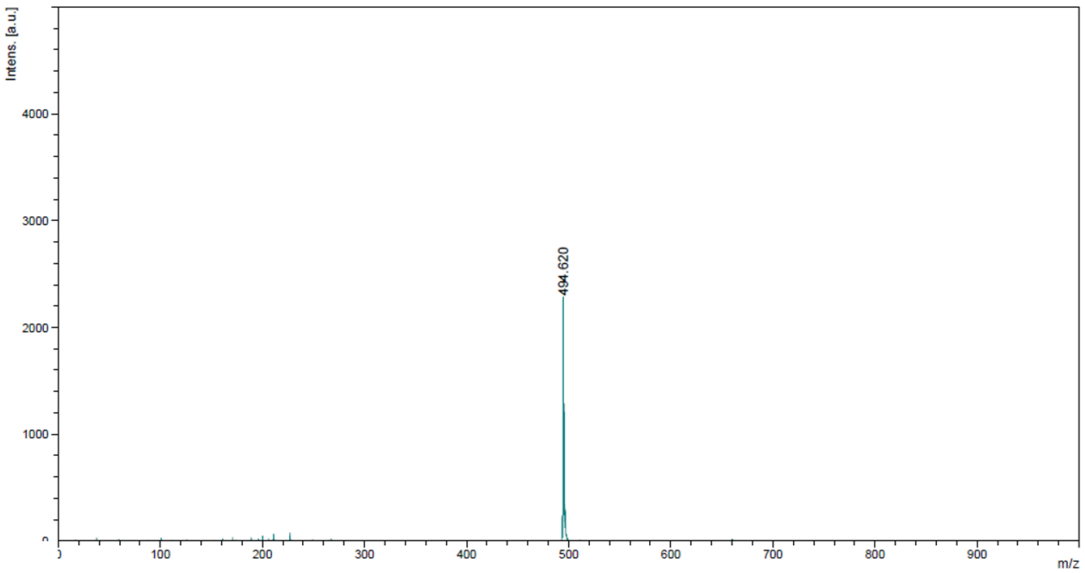

Figure A. 52 *MALDI-TOF mass spectrum of 6,13-dihydro-5*H*-benzo[*i*]benzo[6,7]indolo[2,3-*a*]benzo[6,7]indolo[2,3-*c*]carbazole (**A-BTT**)*

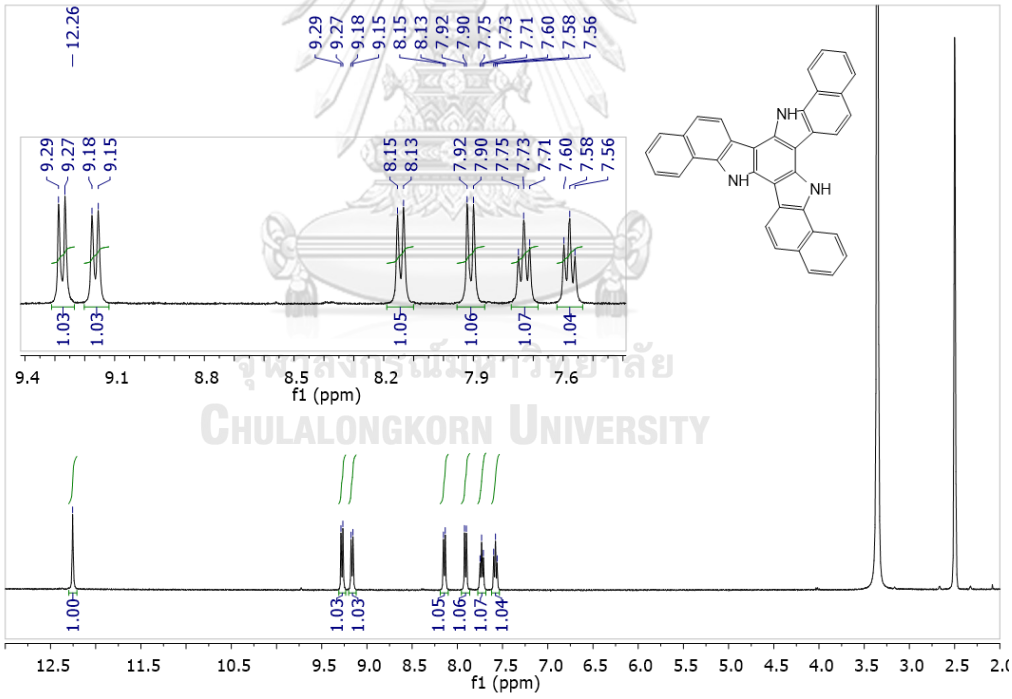

จุฬาลงกรณ์มหาวิทยาลัย
CHULALONGKORN UNIVERSITY

Figure A. 53 *^{1}H-NMR spectrum of 12,19-dihydro-5*H*-benzo[*i*]benzo[6,7]indolo[3,2-*a*]benzo[6,7]indolo[3,2-*c*]carbazole (**S-BTT**)*

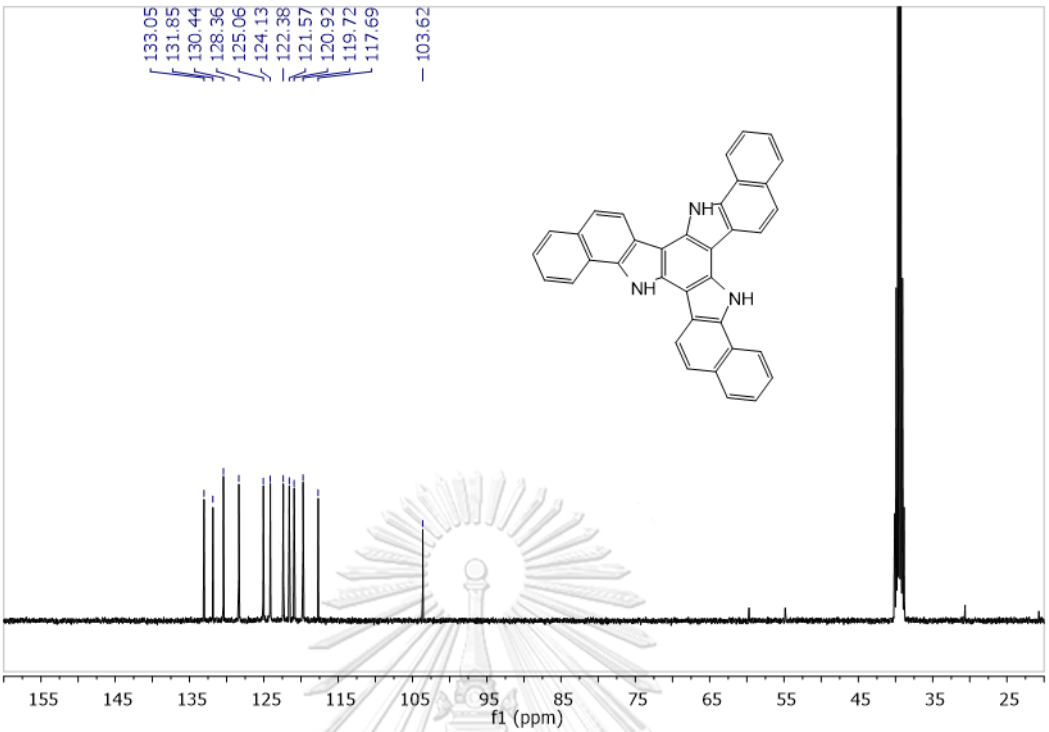

Figure A. 54 *^{13}C-NMR spectrum of 12,19-dihydro-5*H*-benzo[*i*]benzo[6,7]indolo[3,2-*a*]benzo[6,7]indolo[3,2-*c*]carbazole (**S-BTT**)*

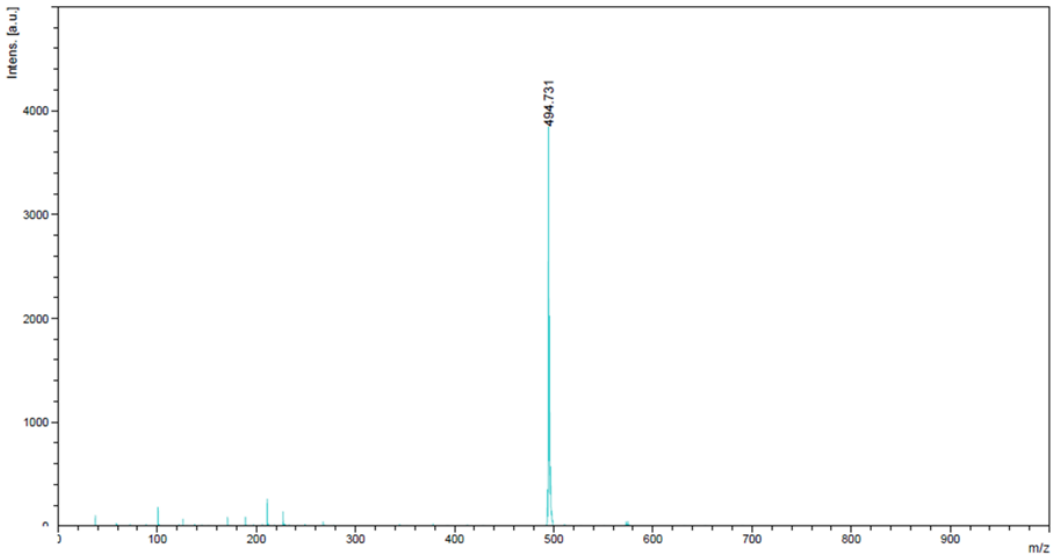

Figure A. 55 *MALDI-TOF mass spectrum of 12,19-dihydro-5*H*-benzo[*i*]benzo[6,7]indolo[3,2-*a*]benzo[6,7]indolo[3,2-*c*]carbazole (S-BTT)*

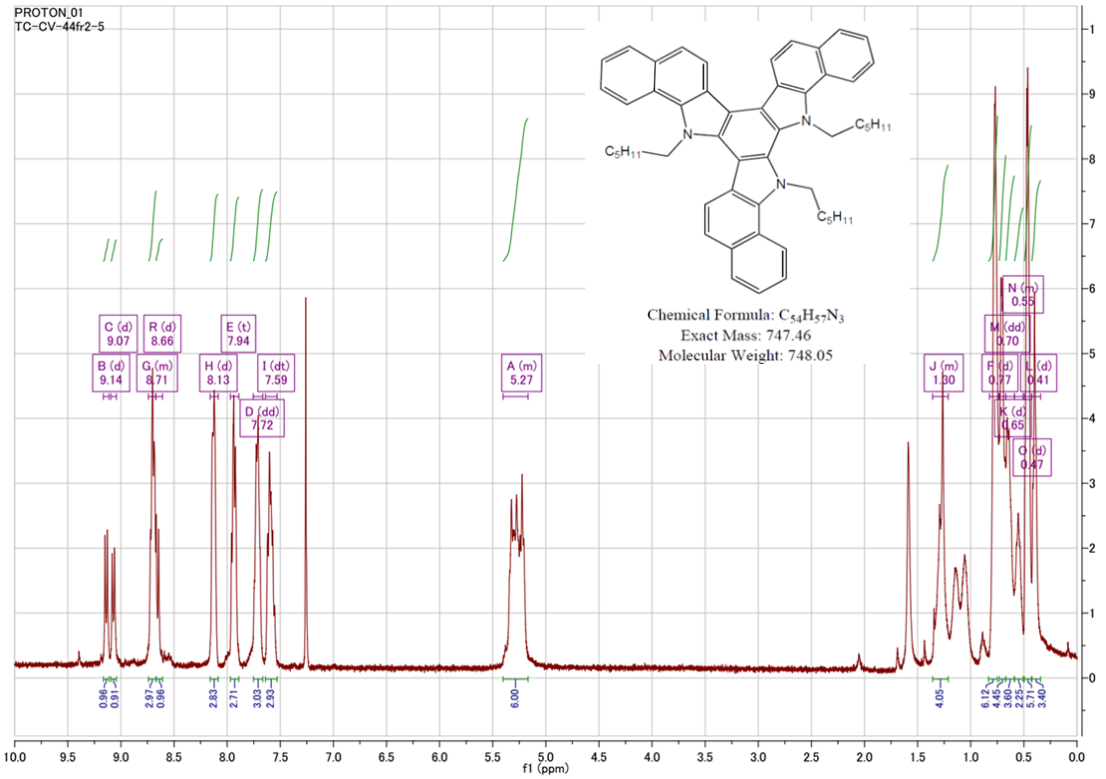

Figure A. 56 *[1]H-NMR spectrum of 5,6,13-trihexyl-6,13-dihydro-5*H*-benzo[i]benzo[6,7]indolo[2,3-*a*]benzo[6,7]indolo[2,3-*c*]carbazole* ***(A-BTT-C6)***

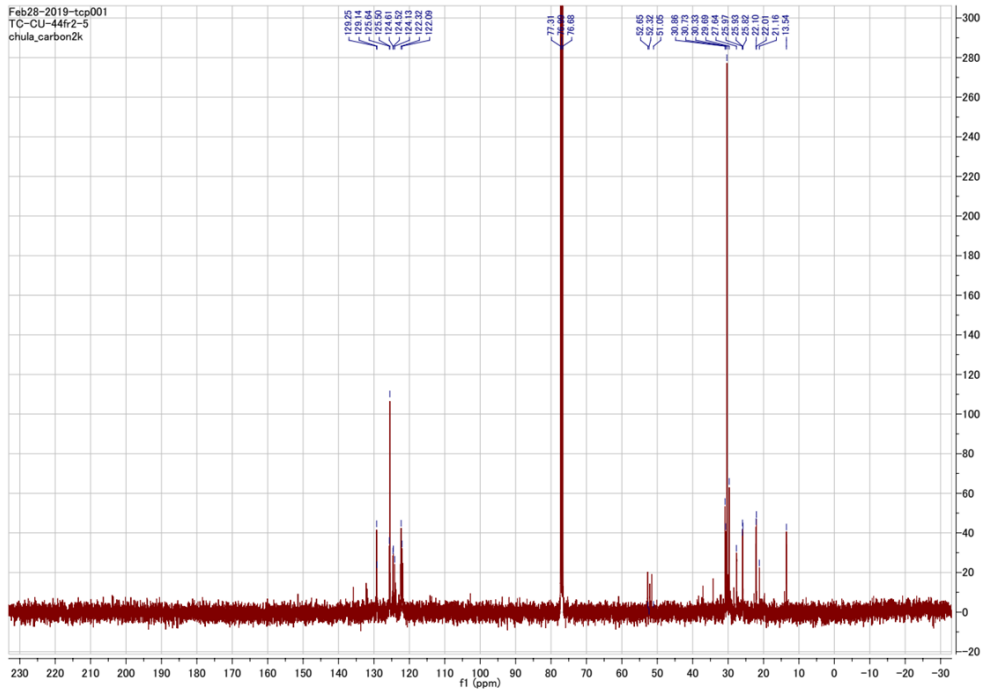

Figure A. 57 *[13]C-NMR spectrum of 5,6,13-trihexyl-6,13-dihydro-5*H*-benzo[i]benzo[6,7]indolo[2,3-*a*]benzo[6,7]indolo[2,3-*c*]carbazole* ***(A-BTT-C6)***

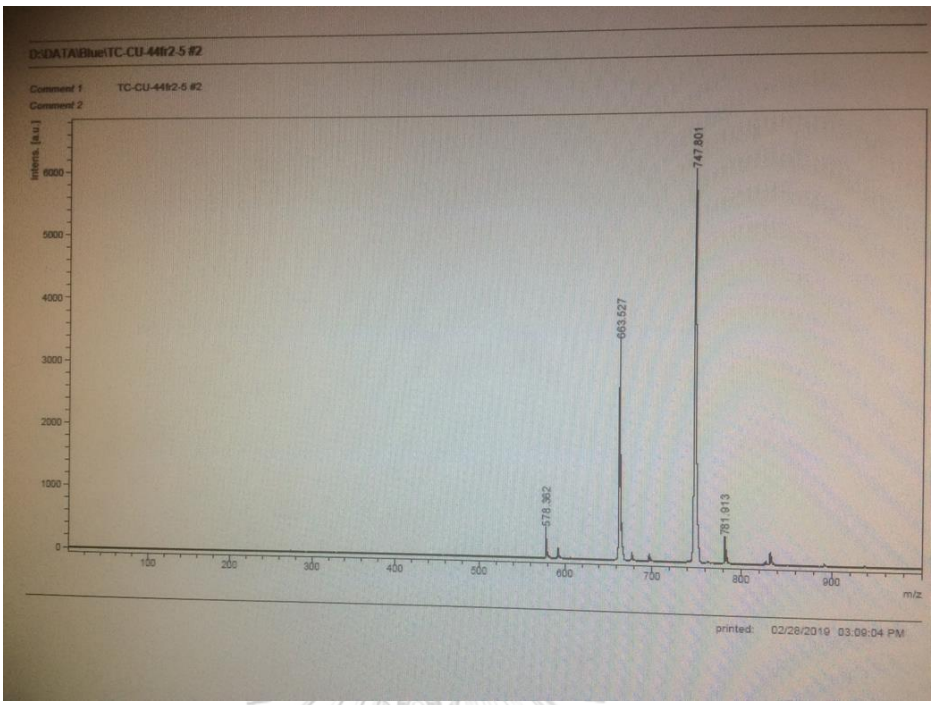

Figure A. 58 *MALDI-TOF mass spectrum of 5,6,13-trihexyl-6,13-dihydro-5H-benzo[i]benzo[6,7]indolo[2,3-a]benzo[6,7]indolo[2,3-c]carbazole* ***(A-BTT-C6)***

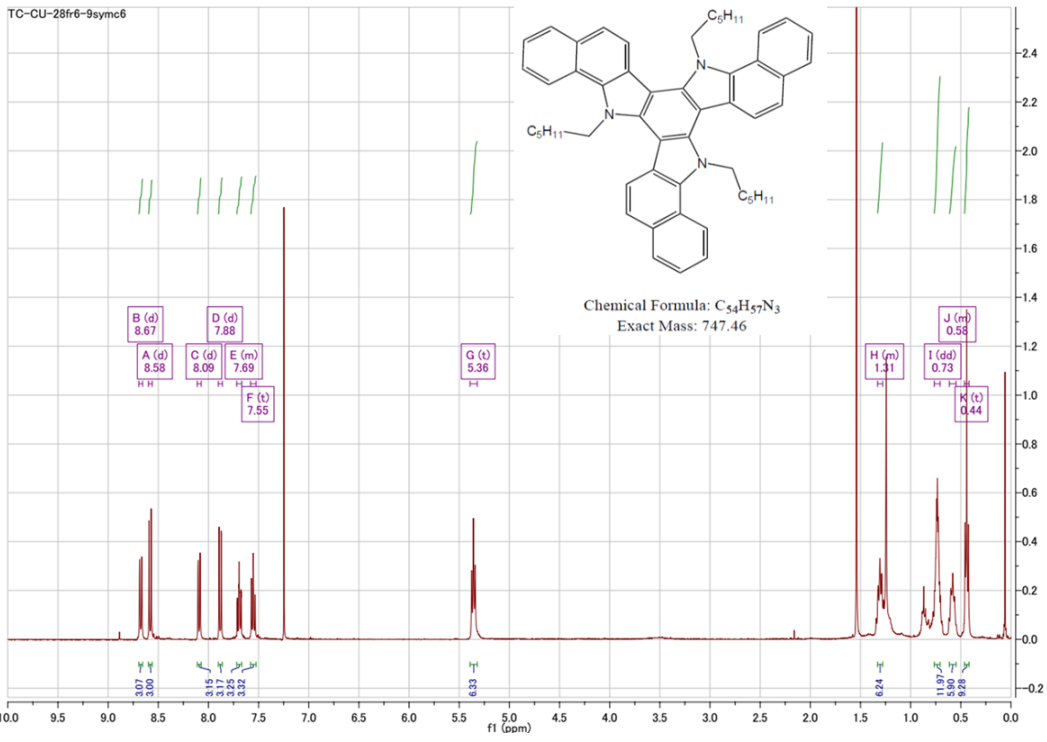

Figure A. 59 *^{1}H-NMR spectrum of 5,12,19-trihexyl-12,19-dihydro-5H-benzo[i]benzo[6,7]indolo[3,2-a]benzo[6,7]indolo[3,2-c]carbazole* ***(S-BTT-C6)***

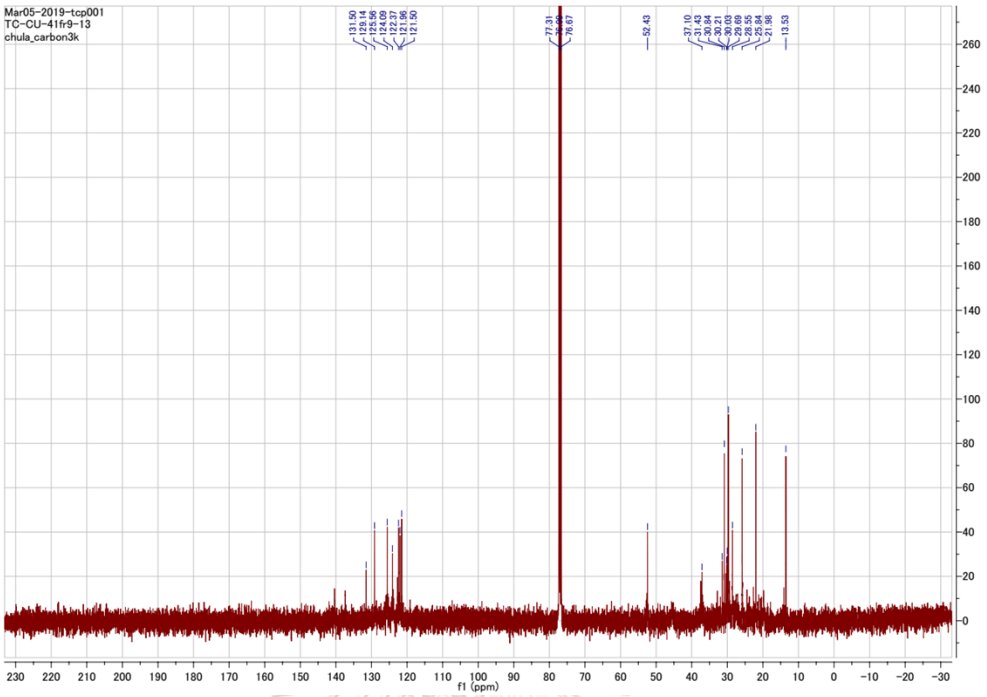

Figure A. 60 *^{13}C-NMR spectrum of 5,12,19-trihexyl-12,19-dihydro-5*H*-benzo[*i*]benzo[6,7]indolo[3,2-*a*]benzo[6,7]indolo[3,2-*c*]carbazole* ***(S-BTT-C6)***

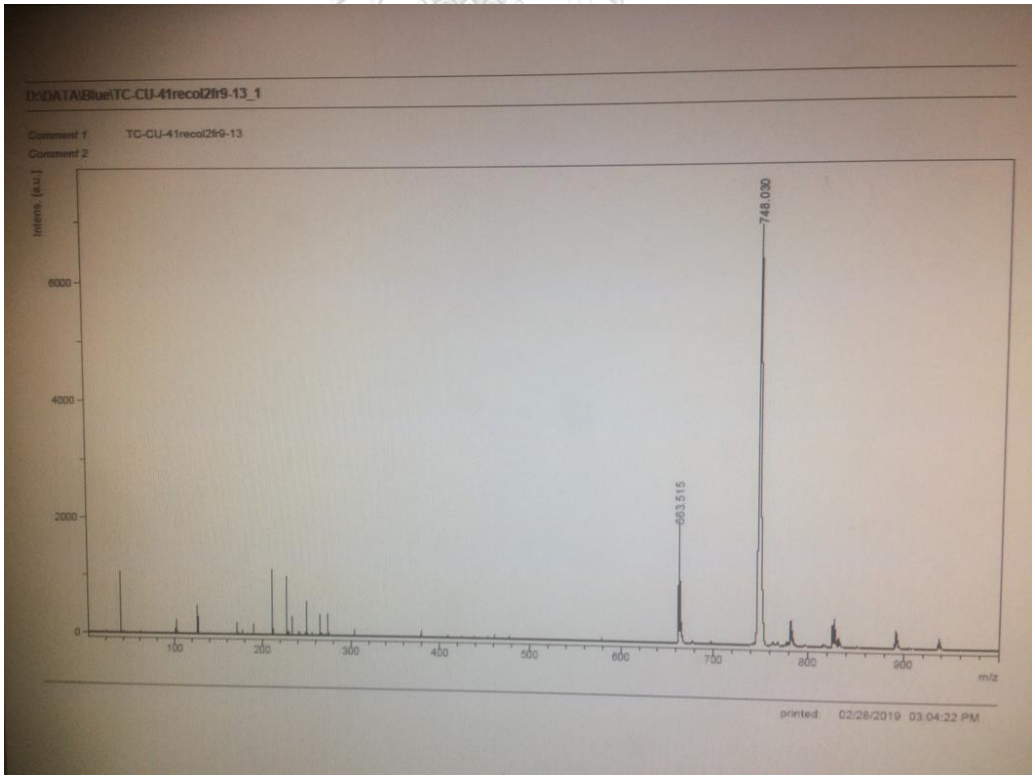

Figure A. 61 *MALDI-TOF mass spectrum of 5,12,19-trihexyl-12,19-dihydro-5*H*-benzo[*i*]benzo[6,7]indolo[3,2-*a*]benzo[6,7]indolo[3,2-*c*]carbazole* ***(S-BTT-C6)***

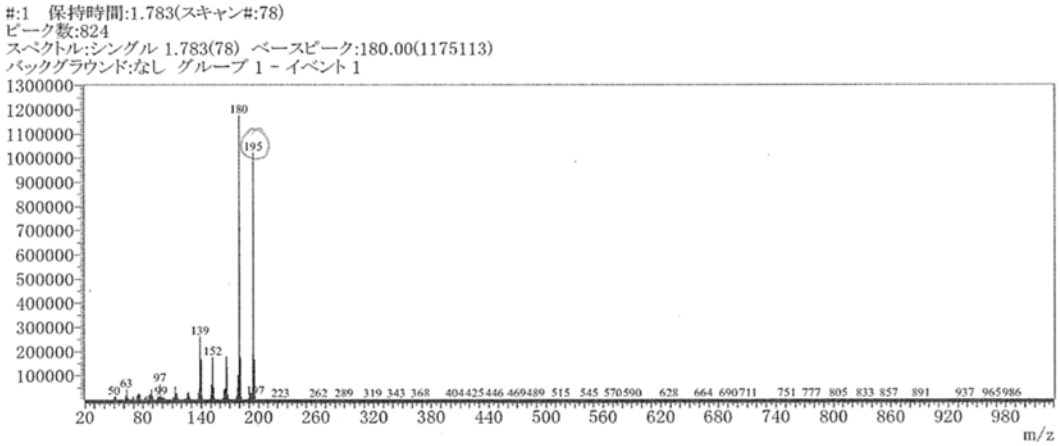

Figure A. 62 *DI-GC-MS spectrum of N-ethyl-benzo[g]indole*

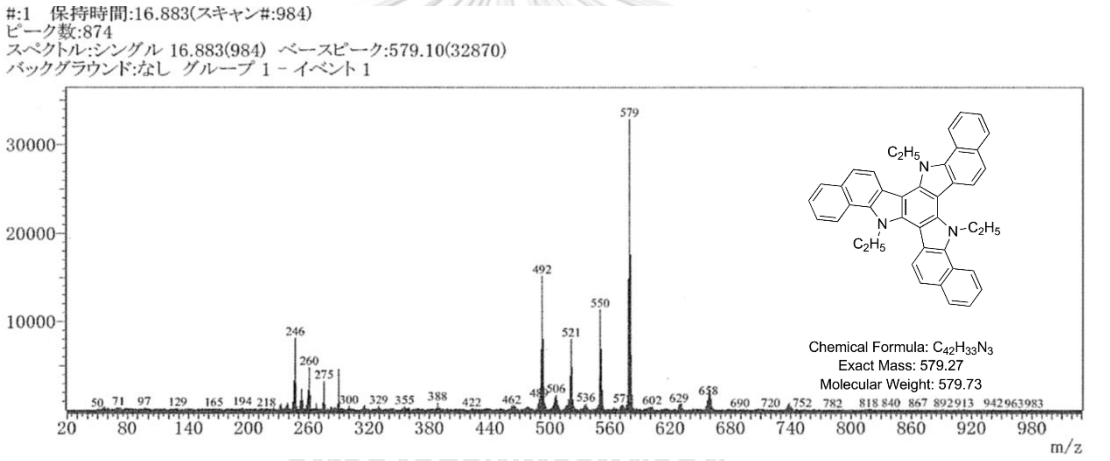

Figure A. 63 *DI-GC-MS spectrum of N, N, N-triethyl-benzotriazatruxene (**S-BTT-C2**)*

จุฬาลงกรณ์มหาวิทยาลัย
Chulalongkorn University

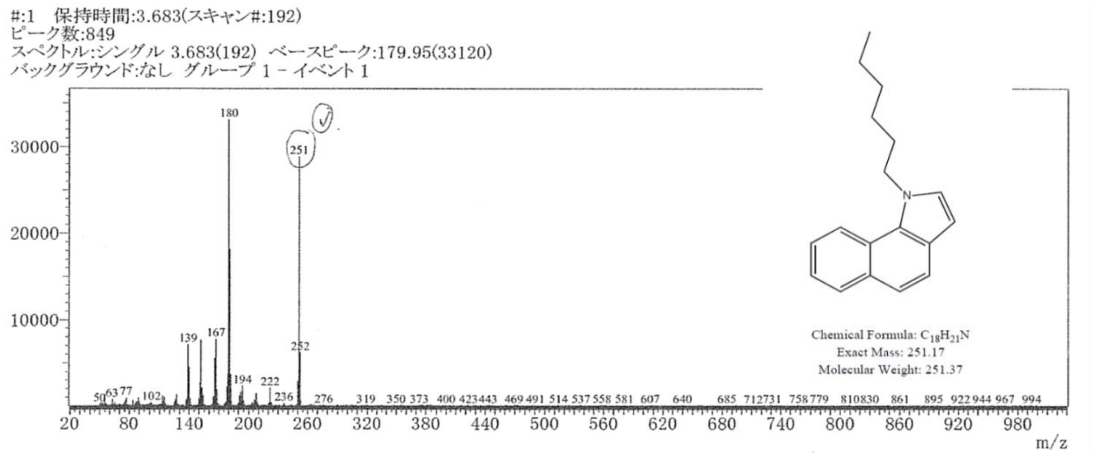

Figure A. 64 *DI-GC-MS spectrum of N-hexyl-benzo[g]indole*

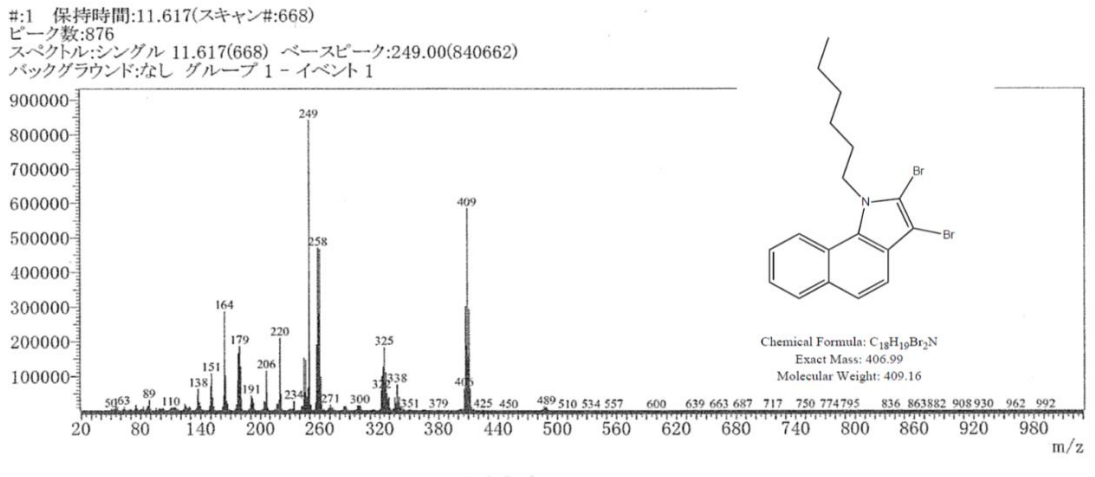

Figure A. 65 *DI-GC-MS spectrum of brominated* N*-hexyl-benzo[g]indole*

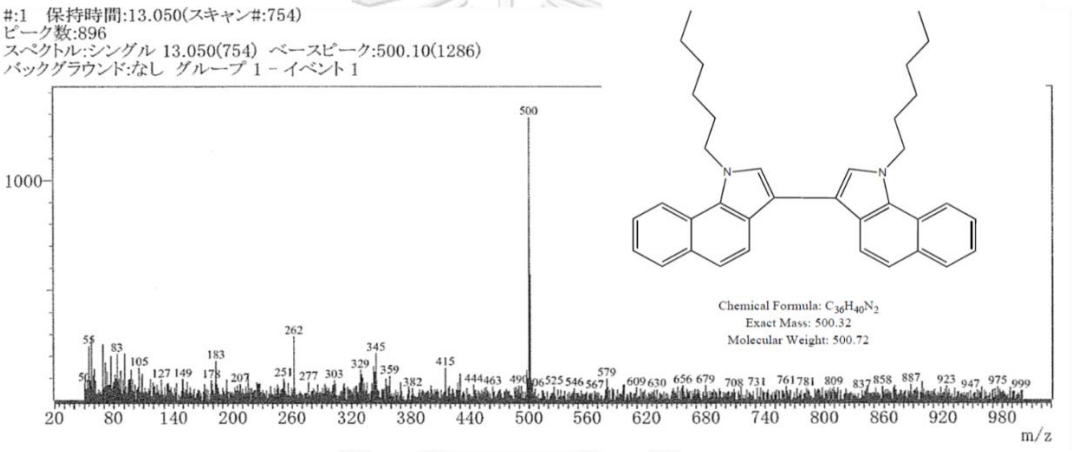

Figure A. 66 *DI-GC-MS spectrum of dimer of* N*-hexyl-benzo[g]indole*

CHULALONGKORN UNIVERSITY

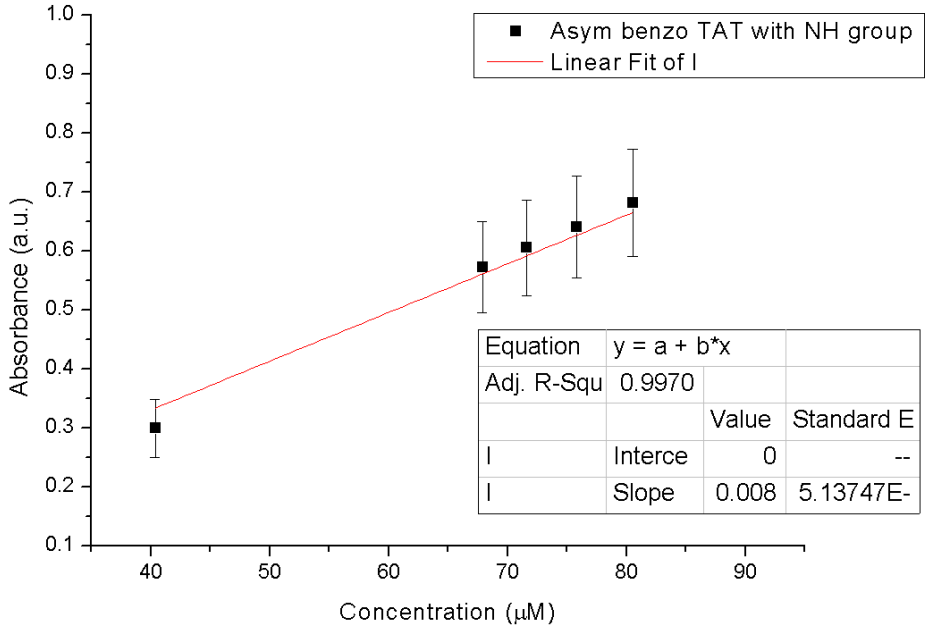

Figure A. 67 *Molar absorption coefficient plot of* ***A-BTT*** *in THF*

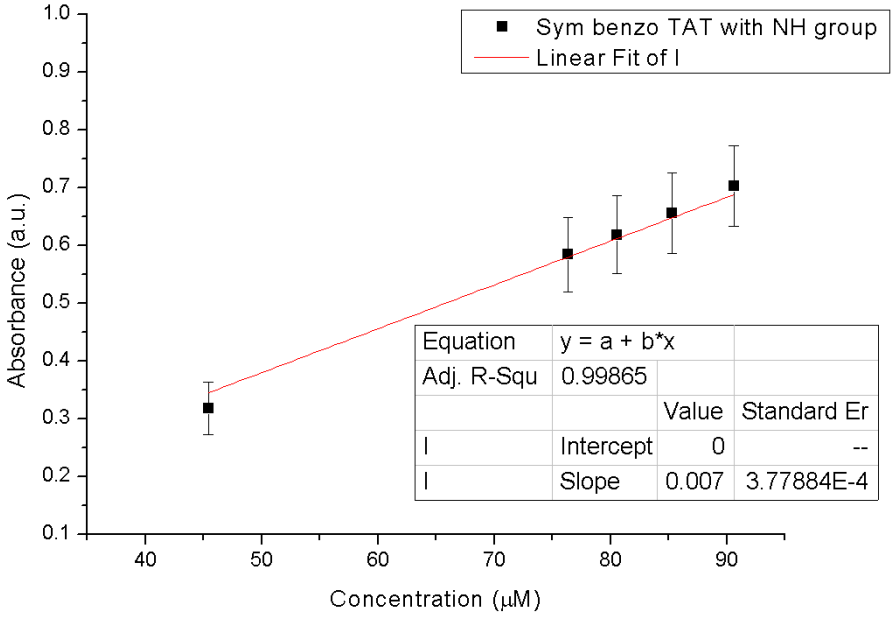

Figure A. 68 *Molar absorption coefficient plot of* ***S-BTT*** *in THF*

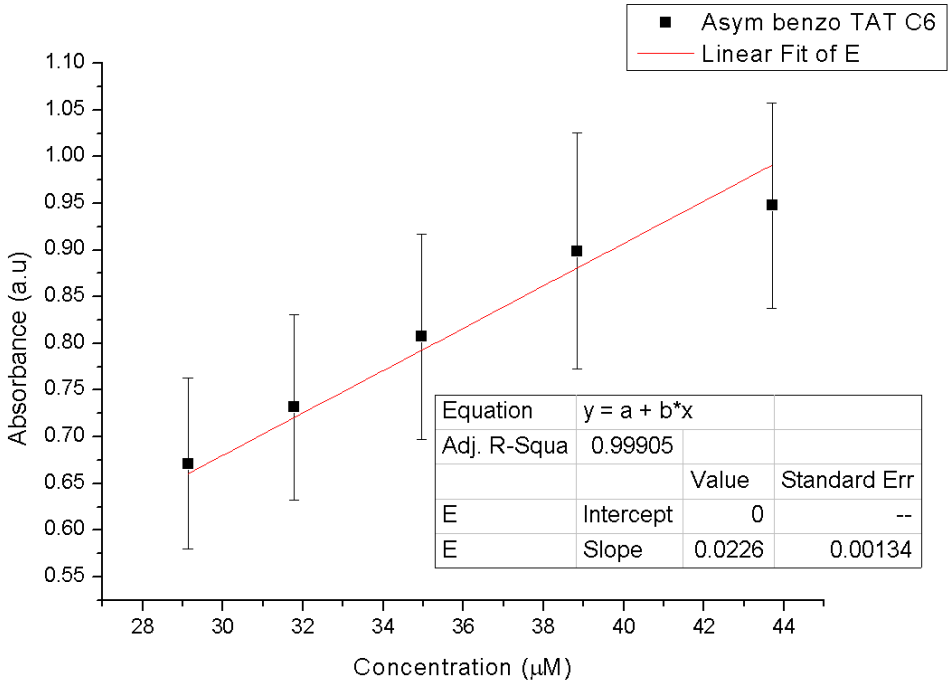

Figure A. 69 *Molar absorption coefficient plot of* ***A-BTT-C6*** *in THF*

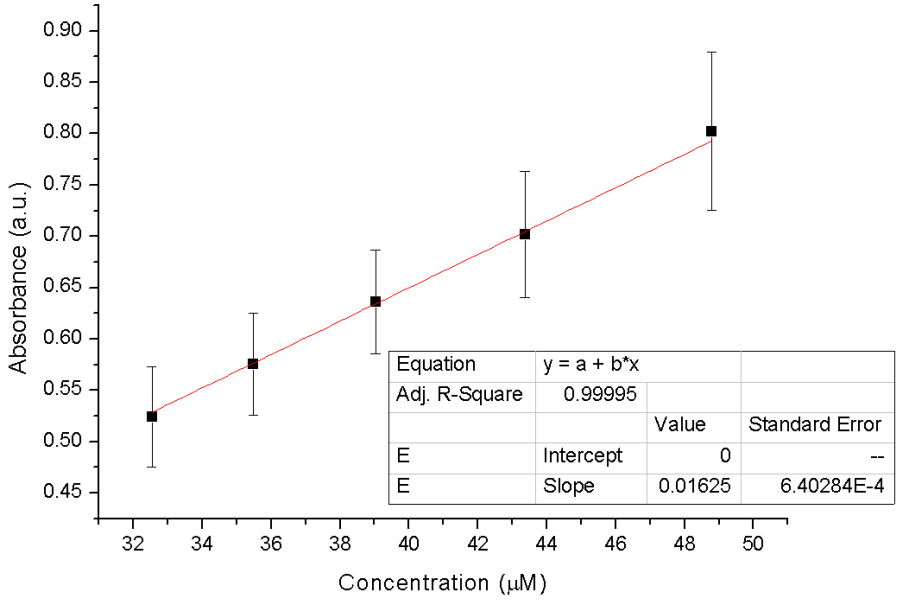

Figure A. 70 *Molar absorption coefficient plot of* ***S-BTT-C6*** *in THF*

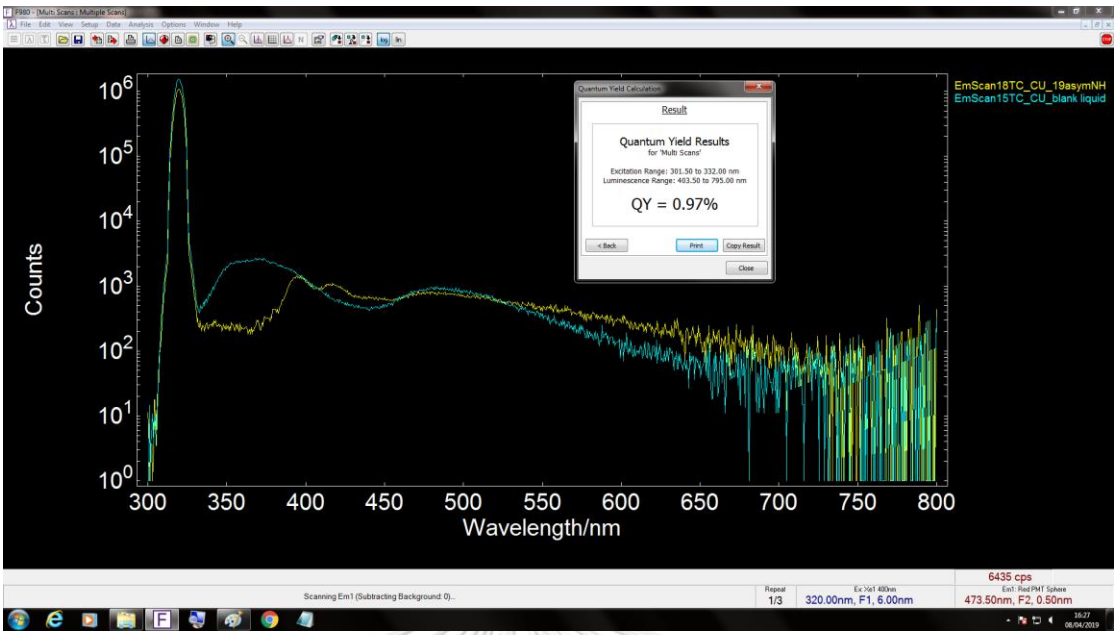

Figure A. 71 *Quantum yield report of* ***A-BTT*** *in* CH_2Cl_2

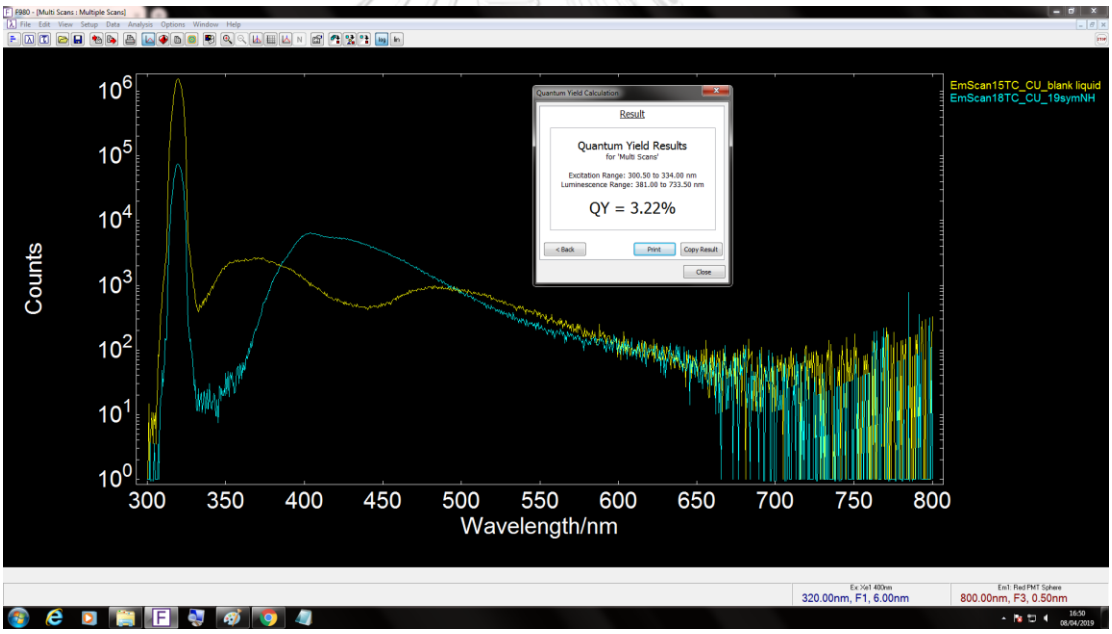

Figure A. 72 *Quantum yield report of* ***S-BTT*** *in* CH_2Cl_2

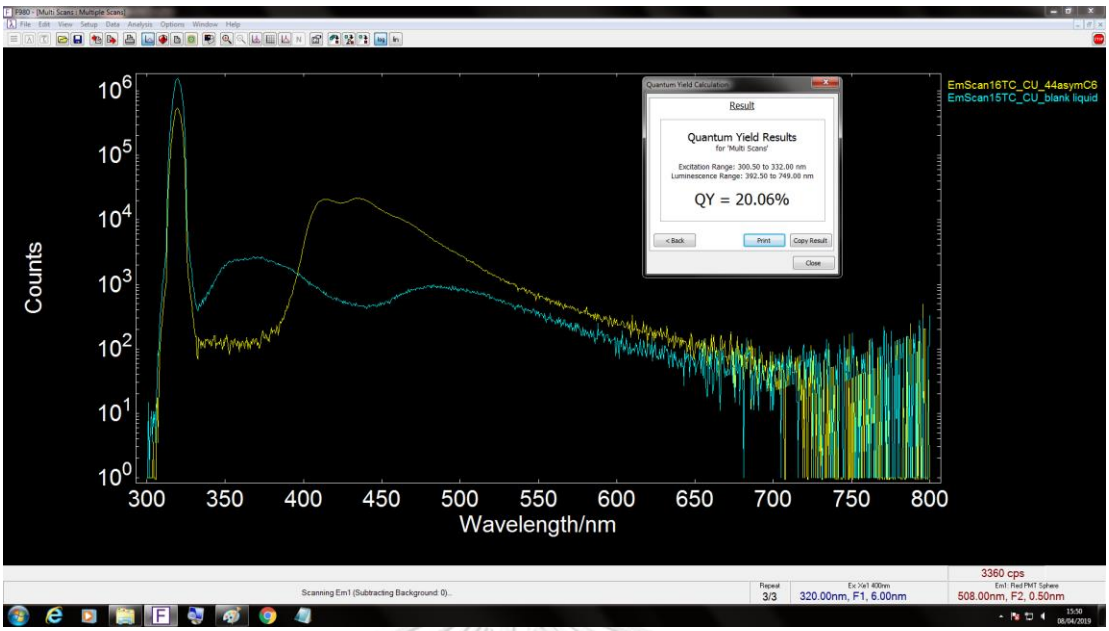

Figure A. 73 *Quantum yield report of* ***A-BTT-C6*** *in* CH_2Cl_2

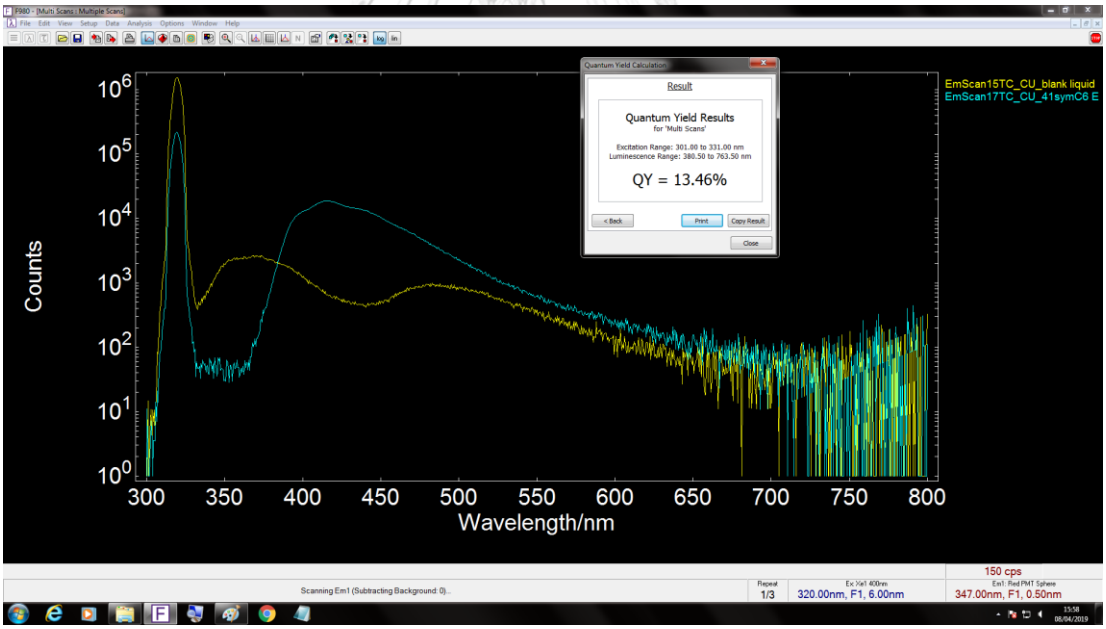

Figure A. 74 *Quantum yield report of* ***S-BTT-C6*** *in* CH_2Cl_2

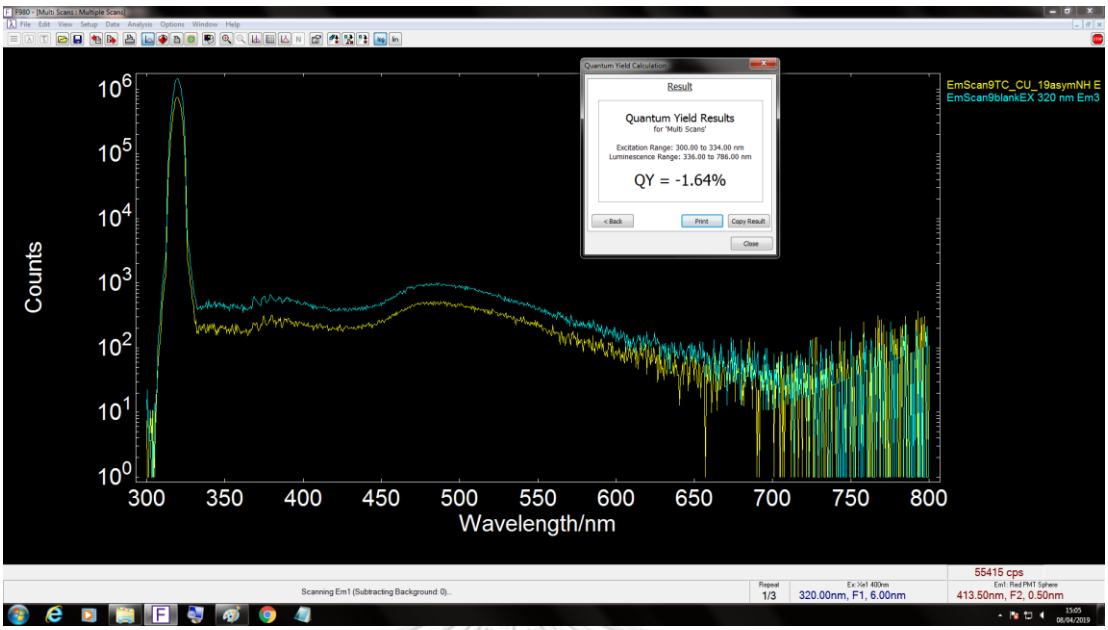

Figure A. 75 *Quantum yield report of* ***A-BTT*** *film*

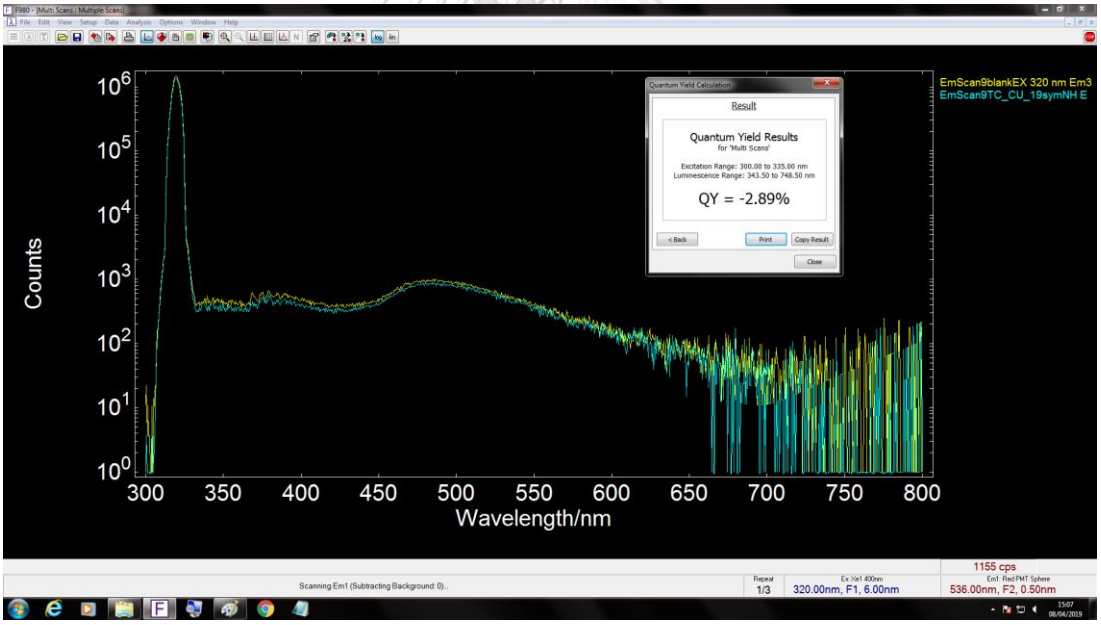

Figure A. 76 *Quantum yield report of* ***S-BTT*** *film*

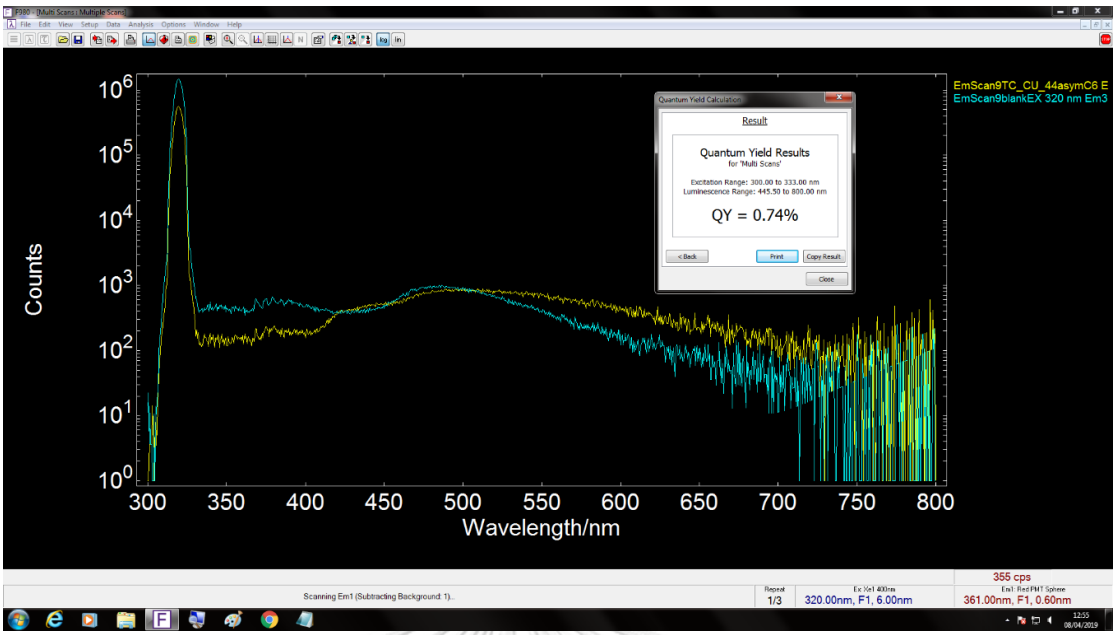

Figure A. 77 *Quantum yield report of* ***A-BTT-C6*** *film*

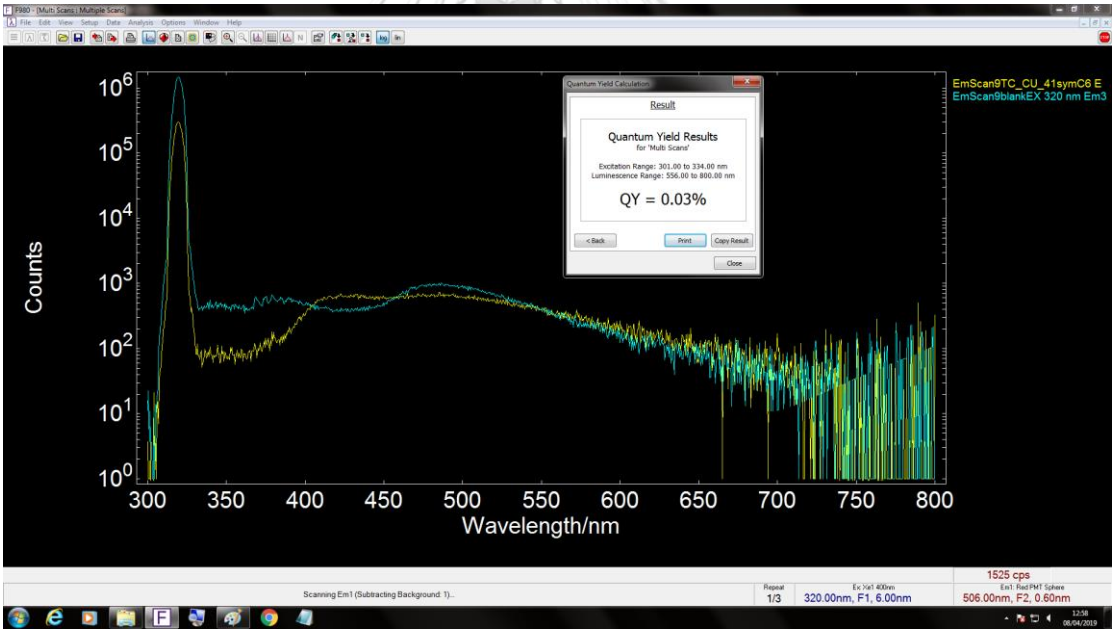

Figure A. 78 *Quantum yield report of* ***S-BTT-C6*** *film*

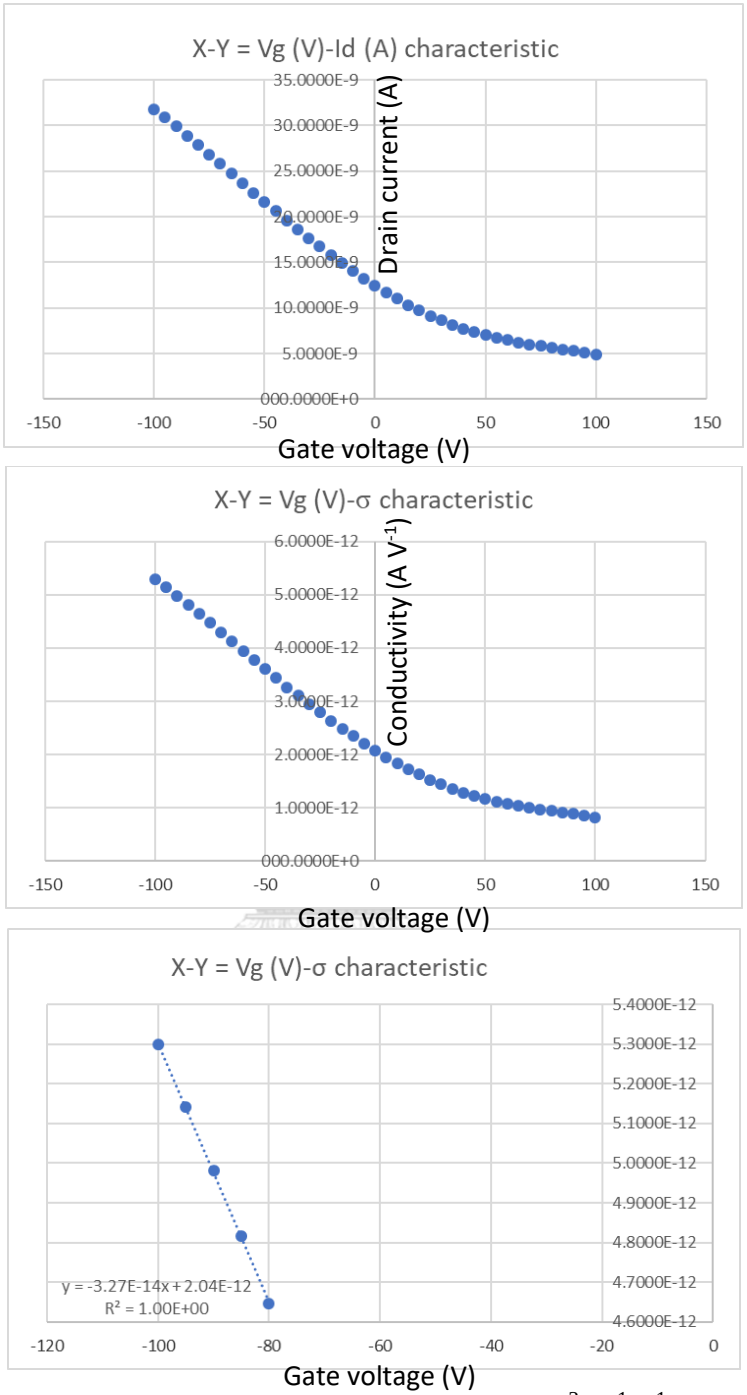

μ = slope*8.69*10^7 = 2.8416E-6 $cm^2\ V^{-1}\ s^{-1}$

Figure A. 79 *One of mobility calculations of evaporated* ***A-BTT*** *film without annealing at 10 µm gap*

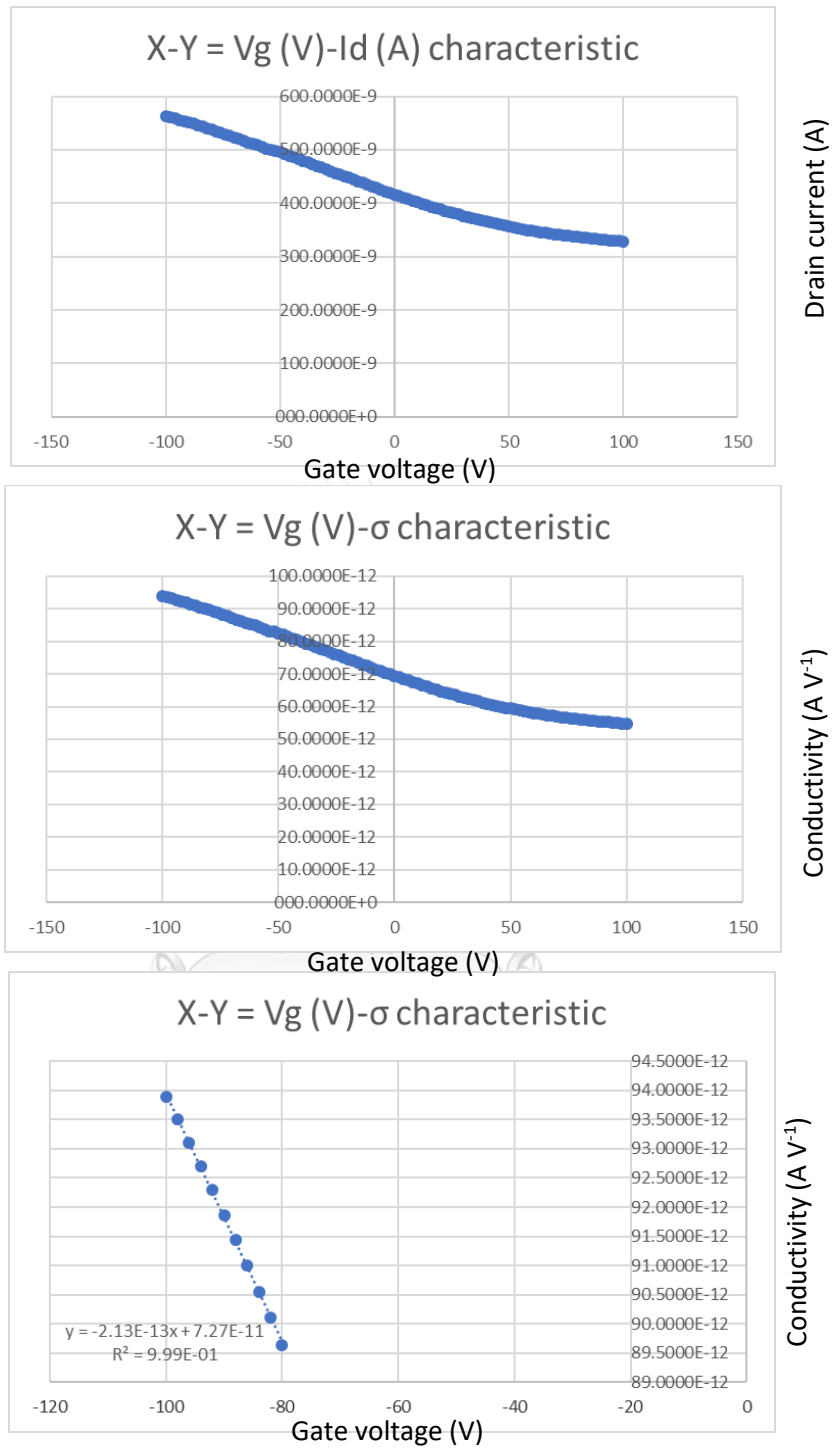

μ = slope*8.69*10^7 = 18.5097E-6 $cm^2\ V^{-1}\ s^{-1}$

Figure A. 80 *One of mobility calculations of evaporated* ***S-BTT*** *film without annealing at 10 µm gap*

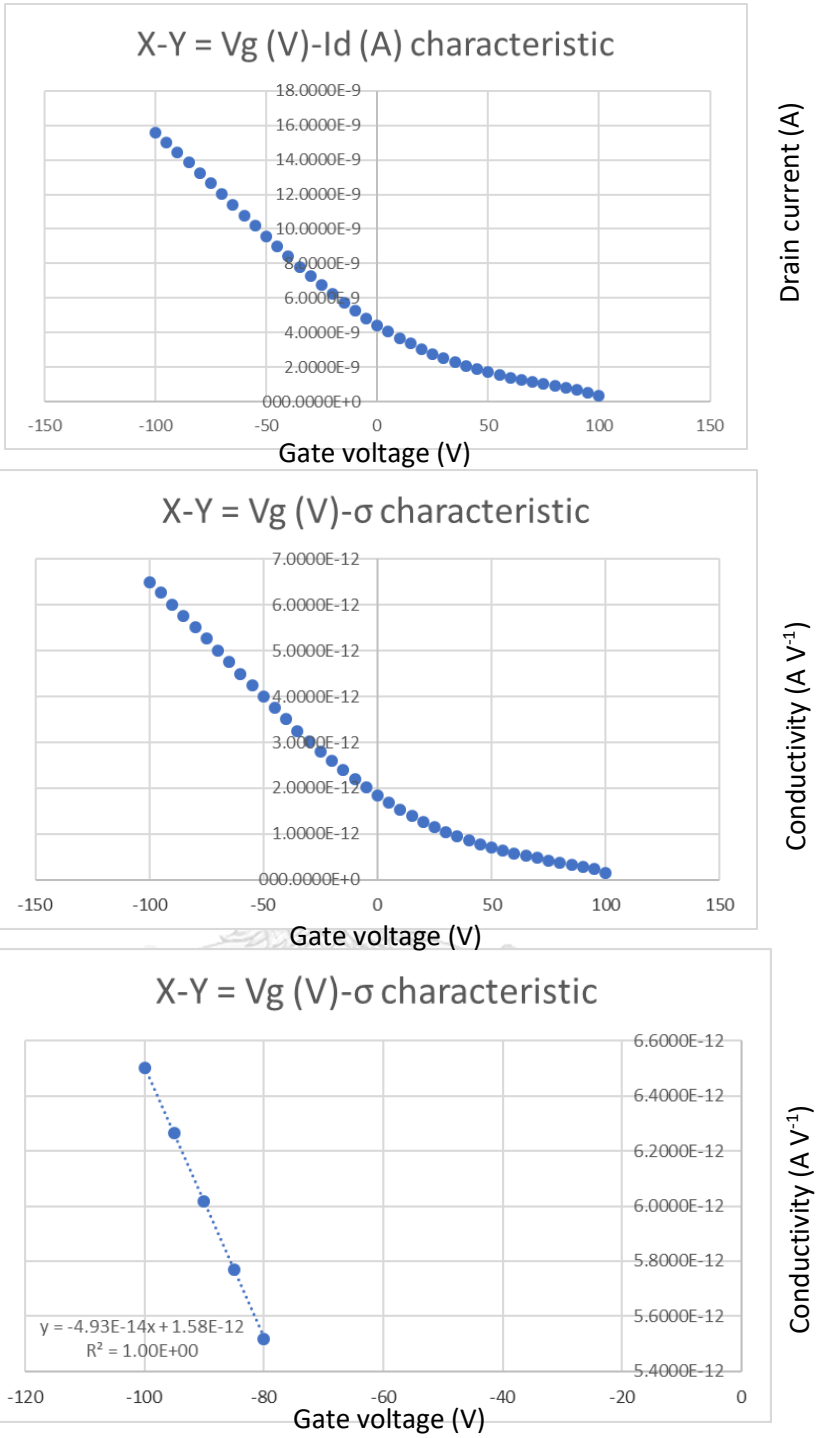

μ = slope*8.69*10^7 = 4.2842E-6 $cm^2\ V^{-1}\ s^{-1}$

Figure A. 81 *One of mobility calculations of evaporated* ***A-BTT*** *film without annealing at 25 µm gap*

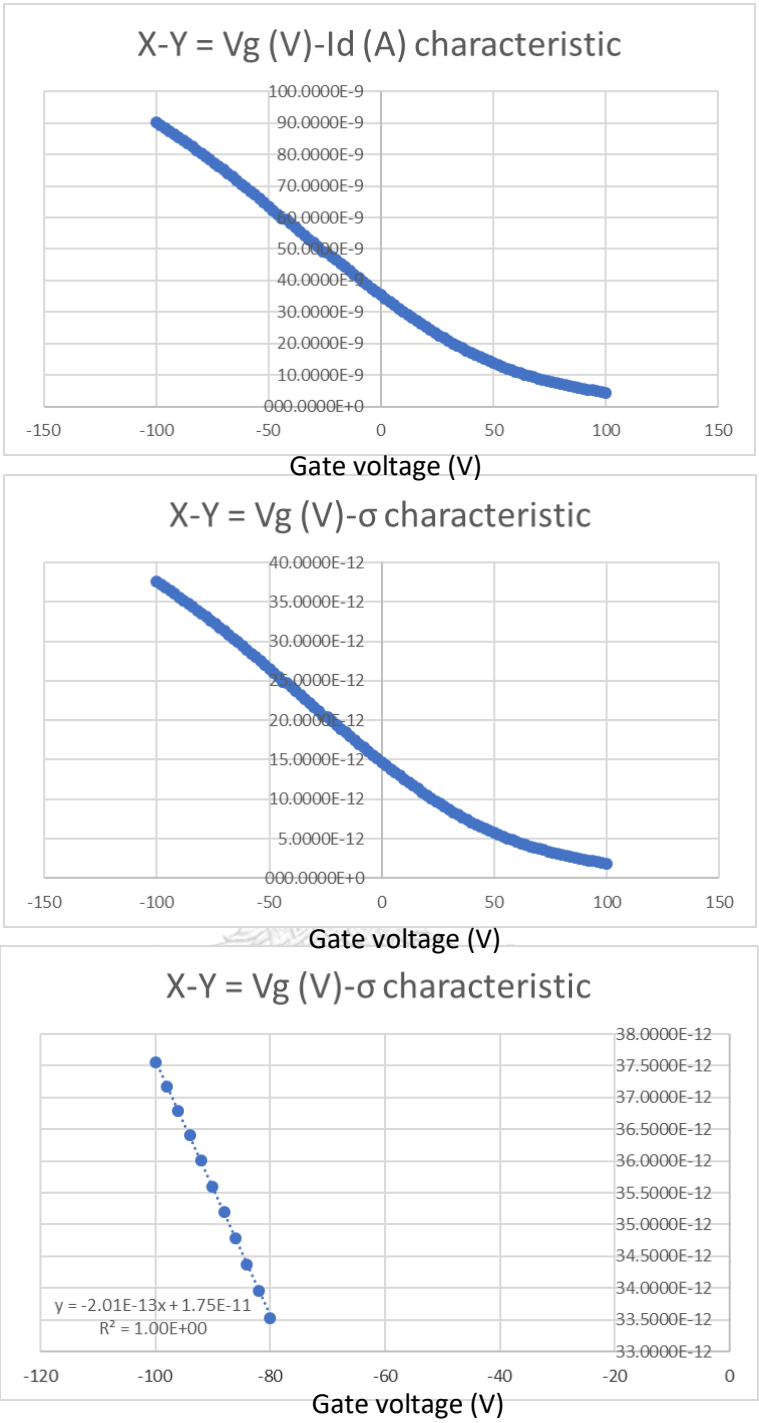

μ = slope*8.69*10^7 = 17.4669E-6 $cm^2\ V^{-1}\ s^{-1}$

Figure A. 82 *One of mobility calculations of evaporated* ***S-BTT*** *film without annealing at 25 µm gap*

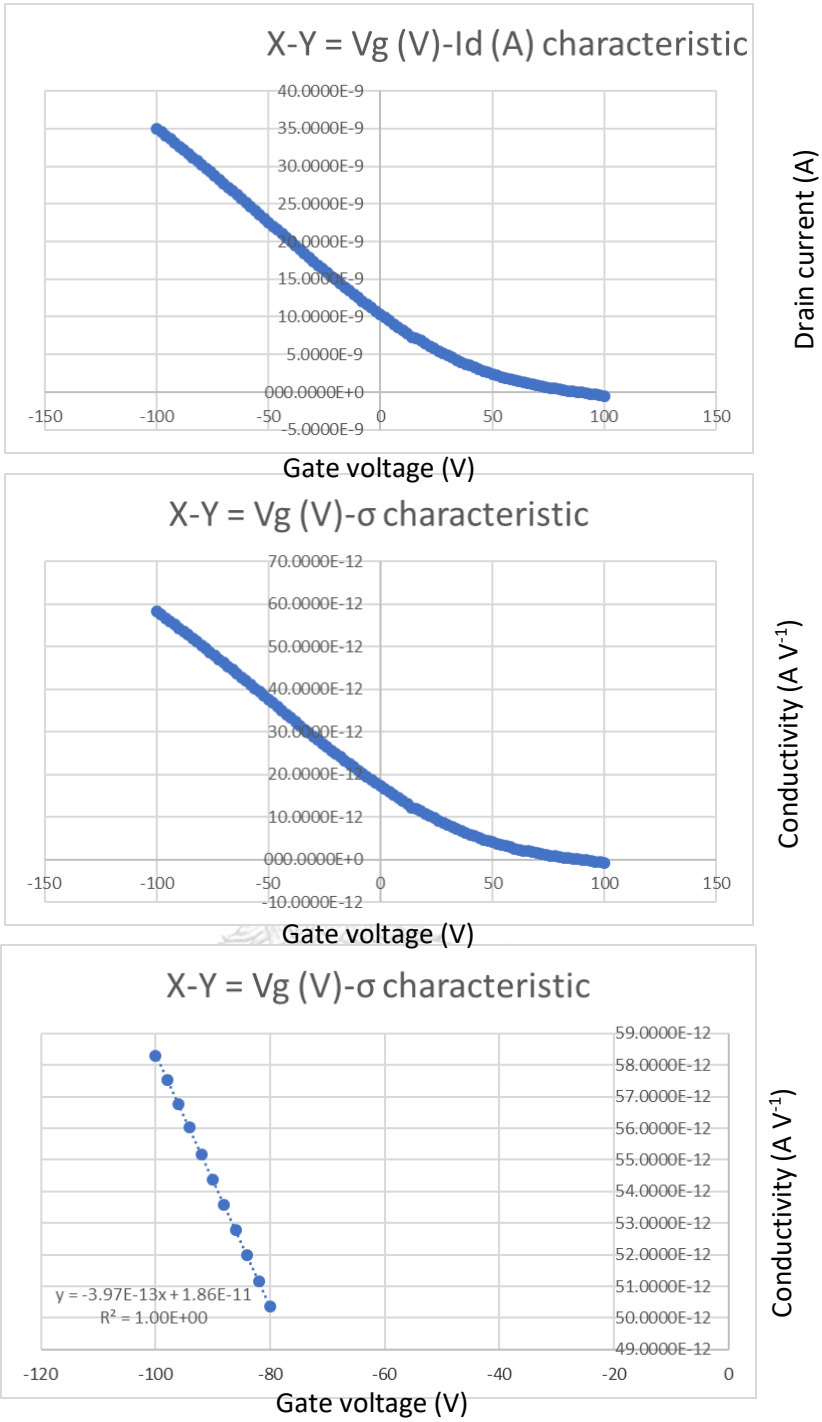

μ = slope*8.69*10^7 = 34.4993E-6 $cm^2\ V^{-1}\ s^{-1}$

Figure A. 83 *One of mobility calculations of evaporated* ***S-BTT*** *film without annealing at 100 µm gap*

VITA

NAME	Tianchai Chooppawa
DATE OF BIRTH	5 December 1987
PLACE OF BIRTH	Bangkok
INSTITUTIONS ATTENDED	Chulalongkorn university
HOME ADDRESS	337/2 Rama 1 road Pathum wan Bangkok Thailand
PUBLICATION	Tianchai Choppawa, Mongkol Sukwattanasinitt, Somboon Sahasithiwat, Vithaya Ruangpornvisuti, Paitoon Rashatasakhon, Substituent effect on quantum efficiency in 4-aryloxy-N-(2′,6′-diisopropylphenyl)-1,8-naphthalimides: Experimental and computational investigations, Dyes and Pigments, Volume 109, 2014, Pages 175-180, ISSN 0143-7208, https://doi.org/10.1016/j.dyepig.2014.05.007. (http://www.sciencedirect.com/science/article/pii/S0143720814001879)

จุฬาลงกรณ์มหาวิทยาลัย
Chulalongkorn University